OPTIMIZATION OF NEW MIXTURES OF HCL/METHANESULFONIC ACID IN MATRIX ACIDIZING OF CARBONATE ROCKS

A Thesis

by

SNEHA KANKARIA

Submitted to the Office of Graduate and Professional Studies of
Texas A&M University
in partial fulfillment of the requirements for the degree of

MASTER OF SCIENCE

Chair of Committee,	Hisham A. Nasr-El-Din
Committee Members,	Stephen A. Holditch
	Mahmoud El-Halwagi
Head of Department,	A. Daniel Hill

December 2017

Major Subject: Petroleum Engineering

ABSTRACT

One of the factors for the success of matrix acidizing of carbonate reservoirs is the selection of appropriate stimulation fluids. Till date, the most common acid for carbonate stimulation is HCl due to ease of its availability, inexpensiveness, and soluble reaction products. However, HCl has many drawbacks. It is associated with high corrosion issues and rapid reaction rate with calcite in bottomhole conditions, which, in turn, causes face dissolution problems. Thus, other alternatives are gaining attention in the oil industry.

Methanesulfonic acid (MSA), an organic acid, offers a viable alternative to HCl as they address the issues of corrosion and face dissolution rendered by HCl. In addition, MSA is environmentally benign. In literature, coreflood studies have been carried out using 10 wt% MSA in carbonates at 250°F to investigate its effectiveness. The kinetic parameters of various concentrations of MSA at different temperatures using rotating disk apparatus (RDA) have also been reported. However, MSA is expensive. This study proposes to use a blend of HCl and MSA for carbonate stimulation while enhancing the properties of HCl.

The goal of the present work is to evaluate the performance of the blend and optimize the concentration of individual acids in it using coreflood studies. Three different ratios of HCl and MSA will be studied by conducting coreflood experiments with 6-in. long Indiana Limestone cores at 250°F. The blend performances will also be compared to the equivalent concentration of individual acids at the determined optimum

injection rate. The effluent samples will be analyzed for pH, calcium concentration, and unconsumed acid concentration. Cores will be analyzed using CT scan for identifying wormhole structures and tortuosity determination. The optimum blend will be tested for dissolution kinetics study (mass-transfer or surface reaction limited regime) using RDA.

The advantages rendered by the new acid mixture compared to other standard systems currently used in the oil industry include: (1) extended wormholes that will ultimately lead to enhanced well productivity, and (2) cost-effectiveness in carbonate stimulation.

To my grandparents, parents, husband and my brother.

ACKNOWLEDGEMENTS

I would like to express my sincere gratitude to my advisor, Dr. Hisham A. Nasr-El-Din, for providing me the opportunity to conduct research under his guidance. I thank him for his immense support and encouragement provided throughout the course of this journey. His constant motivation, faith, and patience helped me enormously to execute this study. I am indebted to Dr. Hisham for implanting the art of scientific thoughts and presenting them effectively.

I am also grateful to Dr. Stephen A. Holditch and Dr. Mahmoud El-Halwagi for serving on my graduate committee. I would also like to extend my thanks to BASF Corporation for providing the chemicals and giving the permission to publish this work. I am thankful to Dr. Shawn Rimassa and Dr. Jia Zhou from BASF Global Oilfield Solutions unit for their valuable inputs and feedbacks that directed me to the right path during my research.

Thanks to Dr. Ahmed I. Rabie for training and mentoring me during the early stage of my graduate school. I appreciate the efforts of Sherif Abdelmoneim for teaching me the details and troubleshooting of coreflood. I thank Mahmoud Taha Ali for helping me with the VBA code for wormhole location determination.

I acknowledge my friends, colleagues, department faculty and staff for making my experience at Texas A&M University an exciting one. I thank the department for honoring my research efforts with prestigious award during the student paper contest.

Special thanks to Raja, Abhishek, Taniya and Taylor for the support, countless discussions and cherishable memories in the school.

Thanks to my grandparents and parents for infusing in me the skill of facing and overcoming the obstacles to pursue my dream. I thank my brother for always encouraging me in all of my accomplishments so far. Last but not the least, I thank the pillar of my life, my husband, for his extreme support, guidance, and adoration. This journey would not have been possible without foundation laid by everyone.

CONTRIBUTORS AND FUNDING SOURCES

Contributors

This study was supervised by a thesis committee of Dr. Hisham A. Nasr-El-Din and Dr. Stephen A. Holditch of the Harold Vance Department of Petroleum Engineering and Dr. Mahmoud El-Halwagi of the Artie McFerrin Department of Chemical Engineering.

The VBA code for wormhole location determination in Chapter VI was written by a graduate student, Mahmoud Taha Ali.

All other work on the coreflood and rotating disk reactor studies for the thesis was completed by the student independently.

Funding Sources

This work was made possible in part by BASF Corporation under the project number C13-00209.

NOMENCLATURE

A	cross-sectional area, cm^2
ACS	American Chemical Society
C_b	bulk concentration of acid, $gmol/cm^3$
CRAs	corrosion resistant alloys
C_s	surface concentration of acid, $gmol/cm^3$
CT	computed tomography
D	diffusivity, cm^2/s
ΔP	pressure drop across the core, atm
DI	de-ionized water
E_a	activation energy, kJ/gmol
ft	feet
ICP-OES	Inductively Coupled Plasma-Optical Emission Spectroscopy
in	inch
J_{mt}	rate of mass-transfer, $gmol/cm^2.s$
K	specific reaction rate constant, $(gmol/cm^2.s)(\ gmol/cm^3)^{-n}$
K_0	pre-exponential factor
k	absolute permeability, Darcy
L	length of the wormhole, cm
L_0	length of the core, cm
M	molarity
μ	fluid viscosity, cp

MSA	methanesulfonic acid
n	reaction order, dimensionless
ν	kinematic viscosity, cm^2/s
ϕ	porosity, vol%
pK_a	negative logarithm of acid dissociation constant, dimensionless
psi	pounds per square inch
PV	pore volume, cm^3
ω	disk rotational speed, rad/s
Q	flow rate, cm^3/min
R	universal gas constant, kJ/gmol.K
RDA	rotating disk apparatus
$-r_{HCl}$	rate of consumption of HCl, $gmol/cm^2.s$
ρ	density of de-ionized water, g/cm^3
rpm	rotations per minute
Sc	Schmidt number, dimensionless
T	temperature, °K
V_{bulk}	volume of the core, cm^3
W_{dry}	dry weight of the core, g
W_{sat}	saturated weight of the core, g
XRD	X Ray Diffraction
XRF	X Ray Fluorescence

TABLE OF CONTENTS

Page

ABSTRACT ii

ACKNOWLEDGEMENTS v

CONTRIBUTORS AND FUNDING SOURCES vii

NOMENCLATURE viii

TABLE OF CONTENTS x

LIST OF FIGURES xii

LIST OF TABLES xviii

CHAPTER I INTRODUCTION 1

CHAPTER II LITERATURE REVIEW 7

CHAPTER III PROBLEM STATEMENT 11

CHAPTER IV RESEARCH OBJECTIVE 13

CHAPTER V MATERIALS 14

V.1 Fluids 14
V.2 Rock Properties 15

CHAPTER VI COREFLOOD STUDIES 17

VI.1 Experimental Procedure 18
VI.1.1 Components of coreflood 18
VI.1.2 Core preparation 19
VI.1.3 Coreflood experiments 20
VI.2 Theory of Wormhole Formation 22
VI.3 Results and Discussions 25
VI.3.1 Acid blend 2.5:7.5 wt% HCl:MSA 25
VI.3.2 Acid blend 5:5 wt% HCl:MSA 43
VI.3.3 Acid blend 7.5:2.5 wt% HCl:MSA 59
VI.3.4 Comparative study 76

CHAPTER VII ROTATING DISK APPARATUS (RDA) STUDIES 83

VII.1 Experimental Procedure 83
VII.1.1 Components of RDA 83
VII.1.2 Disk preparation 85
VII.1.3 RDA experiments 85
VII.2 Theory of RDA 85
VII.3 Results and Discussions 88

CHAPTER VIII CONCLUSIONS 99

REFERENCES 102

APPENDIX 107

LIST OF FIGURES

Page

Figure 1 - A schematic of coreflood set-up. 19

Figure 2 - A typical acid efficiency curve showing the effect of flow rate on acid pore volume required to breakthrough. 24

Figure 3 - Effect of Damköhler number on wormhole structures. 24

Figure 4 - CT scan image of Indiana limestone core after acidizing by 2.5:7.5 wt% HCl:MSA blend at 2 cm^3/min. 26

Figure 5 - Pressure drop across the core for 2.5:7.5 wt% HCl:MSA at 2 cm^3/min as a function of the cumulative volume injected at 250°F. 27

Figure 6 - Calcium ion concentration for 2.5:7.5 wt% HCl:MSA at 2 cm^3/min as a function of the cumulative volume injected at 250°F. 28

Figure 7 - Acid concentration in terms of equivalent HCl and pH of core effluent samples for 2.5:7.5 wt% HCl:MSA at 2 cm^3/min as a function of the cumulative volume injected at 250°F. 29

Figure 8 - Pressure drop across the core for 2.5:7.5 wt% HCl:MSA at 5 cm^3/min as a function of the cumulative volume injected at 250°F. 30

Figure 9 - CT scan image of Indiana limestone core after acidizing by 2.5:7.5 wt% HCl:MSA blend at 5 cm^3/min. 30

Figure 10 - Calcium ion concentration for 2.5:7.5 wt% HCl:MSA at 5 cm^3/min as a function of the cumulative volume injected at 250°F. 31

Figure 11 - Acid concentration in terms of equivalent HCl and pH of core effluent samples for 2.5:7.5 wt% HCl:MSA at 5 cm^3/min as a function of the cumulative volume injected at 250°F. 32

Figure 12 - Pressure drop across the core for 2.5:7.5 wt% HCl:MSA at 7.5 cm^3/min as a function of the cumulative volume injected at 250°F. 33

Figure 13 - CT scan image of Indiana limestone core after acidizing by 2.5:7.5 wt% HCl:MSA blend at 7.5 cm^3/min. 33

Figure 14 - Calcium ion concentration for 2.5:7.5 wt% HCl:MSA at 7.5 cm^3/min as a function of the cumulative volume injected at 250°F. 34

Figure 15 - Acid concentration in terms of equivalent HCl and pH of core effluent samples for 2.5:7.5 wt% HCl:MSA at 7.5 cm^3/min as a function of the cumulative volume injected at 250°F. 35

Figure 16 - Pressure drop across the core for 2.5:7.5 wt% HCl:MSA at 10 cm^3/min as a function of the cumulative volume injected at 250°F. 36

Figure 17 - CT scan image of Indiana limestone core after acidizing by 2.5:7.5 wt% HCl:MSA blend at 10 cm^3/min. 36

Figure 18 - Calcium ion concentration for 2.5:7.5 wt% HCl:MSA at 10 cm^3/min as a function of the cumulative volume injected at 250°F. 37

Figure 19 - Acid concentration in terms of equivalent HCl and pH of core effluent samples for 2.5:7.5 wt% HCl:MSA at 10 cm^3/min as a function of the cumulative volume injected at 250°F. 38

Figure 20 - Acid efficiency curve for 2.5:7.5 wt% HCl:MSA at 250°F. 39

Figure 21 - Pressure drop across the core for 2.5:7.5 wt% HCl:MSA and its respective HCl and MSA controls at 7.5 cm^3/min as a function of the cumulative volume injected at 250°F. 40

Figure 22 - Calcium ion concentration for 2.5:7.5 wt% HCl:MSA and its respective HCl and MSA controls at 7.5 cm^3/min as a function of the cumulative volume injected at 250°F. 40

Figure 23 - Acid concentration in terms of equivalent HCl concentration for 2.5:7.5 wt% HCl:MSA and its respective HCl and MSA controls at 7.5 cm^3/min as a function of the cumulative volume injected at 250°F. 42

Figure 24 - CT scan images of Indiana limestone cores after acidizing by 2.5:7.5 wt% HCl:MSA, 6 wt% HCl control, and 15 wt% MSA control equivalent at 7.5 cm^3/min. 42

Figure 25 - Pressure drop across the core for 5:5 wt% HCl:MSA at 2 cm^3/min as a function of the cumulative volume injected at 250°F. 44

Figure 26 - CT scan image of Indiana limestone core after acidizing by 5:5 wt% HCl:MSA blend at 2 cm^3/min. 44

Figure 27 - Calcium ion concentration for 5:5 wt% HCl:MSA at 2 cm^3/min as a function of the cumulative volume injected at 250°F. 45

Figure 28 - Acid concentration in terms of equivalent HCl and pH of core effluent samples for 5:5 wt% HCl:MSA at 2 cm^3/min as a function of the cumulative volume injected at 250°F. 46

Figure 29 - Pressure drop across the core for 5:5 wt% HCl:MSA at 5 cm^3/min as a function of the cumulative volume injected at 250°F. 47

Figure 30 - CT scan image of Indiana limestone core after acidizing by 5:5 wt% HCl:MSA blend at 5 cm^3/min. 47

Figure 31 - Calcium ion concentration for 5:5 wt% HCl:MSA at 5 cm^3/min as a function of the cumulative volume injected at 250°F. 48

Figure 32 - Acid concentration in terms of equivalent HCl and pH of core effluent samples for 5:5 wt% HCl:MSA at 5 cm^3/min as a function of the cumulative volume injected at 250°F. 49

Figure 33 - Pressure drop across the core for 5:5 wt% HCl:MSA at 7.5 cm^3/min as a function of the cumulative volume injected at 250°F. 50

Figure 34 - CT scan image of Indiana limestone core after acidizing by 5:5 wt% HCl:MSA blend at 7.5 cm^3/min. 50

Figure 35 - Calcium ion concentration for 5:5 wt% HCl:MSA at 7.5 cm^3/min as a function of the cumulative volume injected at 250°F. 51

Figure 36 - Acid concentration in terms of equivalent HCl and pH of core effluent samples for 5:5 wt% HCl:MSA at 7.5 cm^3/min as a function of the cumulative volume injected at 250°F. 52

Figure 37 - Pressure drop across the core for 5:5 wt% HCl:MSA at 10 cm^3/min as a function of the cumulative volume injected at 250°F. 53

Figure 38 - CT scan image of Indiana limestone core after acidizing by 5:5 wt% HCl:MSA blend at 10 cm^3/min. 53

Figure 39 - Calcium ion concentration for 5:5 wt% HCl:MSA at 10 cm^3/min as a function of the cumulative volume injected at 250°F. 54

Figure 40 - Acid concentration in terms of equivalent HCl and pH of core effluent samples for 5:5 wt% HCl:MSA at 10 cm^3/min as a function of the cumulative volume injected at 250°F. 55

Figure 41 - Acid efficiency curve for 5:5 wt% HCl:MSA at 250°F. 56

Figure 42 - Pressure drop across the core for 5:5 wt% HCl:MSA and its respective HCl and MSA controls at 7.5 cm^3/min as a function of the cumulative volume injected at 250°F. 57

Figure 43 - Calcium ion concentration for 5:5 wt% HCl:MSA and its respective HCl and MSA controls at 7.5 cm^3/min as a function of the cumulative volume injected at 250°F. 58

Figure 44 - Acid concentration in terms of equivalent HCl concentration for 5:5 wt% HCl:MSA and its respective HCl and MSA controls at 7.5 cm^3/min as a function of the cumulative volume injected at 250°F. 58

Figure 45 - CT scan images of Indiana limestone cores after acidizing by 5:5 wt% HCl:MSA, 7.2 wt% HCl control, and 17.7 wt% MSA control equivalent at 7.5 cm^3/min. 59

Figure 46 - Pressure drop across the core for 7.5:2.5 wt% HCl:MSA at 2 cm^3/min as a function of the cumulative volume injected at 250°F. 60

Figure 47 - CT scan image of Indiana limestone core after acidizing by 7.5:2.5 wt% HCl:MSA blend at 2 cm^3/min. 61

Figure 48 - Calcium ion concentration for 7.5:2.5 wt% HCl:MSA at 2 cm^3/min as a function of the cumulative volume injected at 250°F. 62

Figure 49 - Acid concentration in terms of equivalent HCl and pH of core effluent samples for 7.5:2.5 wt% HCl:MSA at 2 cm^3/min as a function of the cumulative volume injected at 250°F. 62

Figure 50 - Pressure drop across the core for 7.5:2.5 wt% HCl:MSA at 5 cm^3/min as a function of the cumulative volume injected at 250°F. 63

Figure 51 - CT scan image of Indiana limestone core after acidizing by 7.5:2.5 wt% HCl:MSA blend at 5 cm^3/min. 64

Figure 52 - Calcium ion concentration for 7.5:2.5 wt% HCl:MSA at 5 cm^3/min as a function of the cumulative volume injected at 250°F. 65

Figure 53 - Acid concentration in terms of equivalent HCl and pH of core effluent samples for 7.5:2.5 wt% HCl:MSA at 5 cm^3/min as a function of the cumulative volume injected at 250°F. 65

Figure 54 - Pressure drop across the core for 7.5:2.5 wt% HCl:MSA at 7.5 cm^3/min as a function of the cumulative volume injected at 250°F. 66

Figure 55 - CT scan image of Indiana limestone core after acidizing by 7.5:2.5 wt% HCl:MSA blend at 7.5 cm^3/min. 67

Figure 56 - Calcium ion concentration for 7.5:2.5 wt% HCl:MSA at 7.5 cm^3/min as a function of the cumulative volume injected at 250°F. 68

Figure 57 - Acid concentration in terms of equivalent HCl and pH of core effluent samples for 7.5:2.5 wt% HCl:MSA at 7.5 cm^3/min as a function of the cumulative volume injected at 250°F. 68

Figure 58 - Pressure drop across the core for 7.5:2.5 wt% HCl:MSA at 10 cm^3/min as a function of the cumulative volume injected at 250°F. 69

Figure 59 - CT scan image of Indiana limestone core after acidizing by 7.5:2.5 wt% HCl:MSA blend at 10 cm^3/min. 70

Figure 60 - Calcium ion concentration for 7.5:2.5 wt% HCl:MSA at 10 cm^3/min as a function of the cumulative volume injected at 250°F. 71

Figure 61 - Acid concentration in terms of equivalent HCl and pH of core effluent samples for 7.5:2.5 wt% HCl:MSA at 10 cm^3/min as a function of the cumulative volume injected at 250°F. 71

Figure 62 - Acid efficiency curve for 7.5:2.5 wt% HCl:MSA at 250°F. 73

Figure 63 - Pressure drop across the core for 7.5:2.5 wt% HCl:MSA and its respective HCl and MSA controls at 5 cm^3/min as a function of the cumulative volume injected at 250°F. 73

Figure 64 - Calcium ion concentration for 7.5:2.5 wt% HCl:MSA and its respective HCl and MSA controls at 5 cm^3/min as a function of the cumulative volume injected at 250°F. 74

Figure 65 - Acid concentration in core effluent samples in terms of equivalent HCl concentration for 7.5:2.5 wt% HCl:MSA and its respective HCl and MSA controls at 5 cm^3/min as a function of the cumulative volume injected at 250°F. 75

Figure 66 - CT scan images of Indiana limestone cores after acidizing by 7.5:2.5 wt% HCl:MSA, 8.8 wt% HCl control, and 21.31 wt% MSA control equivalent at 5 cm^3/min. 75

Figure 67 - CT scan images of Indiana limestone cores after acidizing by different acid blends and their controls at the optimum injection rate. 78

Figure 68 - Comparison of acid volume required to reach breakthrough between different acid blends and their respective HCl and MSA controls at optimum injection rates. 80

Figure 69 - Rotating disk reactor. 84

Figure 70 - A typical plot of dissolution rate vs. square root of disk rotational speed. ... 87

Figure 71 - Dissolved Ca^{2+} vs. time plots for RDA tests at 77°F with 5:5 wt% HCl:MSA blend at a) 100, b) 300, c) 500, and d) 800 rpm. 89

Figure 72 - Dissolved Ca^{2+} vs. time plots for RDA tests at 250°F with 5:5 wt% HCl:MSA blend at a) 100, b) 300, c) 500, and d) 800 rpm. 90

Figure 73 - Dissolved H^{+} vs. time plots for RDA tests at 77°F with 5:5 wt% HCl:MSA blend at a) 100, b) 300, c) 500, and d) 800 rpm. 91

Figure 74 - Dissolved H^{+} vs. time plots for RDA tests at 250°F with 5:5 wt% HCl:MSA blend at a) 100, b) 300, c) 500, and d) 800 rpm. 92

Figure 75 - Marble disks after RDA tests with 5:5 wt% HCl:MSA at 77°F at a) 100, b) 300, c) 500, and d) 800 rpm. 93

Figure 76 - Marble disks after RDA tests with 5:5 wt% HCl:MSA at 250°F at a) 100, b) 300, c) 500, and d) 800 rpm. 93

Figure 77 - Rate of dissolution as a function of square root of angular velocity at 77 and 250°F. 94

Figure 78 - Kinematic viscosity of 5:5 wt% HCl:MSA blend as a function of temperature. 96

LIST OF TABLES

Page

Table 1 - Density and viscosity of acid blends as a function of temperature..... 15

Table 2 - Mineralogy of Indiana limestone..... 16

Table 3 - Mineralogy of calcite marble disks..... 16

Table 4 - Porosities and permeabilities of cores used in coreflood experiments. 21

Table 5 - Comparison of various post-coreflood parameters between different acid blends and their respective HCl and MSA controls at optimum injection rates. 82

Table 6 - Kinematic viscosity and density as a function of temperature for 5:5 wt% HCl:MSA blend. 95

Table 7 - Diffusion coefficient values of HCl at different concentration and temperature. 97

Table 8 - Diffusion coefficient values of MSA at different concentration and temperature. 97

CHAPTER I

INTRODUCTION

Mankind has always been on the hunt for various sources of energy to meet the world energy demands. However, fossil fuels continue to dominate over all the other sources. In attempts of oil and gas exploration, wells are drilled both on land and offshore environments. After the geologists analyze a basin and determine its potential to produce oil or gas, which is based on several parameters like permeability and reserve, wells are drilled to start the production. During drilling, mud comprising of solid particles and certain chemicals are injected to maintain pressure in the wellbore to provide wellbore stability, cool and lubricate the drill bit, and remove cuttings from the downhole. Casings are set to provide stabilization of the hole, protect fresh water and isolates zones of interest. The production tubing is a conduit for formation fluids. During all these steps, there are many occasions when the pores might get plugged, thereby declining the productivity. For conventional reservoirs, stimulation is an efficient technique to improve the productivity.

Formation damage refers to oil/gas well production impairment due to plugging of pore throats and spaces. This blockage can be caused by mineral or organic deposits (Muecke 1982). Mineral deposit-induced damage can occur during various stages of a well's life (McLeod 1984) such as drilling, perforating, cementing, chemical treatments, production, etc. Poorly conditioned drilling mud containing improperly sized bridging particles can cause invasion of mud filtrate into a permeable formation. Bentonite mud

can affect the sandstone formations. Mud filtrates can swell and migrate the clays present in the formation. Use of such fluids can also result in washout that leads to a poor cement job (Ghalambor and Economides 2000). On the other hand, cement should be formulated with good fluid loss control additives to prevent the infiltration and precipitation of the slurry containing calcium silicate and calcium hydroxide into the formation.

Damage is usually quantified by skin factor; higher the skin factor, greater is the extent of damage. Perforation of the casing can lead to intrusion of debris and crushed fines into the perforating fluid (Klotz et al. 1974) that permeates into the formation. Completion jobs such as gravel packing to control sand production involve gravel slurry/gel that can squeeze pipe dope and scales into the perforation that causes high pressure drop (Houchin et al. 1988). High drawdown can cause fines migration, thereby plugging the pores. Scale formation and casing leaks are other reasons of formation damage. Chemical treatments such as acidizing are targeted to remove calcite scales, but pumping acid downhole squeezes pipe dope and iron scale into the formation that can precipitate. HF/HCl-induced damage causes a significant amount of precipitation and reduces the permeability of the formation (Bryant and Buller 1990). Scale and corrosion inhibitors can alter the wettability of the formation that indirectly aids in impairment of production. Surfactants used to reduce interfacial tension between oil and water also affects the wettability of the rock. Asphaltene and wax deposition resulting from a change in temperature (caused by injection of cold fluids) are one of the major causes of damage. Certain injection operations involve the introduction of bacteria and corrosion

products downhole. All these mechanisms of formation damage demand a necessity of their removal and prevention techniques.

The objective of well stimulation technique is to improve the productivity of oil or gas wells by removing the damage. Acid treatments are commonly employed to combat the issues of impaired productivity. They are divided into two categories: matrix acidizing and acid fracturing (Muecke 1982). Near-wellbore damage can be remedied by matrix acidizing treatment, where the stimulation fluid is introduced at a pressure below the fracture pressure of the formation. The acid based fluids are introduced at a low injection rate that dissolve and remove the damaging material. The closer the damage is to the perforations, the more easily it can be removed (McLeod 1984). This treatment method is commonly used in sandstones to restore the permeability to its original condition. Typically, the treatment comprises of HCl preflush to remove carbonates from the vicinity in order to avoid precipitation of calcium fluoride by HF present in the main stage acid that consists of HF/HCl mixture to dissolve the silicates. It is followed by post-flush of diesel, brine or HCl that displaces the precipitates formed from HF/HCl.

In carbonates, matrix acidizing is applied to increase the permeability of the formation by the creation of conductive channels that bypass the damaged zone (Coulter and Jennings 1999). Typically, in sandstone formations, the acid treatment is effective within 1–3 ft from the perforation while that in carbonates, it is up to 20 ft. Thus, the success of carbonate acidizing by matrix stimulation is an attractive procedure due to the very high production enhancement compared to that of sandstone acidizing. Deep damages and low permeability reservoirs could be amended using acid fracturing

technique which involves the generation of large conductive fractures by etching the rock. The fluid is introduced at a rate high enough to crack the formation open. Matrix acidizing is preferable over acid fracturing where it is desirable to maintain a natural boundary of shale or an impermeable layer to prevent early water/gas breakthrough (Fredd and Fogler 1998a), or in chalk formations where fracturing is ineffective, or in moderate to high permeability reservoir. The success of the treatment is highly dependent on the type of the stimulation fluid and how well it correlates with the damage (Coulter and Jennings 1999).

Acidizing technique has been used in the oil and gas industry since the 1890s (Coulter and Jennings 1999). It was started by Standard Oil who patented the use of HCl to stimulate carbonate formations. However, HCl was associated with severe corrosion issues that declined its usage for 30 years until arsenic based inhibitors were invented by Dow Chemical Company (Crowe et al. 1992). Till date, HCl is the most commonly used acid in the oil industry as it is cheap, readily available, and has soluble reaction products in carbonates treatment (Buijse et al. 2004). Though HCl has a high rock dissolving power, it has a rapid reaction rate with calcite that limits the penetration depth of the acid, particularly at the low injection rates. This results in face dissolution problems and negligible increment in the conductivity of the formation (Fredd and Fogler 1998a). High concentration of HCl is associated with acid/oil sludge issues (Coulter and Jennings 1999). In addition, HCl has corrosion issues at high temperature conditions (Harris 1961) that require expensive corrosion inhibitors.

The above-mentioned drawbacks of HCl necessitate the discovery of alternative stimulation fluids that have low corrosion profiles and slow reaction rates with calcite. Organic acids address the rapid reaction rate and corrosion issues of HCl, especially in the high temperature applications (Buijse et al. 2004). A slow reacting fluid promotes deeper penetration of the solution before it gets completely spent. But, the reaction products have solubility limitations (Chang et al. 2008). For instance, acetic and formic acid cannot be used beyond 13 and 9 wt% respectively, due to the potential calcium acetate and calcium formate precipitation in the formation. Retarded acid systems, such as oil-based-microemulsions, are other viable options that provide a physical barrier between the acid and the rock, thereby reducing the diffusion of the acid to the surface (Nasr-El-Din et al. 2001). Foamed acids involving co-injection of nitrogen gas and HCl, prevents the acid spending outside the main channel, thus helping in the extension of wormholes to greater depths (Bernadiner et al. 1992). However, both retarded and foamed acid systems have potential to induce asphaltene sludge from the crude oil. This issue becomes even more severe when ferric ions are present. Chelating agents are claimed to be an excellent alternative to HCl since they complex the metal ion and keep them in solution, thereby reducing the chances of unwanted precipitation. However, they have thermal stability (Sokhanvarian et al. 2016) and biodegradability limitations (Frenier et al. 2003) that need to be considered. Moreover, they are expensive chemicals.

Mixture of HCl and organic acids are other alternative stimulation fluids that are capable of promoting the growth of wormholes in the formation by reducing the reaction rate of HCl with the rock, as well as provide good corrosion properties. Many laboratory

studies and field applications have been carried out in literature. The current study deals with a novel organic acid blended with HCl that has rendered improved properties to HCl.

CHAPTER II

LITERATURE REVIEW

Many studies have been conducted in the past, whereby HCl has been blended with weak organic acids such as acetic and formic acid. Dill (1961) disclosed the uses of the HCl-acetic acid mixture in stimulating limestone to produce calcium acetate, $CaCl_2$, and CO_2 that acted as a buffering agent, and provided synergy to maintain unreacted acid for a longer period of time. As the concentration of acetic acid increased in the blend (keeping other things constant), the unreacted acid concentration also increased. A model study was conducted using 15 wt% HCl-10 wt% acetic acid mixture with carbonates (Chang et al. 2008). It was found that the release of Ca^{2+} ions, which was produced from the reaction of HCl with calcite, resulted in the formation of calcium monoacetate aiding in the dissociation of the acetic acid. A synergistic effect, due to the buffering action of acetic acid, was noted with the mixture of 5 wt% HCl-5 wt% acetic acid applied in a sandstone reservoir to stimulate water supply and injection wells in Saudi Arabia (Nasr-El-Din et al. 1997, Hashem et al. 1999).

HCl-formic acid system was studied with Bedford limestone for acid fracturing (Dill and Keeney 1978), whereby the retardation effect, due to the organic acid, changed the reaction kinetics from a mass-transfer-limited to a surface-reaction-limited regime. A mixture of 7.5 wt% HCl-10 wt% formic acid exhibited a penetration depth of 300 and 116 ft compared to 128 and 92 ft with 15 wt% HCl at 200 and 250°F, respectively. 15 wt% HCl-9 wt% formic acid blend was extensively applied in deep gas wells completed

with Super Cr-13 (Nasr-El-Din et al. 2003) and low carbon steel (Nasr-El-Din et al. 2002) in carbonate reservoirs. The acid fracture job with the blend rendered excellent corrosion inhibition and improved gas production. Corrosion of CRAs was minimized in the presence of acetic acid and formic acid blend (Van Domelen and Jennings 1995). The mixture also removed calcium carbonate scales from gas wells (da Motta et al. 1998).

In the present study, a novel and strong organic acid called methanesulfonic acid (MSA, CH_3SO_3H), with a pK_a value of -2, has been recommended to be blended with HCl. MSA has several advantages over HCl. Shank and McCartney (2013) mentioned that MSA has a much lower vapor pressure and almost half H^+ ions activity coefficient than HCl. This property of MSA renders it useful for high temperature applications due to reduced corrosion profile and lower reactivity. MSA is commonly used in electrochemical applications as an acid electrolyte due to the following reasons: 1) high solubility of the metal salt (no precipitation problems), 2) the effluent can be easily treated (no waste release in the environment), and 3) its eco-friendly behavior (Gernon et al. 1999). Since its acidity is comparatively higher than most of the organic acids currently used in oil industry, MSA can be utilized as a standalone stimulation fluid in oilfield applications. In addition, it addresses most of the issues of other organic acids in terms of generating soluble reaction products, comparatively lower corrosivity, and low toxicity.

Heidenfelder et al. (2009) stimulated carbonate reservoirs using several alkanesulfonic acids, specifically MSA, and observed a 20 times reduction in the

corrosion rate of steel compared to an equivalent concentration of HCl in the absence of any corrosion inhibitor. The corrosion behavior of 22Cr steel was also studied (Finšgar and Jackson 2015) using 20 wt% MSA, without any corrosion inhibitor, at various temperatures. At temperatures up to 150°C, the corrosion rate was found to be below the acceptable industrial limit of 0.03 lb/ft^2 per test period. MSA bearing microcapsules were used as an additive in carbonate stimulation (Bertkau and Steidl 2012) that provided retardation effect on the fissures and pore spaces. Shank and McCartney (2013) observed a 33% decrease in $CaCO_3$ scale dissolution at 60°C and 1M acid concentration when MSA was used instead of HCl. The retardation effect was enhanced in the presence of non-ionic surfactants. Dissolution kinetics of MSA with calcite was studied by Reyath et al. (2015) using a rotating disk apparatus. The reaction with calcite marble was diffusion limited at higher temperatures (150 and 250°F) for 5, 10, and 20 wt% MSA. Coreflood studies were conducted by Ortega et al. (2014) with 10 wt% MSA in limestone at 250°F. The optimum injection rate was found to be between 5–7.5 cm^3/min and the wormholing characteristics were described. Even though the MSA application was found to be successful in carbonate acidizing, there is more unexplored potential in it.

Due to MSA being an expensive acid, blending it with HCl will lower the overall cost. In addition, the corrosion inhibitor requirement will be reduced in the presence of MSA. It has seven orders of magnitude higher solubility in water than HCl (Clegg and Brimblecombe 1985) and a high rock-dissolving power. According to Le Chatelier principle, if the dynamic equilibrium of any reaction is perturbed in terms of pressure,

volume, temperature or concentration, the position of the equilibrium shifts to counteract the change. Thus, the presence of HCl should lower the ionization of organic acids in accordance with their ionization constants (Harp et al. 1968), which will lead to increase in the spending time of the acid mixture and lengthy extension of the reaction time. In the current study, MSA, being an organic acid, should prolong the blend spending time and extend the tip of the advancing wormhole to a greater depth. The objective of the current work is to optimize the concentration of individual acids in the blend to obtain the most effective wormhole in terms of least volume of acid required to reach breakthrough and relatively thinner and uniform wormholes with less tortuosity.

CHAPTER III

PROBLEM STATEMENT

In-depth laboratory and field studies have been reported in the literature in the area of acidizing. Historically, HCl is the most commonly used acid in the oil industry. Standard Oil patented the use of HCl for stimulation technique (Coulter and Jennings 1999). However, it has many drawbacks, such as rapid reaction rate with calcite, which results in early acid spending and a negligible increase in permeability, and severe corrosion at elevated temperatures. Various alternative stimulation fluids have been tried, each having their pros and cons. Organic acid, such as MSA, has been reported to be used as a standalone stimulation fluid in carbonate reservoir (Heidenfelder et al. 2009) that yields soluble products, lower corrosion, and exhibits higher acidity than other commonly known organic acids. Blending HCl with organic acids has also been suggested as a viable option to mitigate the drawbacks of HCl. Early studies on acid blends include HCl-acetic acid and HCl-formic acid mixtures (Dill 1961, Dill and Keeney 1978).

However, there is a gap in the literature. Blending HCl with MSA did not receive any attention and requires a systematic approach to be evaluated in the carbonate stimulation. A novel acid blend comprising of HCl and MSA is recommended as an alternative to HCl that will retard it and promote the advancement of the wormhole. This study deals with optimizing the ratio of the individual acids in order to achieve the best

performance of the blend in terms of least volume of acid requirement and single dominant wormhole with least tortuosity.

CHAPTER IV

RESEARCH OBJECTIVE[1]

Three blends, each having different ratios of the individual acids, were used to conduct the coreflood tests with Indiana limestone cores. The objective of the present work was to optimize the concentration of individual acids in the blend using coreflood study at 250°F to: 1) obtain the most effective and dominant wormhole in terms of least volume of acid required to reach breakthrough, and 2) obtain relatively thinner wormholes with less tortuosity. The blend performances were compared to the equivalent concentration of individual acids at the determined optimum injection rate. The degree of retardation imparted by MSA to the blend was determined by diffusion coefficient calculations from rotating disk reactor experiments.

[1] Part of this chapter is reprinted with permission from: "Matrix Acidizing of Carbonate Rocks Using New Mixtures of HCl/Methanesulfonic Acid" by Sneha Kankaria, Hisham A. Nasr-El-Din, and Shawn Rimassa, 2017. SPE Proceedings, Copyright [2017] by Society of Petroleum Engineers.

CHAPTER V

MATERIALS[2]

V.1 Fluids

ACS grade hydrochloric acid was purchased from Macron Fine chemicals. MSA and corrosion inhibitor were supplied by a local chemical company. The corrosion inhibitor was a blend of potassium iodide that acts as an intensifier, and environmentally improved propargyl alcohol-based derivative. The strength of HCl and MSA was determined by manual titration with a freshly prepared 1.0M sodium hydroxide solution. The concentrations of HCl and MSA were 36.45±0.15 wt% and 73±0.25wt%, respectively. Acid solutions were prepared by dilution with de-ionized water (resistivity 18.2 MΩ at 77°F). 2 vol% corrosion inhibitor was added to avoid any corrosion of the equipment. The density and viscosity of each of the acid blend were measured as a function of temperature using Anton Paar DMA 4100 density meter and a Ubbelohde capillary viscometer (0 and 0C type), respectively. The density and viscosity results for each blend are tabulated below in **Table 1**.

---

[2] Part of this chapter is reprinted with permission from: "Matrix Acidizing of Carbonate Rocks Using New Mixtures of HCl/Methanesulfonic Acid" by Sneha Kankaria, Hisham A. Nasr-El-Din, and Shawn Rimassa, 2017. SPE Proceedings, Copyright [2017] by Society of Petroleum Engineers.

Acid Blend	Temperature (°C)	Density (g/cm^3)	Viscosity (cP)
2.5:7.5 wt% HCl:MSA	20	1.03	1.19
	40	1.02	0.84
	60	1.01	0.57
	80	0.99	0.43
5:5 wt% HCl:MSA	20	1.00	1.15
	40	0.99	0.81
	60	0.98	0.51
	80	0.975	0.39
7.5:2.5 wt% HCl:MSA	20	1.05	1.24
	40	1.04	0.89
	60	1.03	0.60
	80	1.02	0.46

Table 1 - Density and viscosity of acid blends as a function of temperature

V.2 Rock Properties

A total of 18 cylindrical cores were drilled from a homogeneous outcrop Indiana Limestone block for coreflood studies. The dimension of each core was 1.5 in. diameter and 6 in. length. Cores were drilled in one direction in order to maintain permeability anisotropy. The mineralogy of the Indiana limestone cores was characterized by x-ray diffraction (XRD and x-ray fluorescence (XRF). Limestone is essentially 99 wt% calcite. **Table 2** shows the mineralogy of the limestone rocks.

Mineral	Concentration (wt%)
Calcite, $CaCO_3$	99.06
Silica, SiO_2	0.94

Table 2 - Mineralogy of Indiana limestone

For RDA studies, calcite marble disks were drilled and cut from the marble block. The dimensions of the disks were 1.5 in. diameter and 0.65 in. thickness. The porosity of the marble disks was almost 0 vol%. Its mineralogy was determined using XRF, which is tabulated below (**Table 3**):

Mineral	Concentration (wt%)
Calcite, $CaCO_3$	97.6
Silica, SiO_2	0.41
Magnesium oxide, MgO	1.40
Alumina, Al_2O_3	0.35
Potassium oxide, K_2O	0.17
Ferric oxide, Fe_2O_3	0.07

Table 3 - Mineralogy of calcite marble disks

CHAPTER VI

COREFLOOD STUDIES[3]

Three blends, each having different ratios of the individual acids, were used to conduct the coreflood tests with Indiana limestone cores. Four different injection rates were used for each blend to find the optimum injection rate. Then, the control study was conducted with the individual acid solution having concentration equivalent to that of the blend at the optimum injection rate. The temperature for all the tests was 250°F. Therefore, a total of 18 coreflood tests were conducted. Some of them were repeated to check the reproducibility of the data. The three blends and the corresponding controls that were used are:

- 2.5:7.5 wt% HCl:MSA, 6 wt% HCl, 15 wt% MSA
- 5:5 wt% HCl:MSA, 7.2 wt% HCl, 17.7 wt% MSA
- 7.5:2.5 wt% HCl:MSA, 8.8 wt% HCl, 21.31 wt% MSA

The performance of the blends was compared with their corresponding controls as well as with each other in terms of (1) minimum volume of acid required to breakthrough, (2) dominant and least tortuous wormholes, and (3) maximum acid concentration left to further propagate the wormhole for deeper penetration. Combining all the parameters, the optimum blend was chosen.

---

[3] *Part of this chapter is reprinted with permission from: "Matrix Acidizing of Carbonate Rocks Using New Mixtures of HCl/Methanesulfonic Acid" by Sneha Kankaria, Hisham A. Nasr-El-Din, and Shawn Rimassa, 2017. SPE Proceedings, Copyright [2017] by Society of Petroleum Engineers.

VI.1 Experimental Procedure

VI.1.1 Components of coreflood

A schematic diagram of the coreflood apparatus is shown in **Fig. 1**. It consisted of the following components:

1. An ISCO syringe pump to inject the fluids into the core at constant flow rate or constant pressure mode as per needed.
2. Two accumulators for acid and de-ionized water.
3. A 6 in. stainless steel core holder with a rubber sleeve.
4. An electric oven containing the core holder to maintain the desired temperature.
5. A hydraulic pump to apply overburden/confining pressure on the core. It was used to inject hydraulic oil into the annular space between the internal surface of the core holder and the rubber sleeve. The confining pressure simulated the pressure applied by the overburden layers of the rocks in a typical formation.
6. Gauges and regulators to monitor and control the pressure drop across the core over time.
7. A nitrogen cylinder to apply back pressure and confining pressure.
8. A pressure transducer to measure the pressure drop across the core. The pressure transducer was connected to the data acquisition system (LABVIEW) to record the pressure drop across the core against time.

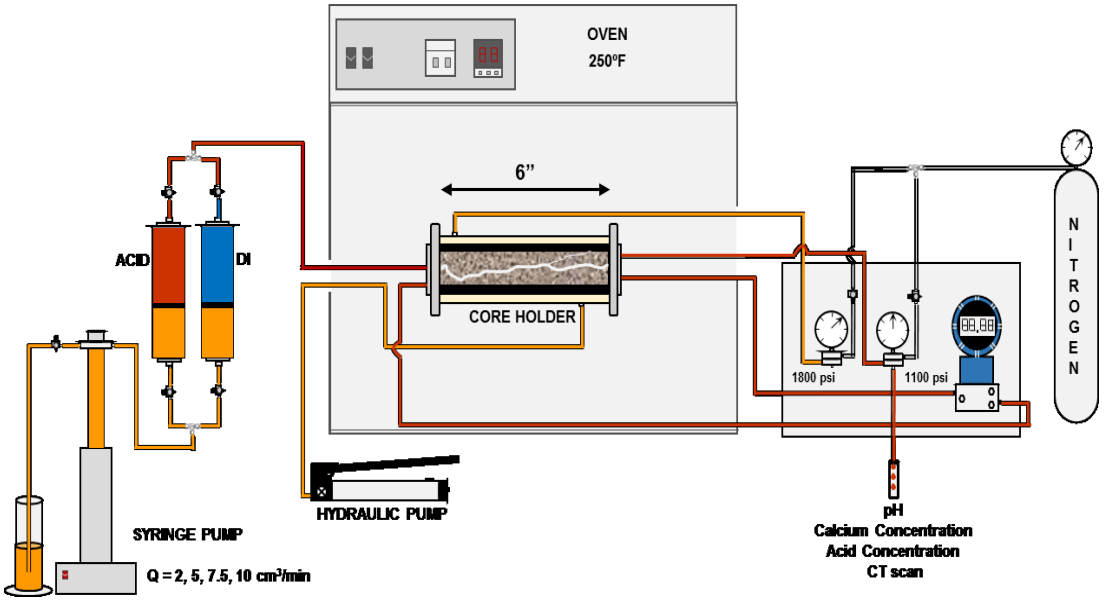

Figure 1 – A schematic of coreflood set-up.

VI.1.2 Core preparation

Core samples with diameter 1.5 in. and length 6 in. were drilled from Indiana limestone block. The cores were dried in an oven at 250ºF for 2 hours followed by complete saturation with de-ionized water under vacuum for 4 hours. The pore volume and porosity were calculated by the weight difference method (**eq. 1 and 2**).

$$PV = \frac{W_{sat} - W_{dry}}{\rho} \quad . \quad \ldots\ldots\ldots\ldots\ldots\ldots\ldots\ldots\ldots\ldots\ldots\ldots\ldots\ldots\ldots\ldots \quad (1)$$

$$\phi = \frac{PV}{V_{bulk}} \times 100 \quad . \quad \ldots\ldots\ldots\ldots\ldots\ldots\ldots\ldots\ldots\ldots\ldots\ldots\ldots\ldots\ldots\ldots \quad (2)$$

where PV is pore volume in cm^3, W_{sat} and W_{dry} is the saturated and dry weight of the core in g, ρ is the density of de-ionized water in g/cm^3, ϕ is porosity in vol%, V_{bulk} is the volume of the core in cm^3.

VI.1.3 Coreflood experiments

The saturated core was loaded into a core holder, and a back pressure of 1,100 psi was applied to ensure that most of CO_2, produced during reaction with acid, is kept in solution. An overburden pressure of 1,800 psi was applied on the core to ensure that flow of different fluids did not bypass the core. Acid injection rates of 2, 5, 7.5, and 10 cm^3/min were used for all the acid blends. Control experiments with an equivalent concentration of only HCl and MSA were also performed to evaluate and compare the efficiency of acid mixture. It is worthwhile to emphasize that the control experiments were conducted only at the corresponding optimum injection rate for each blend.

Firstly, the permeabilities of the cores were determined by injecting de-ionized water at injection rates of 2, 5, and 10 cm^3/min at room temperature, using Darcy's equation (**eq. 3**).

$$k = \frac{Q \times \mu \times L_0}{A \times \Delta P} \quad \ldots\ldots \quad (3)$$

where k is absolute permeability in Darcy, Q is the flow rate in cm^3/min, μ is the fluid viscosity in cP, $L_0$is the length of the core in cm, A is cross-section of the core in cm^2, and ΔP is pressure drop across the core in atm.

The porosities and permeabilities of all the cores used are given in **Table 4**. Then, the cores were heated to 250ºF with continuous injection of de-ionized water (DI Water) until the pressure drop stabilized. This was followed by injection of acid solutions until breakthrough was achieved marked by a negligible pressure drop. Corrections for the dead pore volume to account for the distance between injection valve

and the inlet of the core was applied. Some of the experiments were repeated, and the experimental error was ±6% under the given conditions of temperature, pressure, and flow rates using the same coreflood set-up.

Experiment set	Core ID	Acid injection rates used, cm^3/min	PV, cm^3	Porosity, vol%	Absolute permeability (k), md
2.5:7.5 wt% HCl:MSA	16	5	26.9	15.5	17.4
	20	7.5	25.6	14.7	20.6
	24	10	24.4	14.0	17.9
	25	2	24.2	13.9	19.3
	26 (HCl control)	7.5	24.0	13.8	17.0
	27 (MSA control)	7.5	23.5	13.5	18.6
5:5 wt% HCl:MSA	4	5	25.8	14.8	48.0
	5	7.5	27.4	15.8	31.0
	6	10	28.8	16.6	63.5
	7	2	23.8	13.7	36.5
	8 (HCl control)	7.5	27.3	15.7	44.2
	9 (MSA control)	7.5	23.7	13.6	54.5
7.5:2.5 wt% HCl:MSA	12	5	24.1	13.9	41.7
	15	7.5	23.4	13.5	34.5
	13	10	22.8	13.1	22.7
	17	2	24.3	14.0	18.7
	18 (HCl control)	5	26.0	15.0	24.1
	19 (MSA control)	5	25.3	14.5	24.5

Table 4 - Porosities and permeabilities of cores used in coreflood experiments (Reprinted with permission from Kankaria et al., 2017).

Core effluent samples were collected every 0.1 PV and their pH was measured using Oakton pH meter. They were further diluted to be analyzed for calcium ion concentration by Inductively Coupled Plasma-Optical Emission Spectroscopy (ICP-OES) analysis by Perkin Elmer using Optima 7000 DV ICP-OES system and WinLab 32^{TM} software. The acid concentrations in the core effluent samples were measured by titration with 0.1M NaOH solutions in a Metrohm 907 Titrando autotitrator and were reported in terms of equivalent HCl. The cores were scanned by X-ray computed tomography (CT), and the images for wormhole structures were generated using Osirix software and analyzed using ImageJ software.

VI.2 Theory of Wormhole Formation

Wormholes are highly conductive channels formed when reactive stimulation fluids, like acids, flow in porous media causing dissolution of dissolvable minerals present in the rock. These channels carry acid into the formation during stimulation and provide low resistance path for the oil to flow after the stimulation is over. When the acid enters the core, some of the acid advances ahead of the initial reaction front and dissolves the mineral (Hoefner and Fogler 1988). This results in reduced resistance for the acid to flow in the initial front region, causing more dissolution behind the front, compared to the advancing tip of the wormhole. Flow from other regions is diverted into this channel because the resistance to flow is negligible in a wormhole compared to the remaining areas. Essentially, the wormhole carries all the injected fluid.

Bazin (2001) recognized two resistances that determine the structure of the wormhole: mass-transfer and surface-reaction-limited kinetics (**Fig. 2**). The efficiency of wormhole formation is well explained by a dimensionless parameter, Damköhler number, which is the ratio of the rate of dissolution of acid to the rate of convective transport of acid (Fredd and Fogler 1999; Huang et al. 2000). If the reaction between the acid and rock is faster than the flow/diffusion of acid, the reaction is mass-transfer limited (Hoefner and Fogler 1988; Daccord et al. 1993). The limestone dissolution by HCl is greatly affected by flow rate. At very low injection rates/acid flux or high Damköhler number, the acid is consumed at the inlet face of the core resulting in inefficient stimulation treatment (**Fig. 3**). Compact dissolution patterns are formed indicating convection-limited regime. On the contrary, at very high flow rates (lower Damköhler number) of acid, the dissolution occurs over a large surface area, creating branched wormholes. Ramified wormhole structures and uniform dissolution occurs at such high rates, indicating the surface-reaction-limited regime, thereby reducing the efficiency of stimulation. At intermediate injection rates, narrower wormholes are formed, that can penetrate deeper for the least volume of acid, enhance permeability, and extend the channels deep into the formation to create low resistance paths for oil/gas to flow towards the wellbore. This is the mass transfer-limited regime.

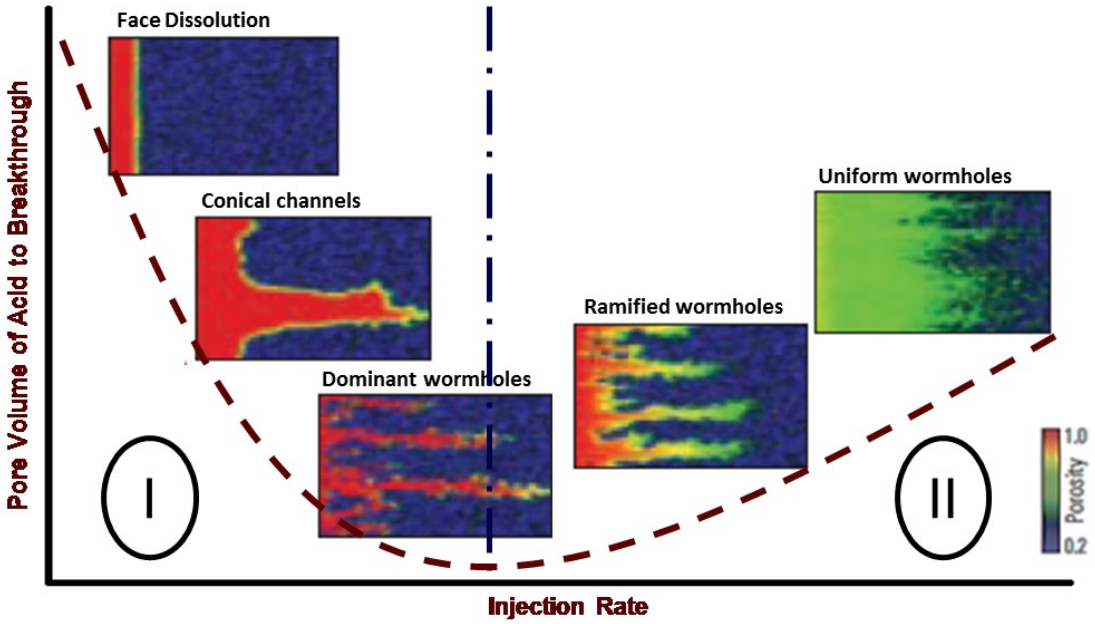

Figure 2 – A typical acid efficiency curve showing the effect of flow rate on acid pore volume required to breakthrough.

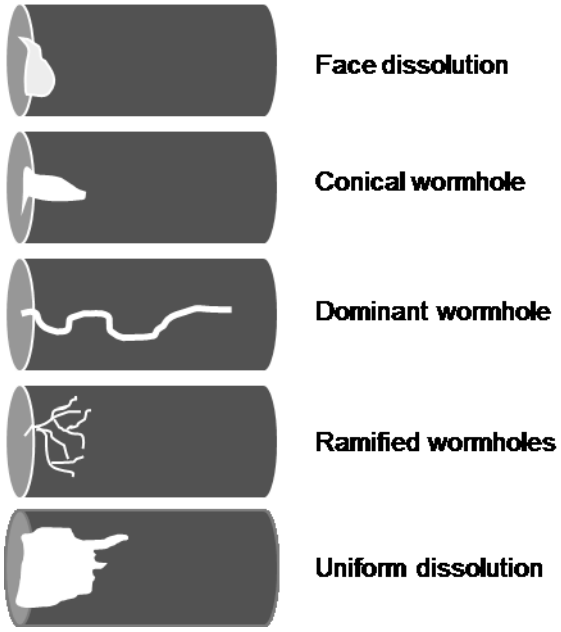

Figure 3 – Effect of Damköhler number on wormhole structures.

An efficient acid system will have (a) least fluid loss through the walls of the wormhole, and (b) least consumption of the acid at the walls of wormholes so that higher acid concentration is maintained at the advancing tip of the wormhole (Bazin 2001). Such an optimum rate would correspond to least volume of acid to enlarge the larger natural pores to propagate the wormholes (Huang et al. 2000), and represents the transition between mass-transfer and surface-reaction-limited regimes (Wang et al. 1993). Thus, the goal of this study is to optimize the two resistances for each composition of the blend by tuning the injection rates so that single dominant wormholes are obtained, since minimum volume of acid is required to achieve wormhole breakthrough. The results will be compared with that of individual acids (controls) having concentration equivalent to the blends.

VI.3 Results and Discussions

VI.3.1 Acid blend 2.5:7.5 wt% HCl:MSA

Six coreflood experiments were performed, including two control studies with an equivalent concentration of only HCl and only MSA. The coreflood experiments with 2.5:7.5 wt% HCl:MSA acid mixture were conducted at injection rates of 2, 5, 7.5 and 10 cm^3/min.

At injection rate 2 cm^3/min:

About 3.41 PV of acid was required to reach breakthrough. A CT scan image shows face dissolution with thick wormhole at the core inlet, which tapers close to the outlet (**Fig. 4**). An arrow in the figure indicates the acid flow direction. At 2 cm^3/min,

the acid blend had a long residence time in the core causing a large volume of acid consumption at the entrance of the core. The dissolution reaction is faster relative to the acid transport that causes a large amount of acid consumption on the wormhole walls close to the core inlet (Hoefner and Fogler 1988; Bazin 2001). Lower acid flux limits the unreacted acid concentration at the advancing channel tip.

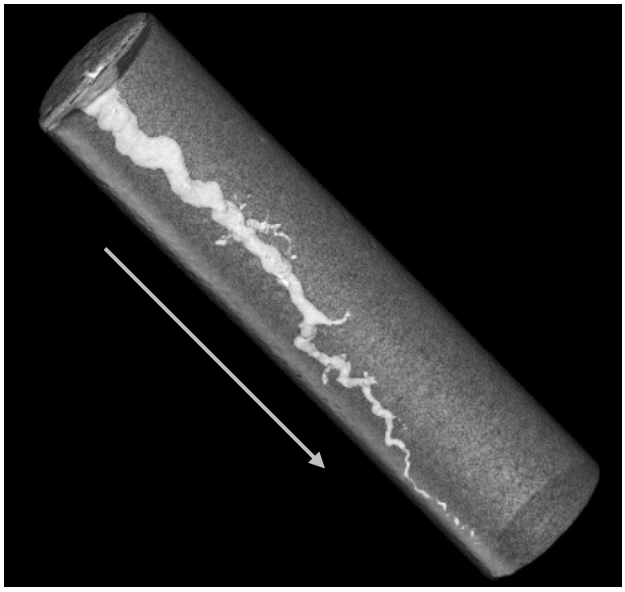

Figure 4 - CT scan image of Indiana limestone core after acidizing by 2.5:7.5 wt% HCl:MSA blend at 2 cm^3/min.

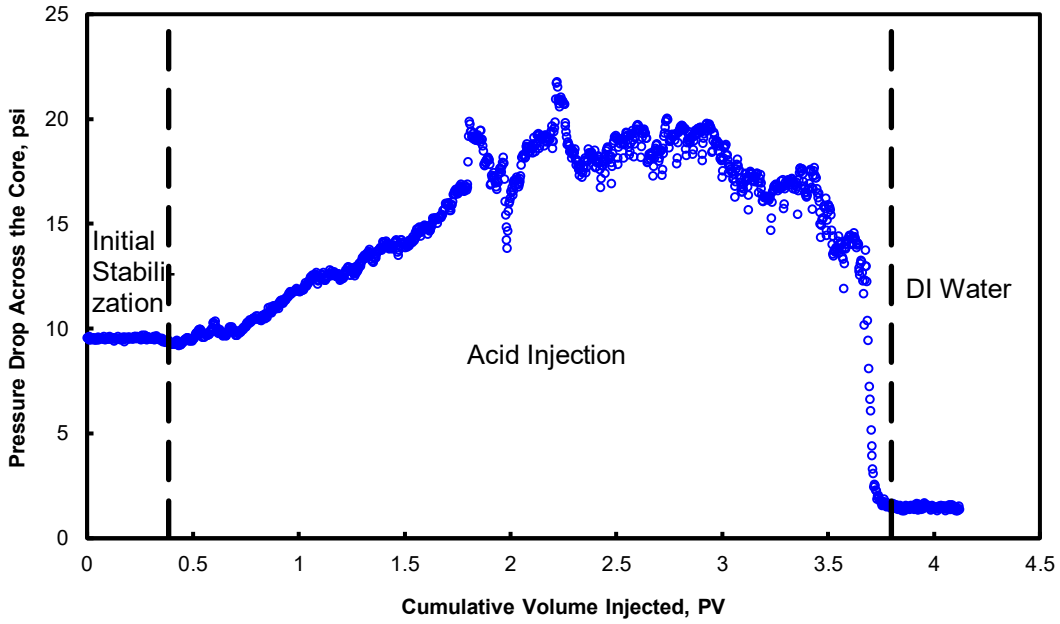

Figure 5 - Pressure drop across the core for 2.5:7.5 wt% HCl:MSA at 2 cm^3/min as a function of the cumulative volume injected at 250°F.

There was an increase in the pressure drop when the acid reached the core entrance (**Fig. 5**). This is because one of the reaction products, gaseous CO_2, is not completely dissolved in the fluid stream. From the pressure vs. temperature diagram (Cheng et al. 2017), at 250°F and 1,100 psi back pressure, CO_2 exists on the boundary of supercritical fluid and gaseous state. When the acid flux is low, gaseous CO_2 evolves and tends to accumulate at the wormhole tip. A local increase in gas phase saturation causes a reduction in the liquid relative permeability of the rock (Shukla et al. 2006, Bernadiner et al. 1992). Gaseous CO_2 increases transport of H^+ ions to the wormhole surface close to the core inlet (Qiu et al. 2014). This retards the wormhole propagation across the length of the core and eventually causes an increase in the diameter of the wormhole close to the core entrance.

Maximum calcium ions dissolved was about 30,000 mg/L (**Fig. 6**). The maximum unconsumed acid concentration at breakthrough, measured in the effluent samples, was less than 0.1 wt% equivalent HCl (**Fig. 7**). This indicates that almost the entire acid that was injected was consumed on the walls of the wormhole, and negligible acid was left for further penetration of the wormhole at the same PV of acid corresponding to breakthrough.

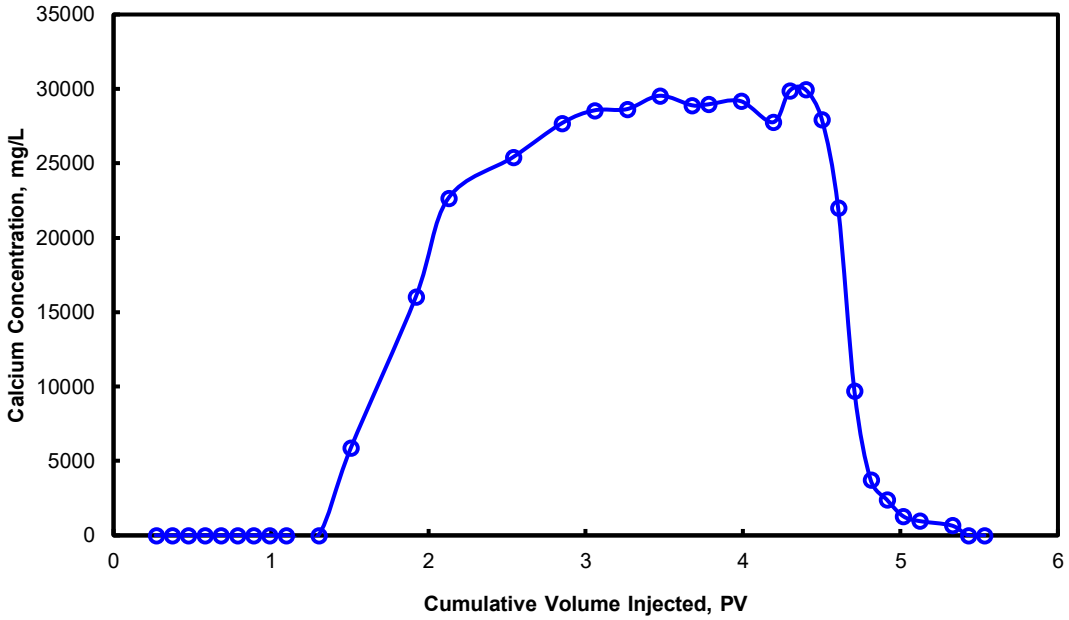

Figure 6 - Calcium ion concentration for 2.5:7.5 wt% HCl:MSA at 2 cm^3/min as a function of the cumulative volume injected at 250°F.

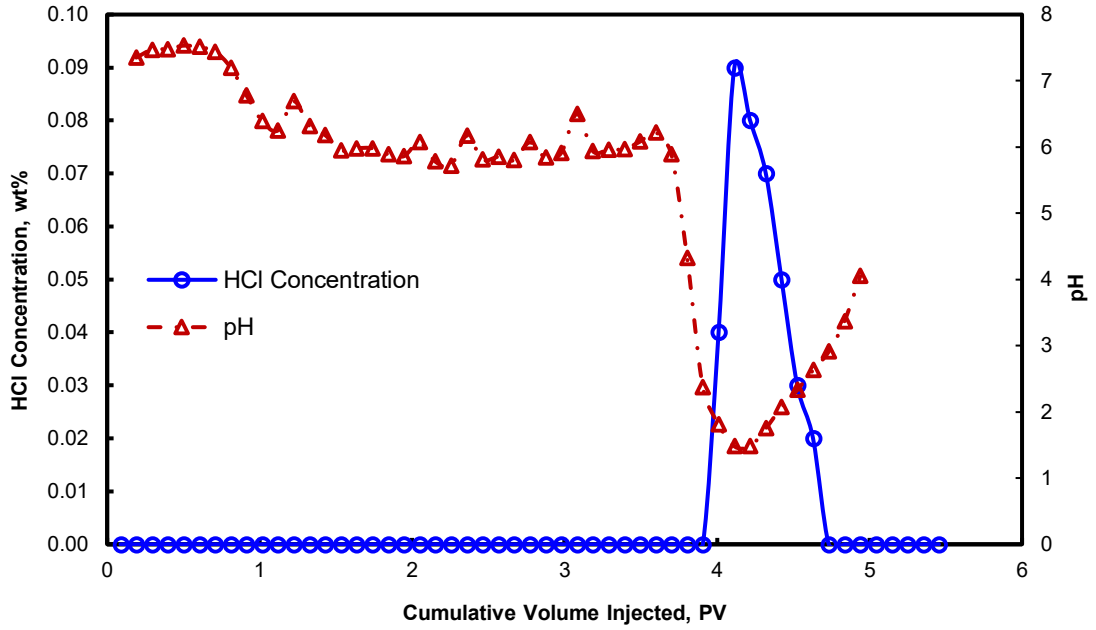

Figure 7 - Acid concentration in terms of equivalent HCl and pH of core effluent samples for 2.5:7.5 wt% HCl:MSA at 2 cm^3/min as a function of the cumulative volume injected at 250°F.

<u>At injection rate 5 cm^3/min:</u>

The blend required 1.59 PV of acid to reach breakthrough, which is comparatively lesser than that at 2 cm^3/min. There was no increase in the pressure drop when the acid reached the inlet of the core (**Fig. 8**). This indicates that the undissolved gaseous CO_2 generated from the acid reaction with calcite was left behind by the advancing tip of the wormhole when the residence time of the acid in the core reduced. Conical wormhole was observed at the inlet face.

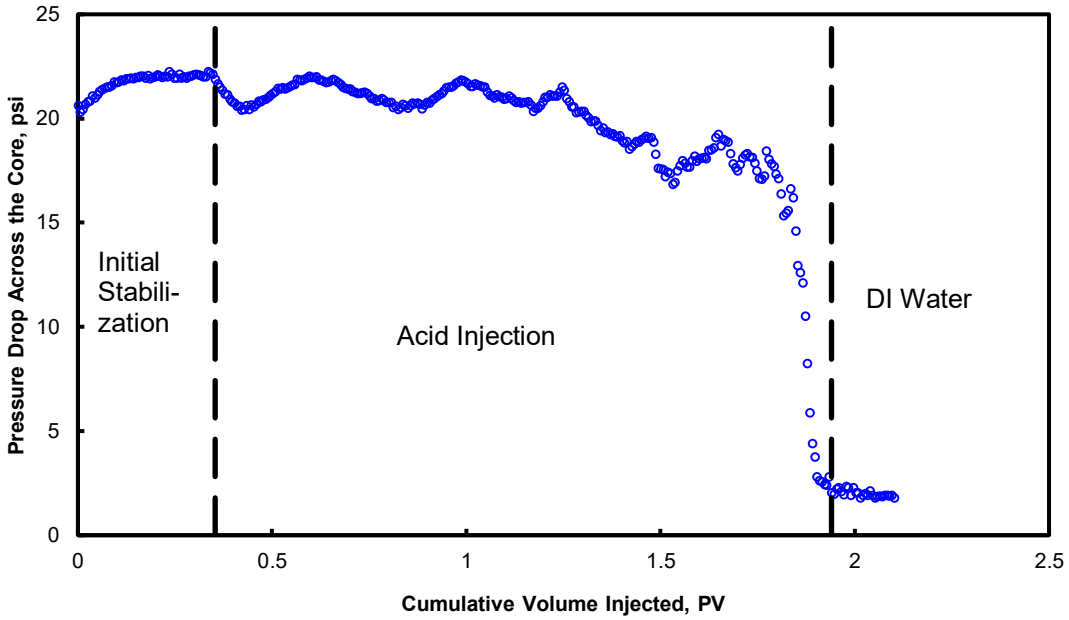

Figure 8 - Pressure drop across the core for 2.5:7.5 wt% HCl:MSA at 5 cm^3/min as a function of the cumulative volume injected at 250°F.

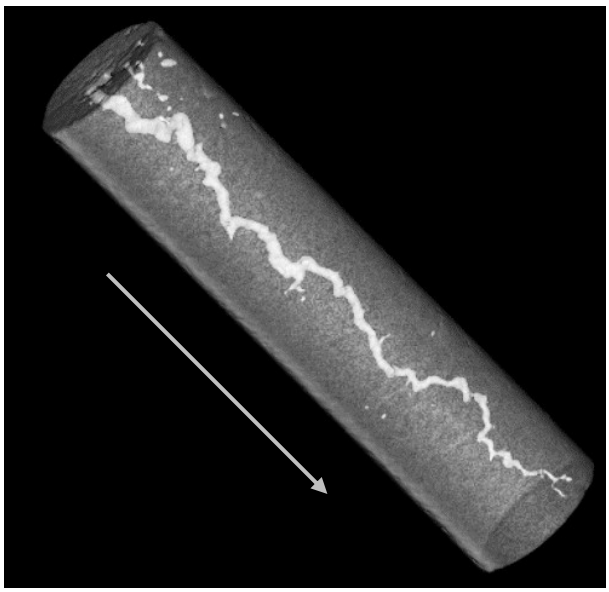

Figure 9 - CT scan image of Indiana limestone core after acidizing by 2.5:7.5 wt% HCl:MSA blend at 5 cm^3/min.

From CT scan result, there was a single wormhole generated, relatively smaller in diameter compared to that obtained at 2 cm^3/min (**Fig. 9**). The acid blend had a shorter residence time in the core at 5 cm^3/min, which resulted in propagation of the wormhole across the length of the core, instead of being consumed on the walls of the wormhole. Maximum calcium ions dissolved was close to 30,000 mg/L (**Fig. 10**). The unspent acid concentration at breakthrough was 0.55 wt% (**Fig. 11**), which was higher than that obtained at 2 cm^3/min. Thus, there was some live acid left to extend the wormhole deeper in formation corresponding to the PV of acid corresponding to breakthrough.

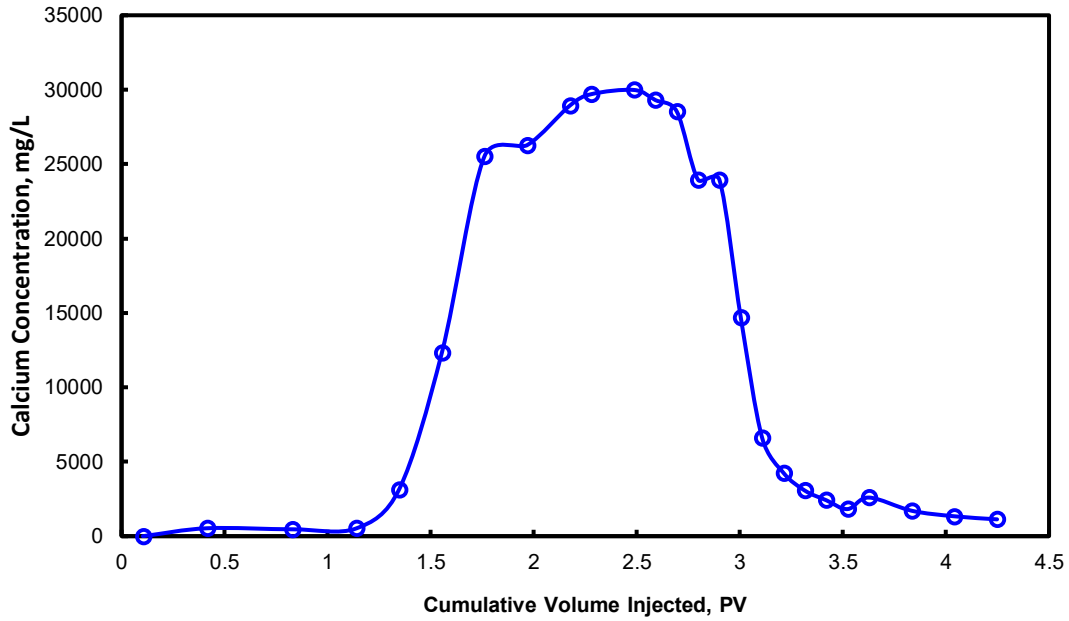

Figure 10 - Calcium ion concentration for 2.5:7.5 wt% HCl:MSA at 5 cm^3/min as a function of the cumulative volume injected at 250°F.

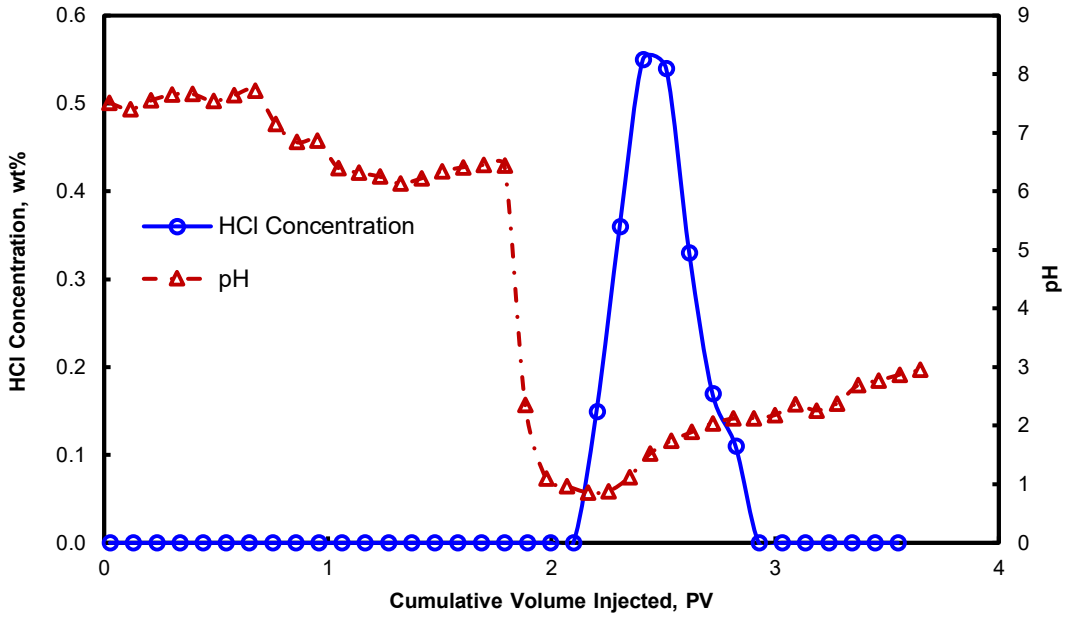

Figure 11 - Acid concentration in terms of equivalent HCl and pH of core effluent samples for 2.5:7.5 wt% HCl:MSA at 5 cm^3/min as a function of the cumulative volume injected at 250°F.

<u>At injection rate 7.5 cm^3/min:</u>

The PV required to reach breakthrough was 1.33, comparatively lower than that for the above-mentioned injection rates. The pressure drop profile showed a linear decline when the acid reached the inlet of the core (**Fig. 12**). The residence time was lower than the previous cases, so the reaction was not very vigorous, and the gaseous CO_2 produced during the reaction was trailing behind the propagating wormhole. The retardation effect of CO_2 on the wormhole advancement diminishes as the injection rate increases.

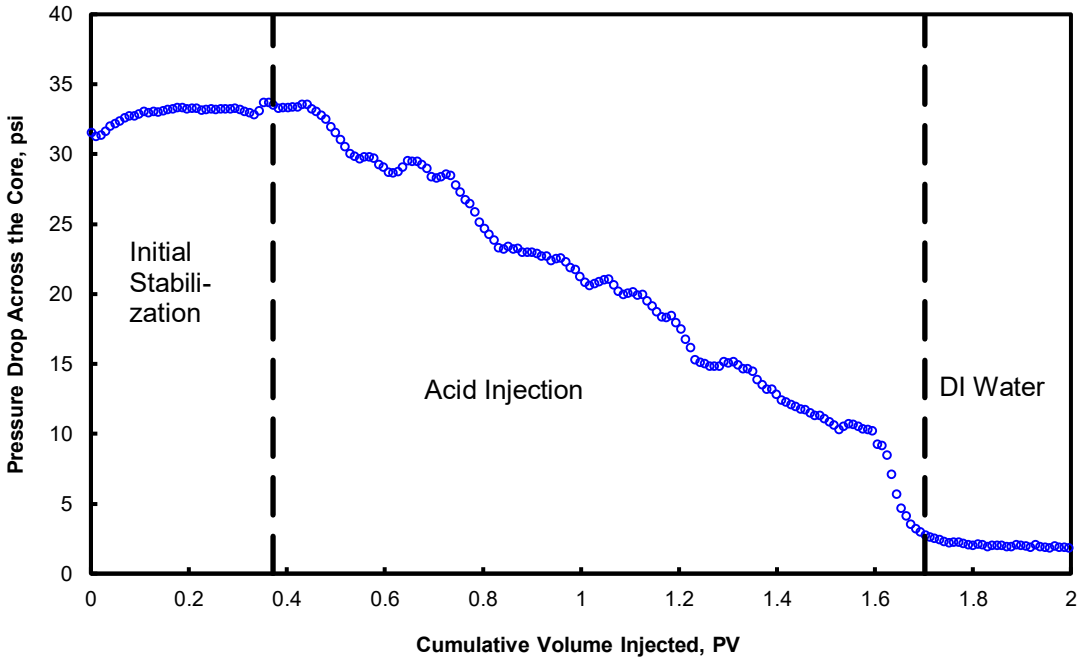

Figure 12 - Pressure drop across the core for 2.5:7.5 wt% HCl:MSA at 7.5 cm^3/min as a function of the cumulative volume injected at 250°F.

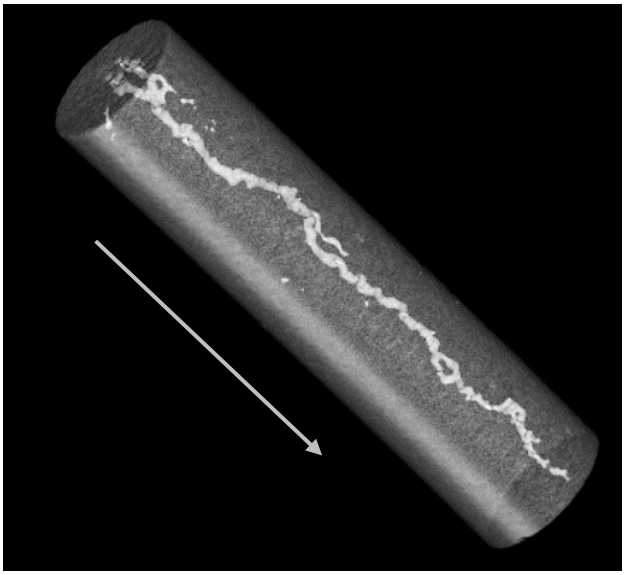

Figure 13 - CT scan image of Indiana limestone core after acidizing by 2.5:7.5 wt% HCl:MSA blend at 7.5 cm^3/min.

A significantly straight, least tortuous and dominant wormhole was observed from the CT scan image (**Fig. 13**). The wormhole was relatively thinner than that for 2 and 5 cm^3/min. This is desirable as such a wormhole will consume less volume of acid to breakthrough and ensure deeper penetration in the formation. In addition, the wormhole has an almost consistent diameter from the inlet to the outlet of the core. Maximum calcium ions dissolved was about 31,800 mg/L (**Fig. 14**). Maximum unconsumed acid concentration in the effluent samples at breakthrough was 0.85 wt% equivalent HCl (**Fig. 15**). This is again higher than the other two flow rates discussed earlier, thus displaying the deeper wormhole penetration ability of the blend at 7.5 cm^3/min.

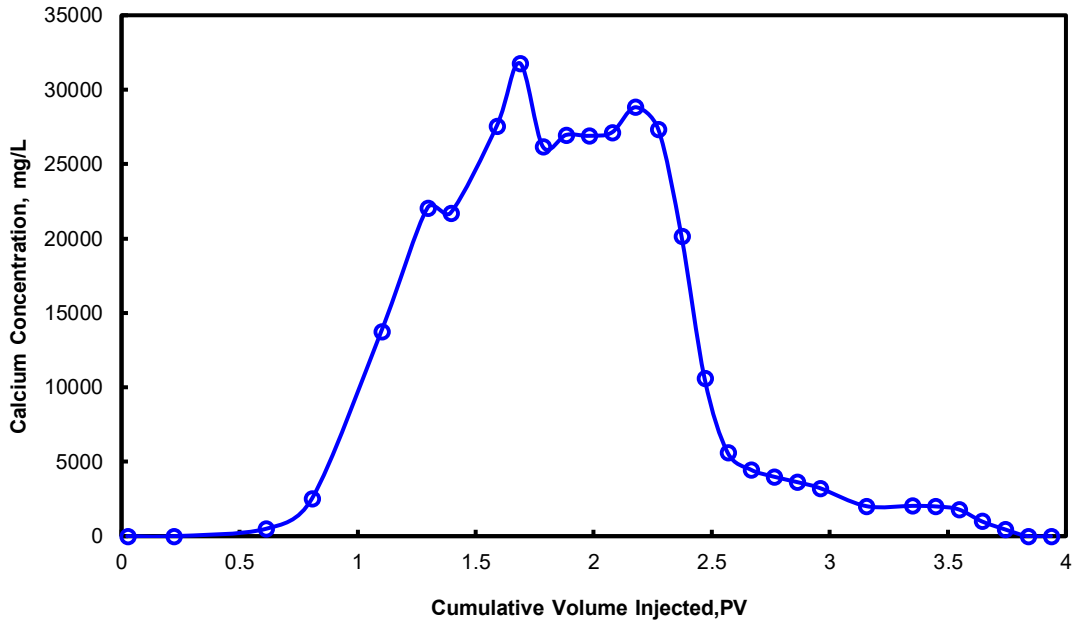

Figure 14 - Calcium ion concentration for 2.5:7.5 wt% HCl:MSA at 7.5 cm^3/min as a function of the cumulative volume injected at 250°F.

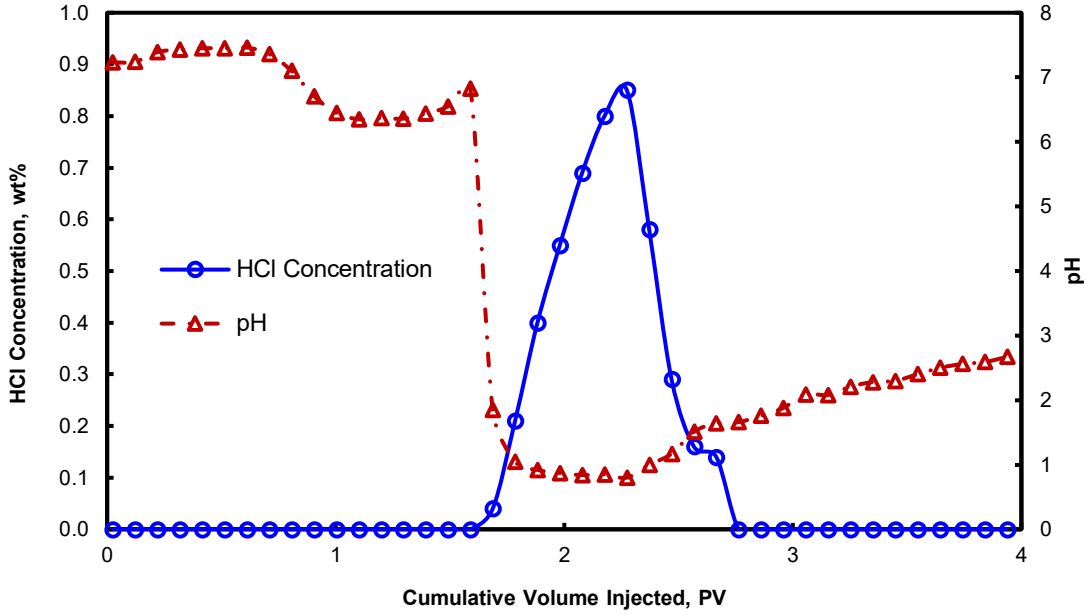

Figure 15 - Acid concentration in terms of equivalent HCl and pH of core effluent samples for 2.5:7.5 wt% HCl:MSA at 7.5 cm^3/min as a function of the cumulative volume injected at 250°F.

<u>At injection rate 10 cm^3/min:</u>

About 2.04 PV of the acid blend was required to breakthrough the core, which is higher than the volume of acid required at 7.5 cm^3/min; hence, the optimum injection rate, which requires the least PV of acid to breakthrough, is 7.5 cm^3/min. There was no increase in the pressure drop when acid reached the core inlet (**Fig. 16**). At high injection rate (10 cm^3/min), the transport of acid is faster than the surface reaction. The produced CO_2 in gas phase trails behind the advancing wormhole, thus its detrimental effect of increasing the pressure drop and face dissolution of the core are eliminated. The effect of back pressure is much more pronounced at low injection rates.

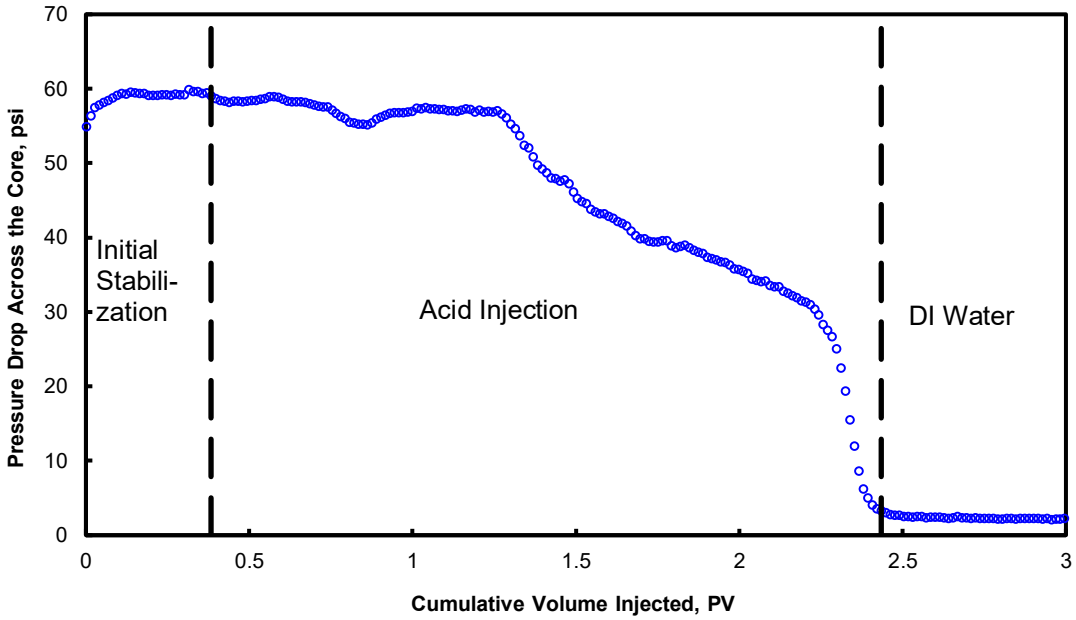

Figure 16 - Pressure drop across the core for 2.5:7.5 wt% HCl:MSA at 10 cm^3/min as a function of the cumulative volume injected at 250°F.

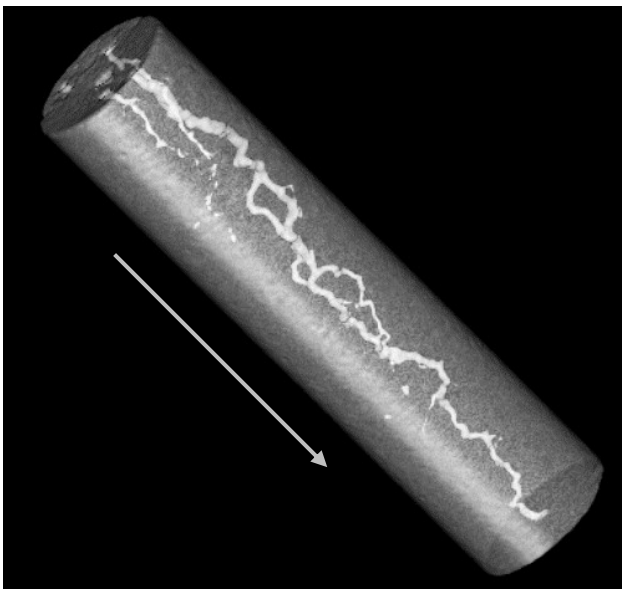

Figure 17 - CT scan image of Indiana limestone core after acidizing by 2.5:7.5 wt% HCl:MSA blend at 10 cm^3/min.

Intertwined branched wormhole is observed at 10 cm^3/min (**Fig. 17**), which results from the fluid leak-off through its walls and is expected when the calcite dissolution shifts towards the surface reaction limited regime. Branching slows down the wormhole propagation, causing a large volume of acid consumption. This further confirms that 7.5 cm^3/min is the optimum injection rate. Maximum calcium ion dissolved was 29,500 mg/L (**Fig. 18**). The dissolved calcium concentration is lower than that at 7.5 cm^3/min, which is due to the blend having a much shorter residence time at 10 cm^3/min. Maximum unspent acid concentration in terms of equivalent HCl in effluent sample reached 1.25 wt% (**Fig. 19**), higher than that corresponding to all the above-mentioned flow rates.

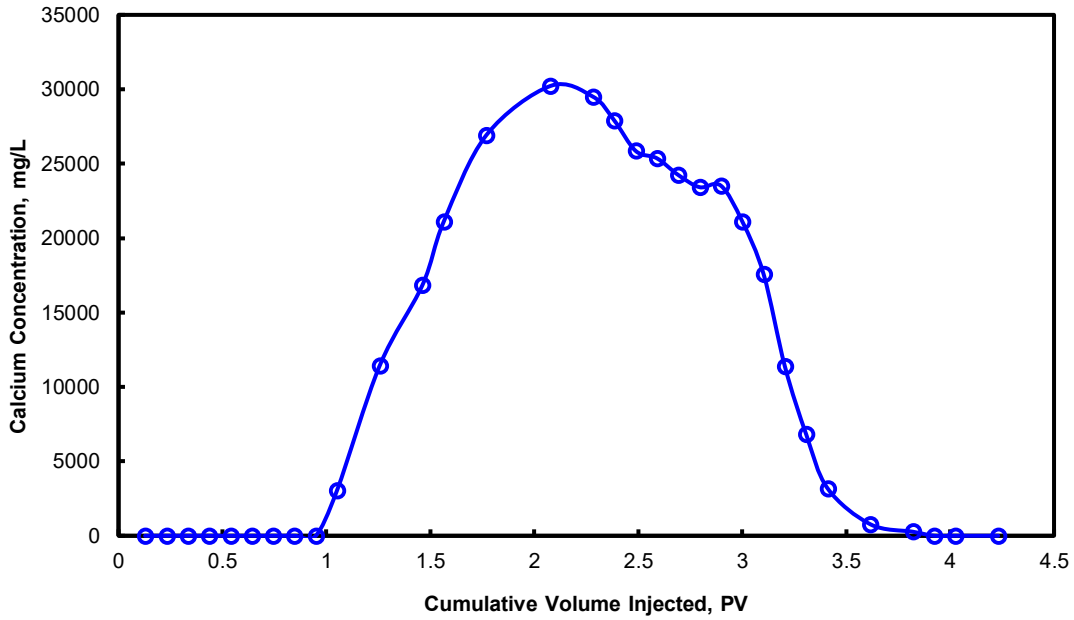

Figure 18 - Calcium ion concentration for 2.5:7.5 wt% HCl:MSA at 10 cm^3/min as a function of the cumulative volume injected at 250°F.

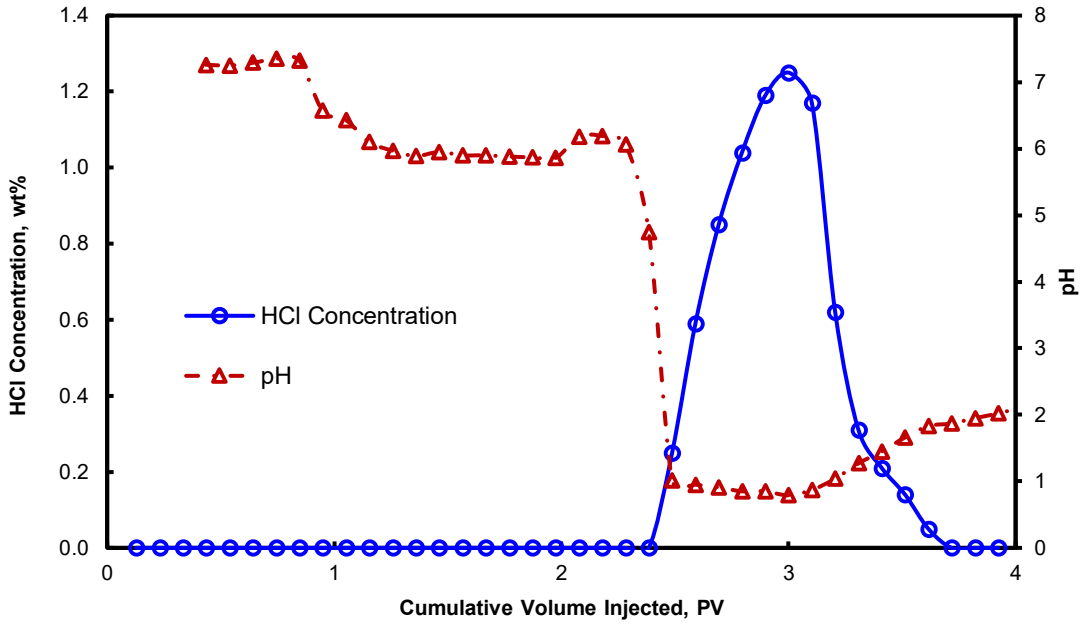

Figure 19 - Acid concentration in terms of equivalent HCl and pH of core effluent samples for 2.5:7.5 wt% HCl:MSA at 10 cm^3/min as a function of the cumulative volume injected at 250°F.

<u>At optimum injection rate 7.5 cm^3/min:</u>

The optimum flow rate at which the lowest PV (1.33 PV) of the acid blend was needed to reach breakthrough was obtained at 7.5 cm^3/min. It marked the transition of mass-transport and surface-reaction limited regime. Control experiments comprising of an equivalent concentration of only HCl (6 wt%) and MSA (15 wt%) were carried out at 7.5 cm^3/min to compare the efficiencies of acid blends and controls. **Fig. 20** shows the acid efficiency curve for the blend. The volume of acid required to reach breakthrough for the equivalent 6 wt% HCl control experiment was 2.08 PV, and that for the 15 wt% MSA control was 1.62 PV. Pressure drop profiles for the acid blend and controls declined with acid injection (**Fig. 21**). This indicates that the reaction with the rock was not very vigorous at 7.5 cm^3/min to increase the pressure drop, and the small amount of

gaseous CO_2 produced during the reaction was left behind the advancing wormhole by the optimum injection rate of the acid solutions.

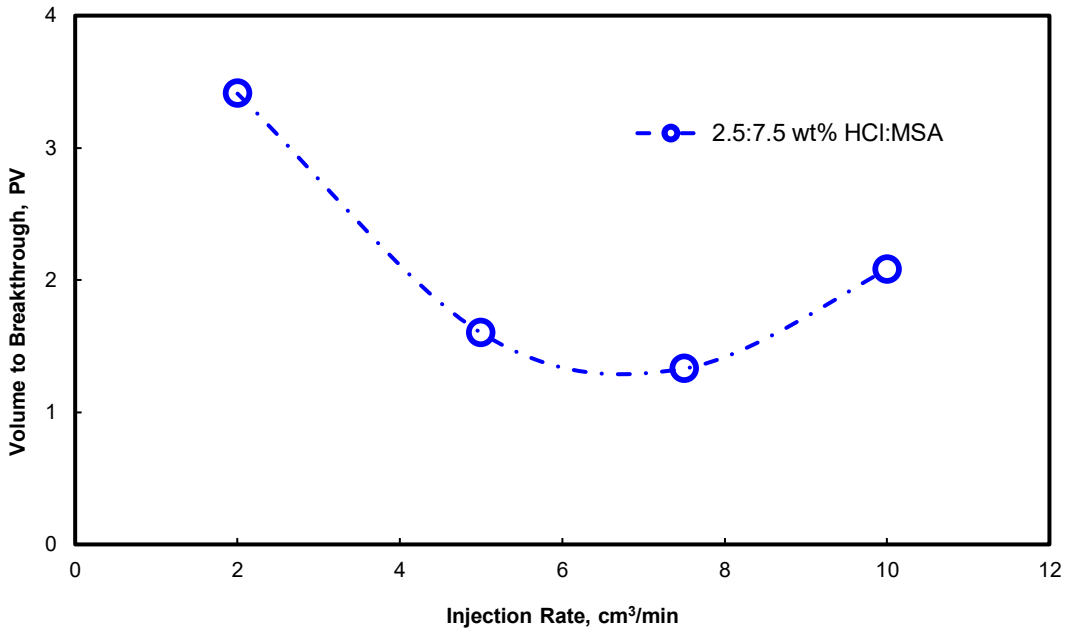

Figure 20 - Acid efficiency curve for 2.5:7.5 wt% HCl:MSA at 250°F (Reprinted with permission from Kankaria et al., 2017).

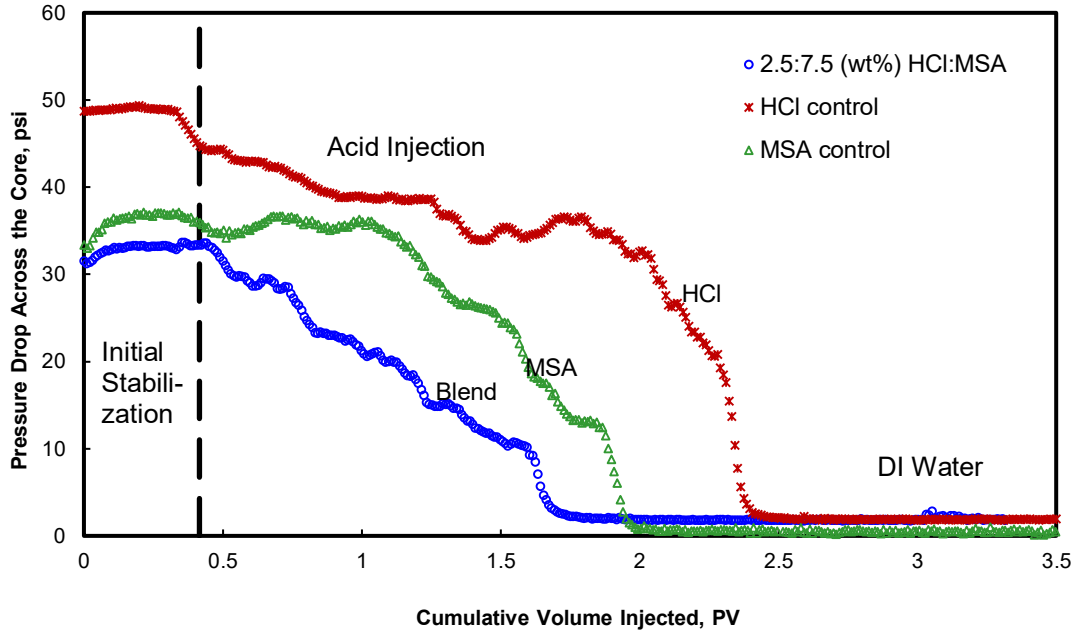

Figure 21 - Pressure drop across the core for 2.5:7.5 wt% HCl:MSA and its respective HCl and MSA controls at 7.5 cm^3/min as a function of the cumulative volume injected at 250°F (Reprinted with permission from Kankaria et al., 2017).

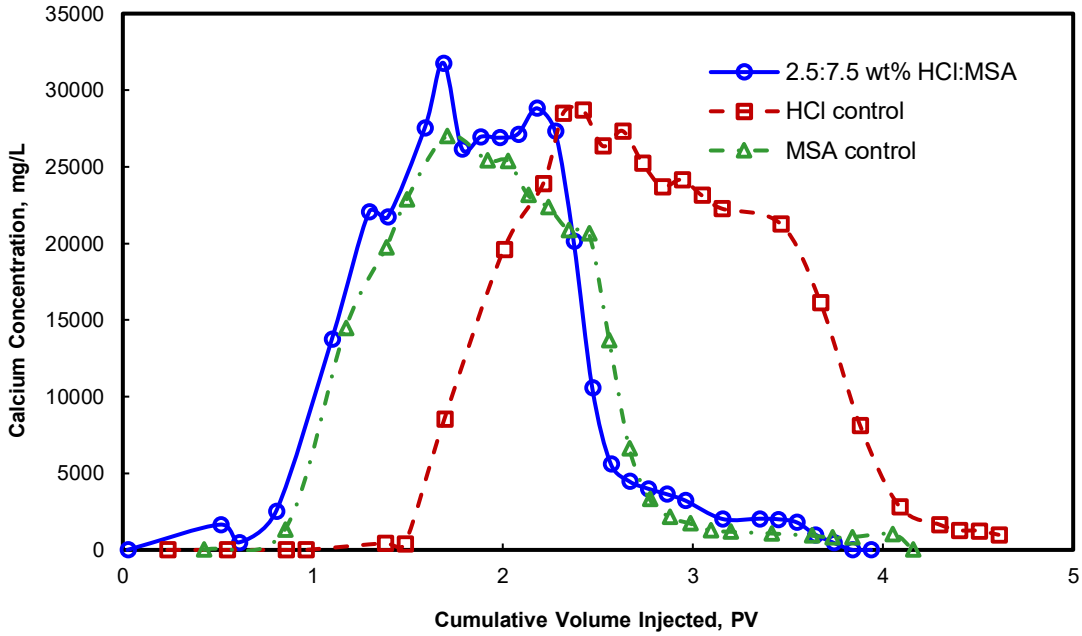

Figure 22 - Calcium ion concentration for 2.5:7.5 wt% HCl:MSA and its respective HCl and MSA controls at 7.5 cm^3/min as a function of the cumulative volume injected at 250°F (Reprinted with permission from Kankaria et al., 2017).

pH of the collected samples was measured, and a sharp drop from 4.5 to 0 was observed at breakthrough. Calcium ion concentration in the core effluent samples was measured and plotted as a function of the cumulative volume injected (**Fig. 22**). The area under the generated curve was calculated by applying the trapezoidal rule of integration using MATLAB, and the total amount of calcium ions dissolved by the acid blend (1.04 g) at the injection rate of 7.5 cm^3/min was found to be less than that of HCl control (1.29 g). **Fig. 23** shows the plot of acid concentration in core effluent samples in terms of equivalent HCl concentration as a function of the cumulative volume injected, and almost the same concentration (0.8-0.95 wt%) of acid remains for the acid blend and controls. Thus, almost negligible acid was left for further penetration in all the cases.

Fig. 24 shows the conductive channels formed for the experiment set of 2.5:7.5 wt% HCl:MSA along with its equivalent controls. CT scan images revealed a single, straight and dominant wormhole for the acid blend, comparatively thinner and uniform in diameter, than the HCl control. This is a clear indication of higher acid consumption on the walls of the wormhole than in propagation of the channel for the HCl control.

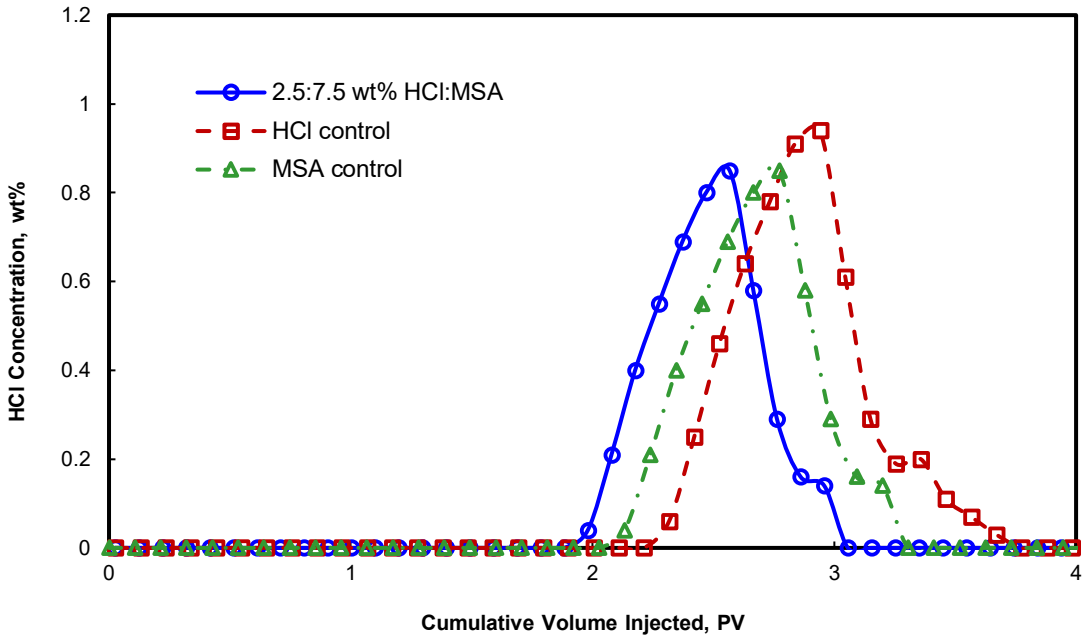

Figure 23 - Acid concentration in terms of equivalent HCl concentration for 2.5:7.5 wt% HCl:MSA and its respective HCl and MSA controls at 7.5 cm^3/min as a function of the cumulative volume injected at 250°F (Reprinted with permission from Kankaria et al., 2017).

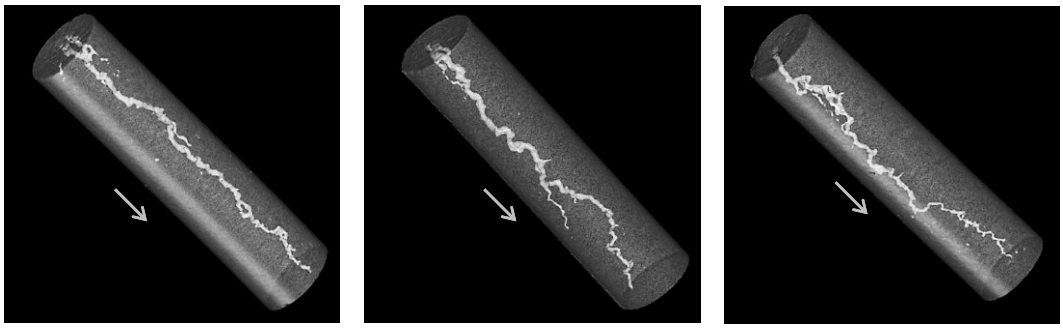

2.5:7.5 wt% HCl:MSA	6 wt% HCl control	15 wt% MSA control

Figure 24 - CT scan images of Indiana limestone cores after acidizing by 2.5:7.5 wt% HCl:MSA, 6 wt% HCl control, and 15 wt% MSA control equivalent at 7.5 cm^3/min (Reprinted with permission from Kankaria et al., 2017).

VI.3.2 Acid blend 5:5 wt% HCl:MSA

The overall acid strength of 5:5 wt% HCl:MSA is higher than the 2.5:7.5 wt% HCl:MSA blend. Four coreflood experiments were carried out with 5:5 wt% HCl:MSA mixture at 2, 5, 7.5 and 10 cm^3/min, along with the two control studies using only HCl (7.2 wt%) and MSA (17.7 wt%).

At injection rate 2 cm^3/min:

Coreflood experiment with 5:5 wt% HCl:MSA was carried out with the lowest flow rate (2 cm^3/min) of this experimental study. The PV of acid required to breakthrough was found to be 2.94. It was lower than the one obtained with the previous blend (2.5:7.5 wt% HCl:MSA) at low injection rate. Pressure drop profile showed an increase when the acid reached the core inlet (**Fig 25**). Such an increase in the pressure drop is due to some gaseous CO_2 which is not in the supercritical phase at 1100 psi. When the residence time of the acid is long, gaseous CO_2 comes out of the solution as it is in the mass-transfer limited regime. As the gas phase saturation increases at the expense of that of the liquid phase locally, the relative permeability of the liquid decreases. CO_2 enhances the conveyance of H^+ ions to the wormhole walls by local mixing (Qiu et al. 2014). The mass transfer coefficient or diffusivity of the acid increases. As a result, the gas phase indirectly causes the radial growth of the wormhole by blocking the tip of the wormhole (Cheng et al. 2017).

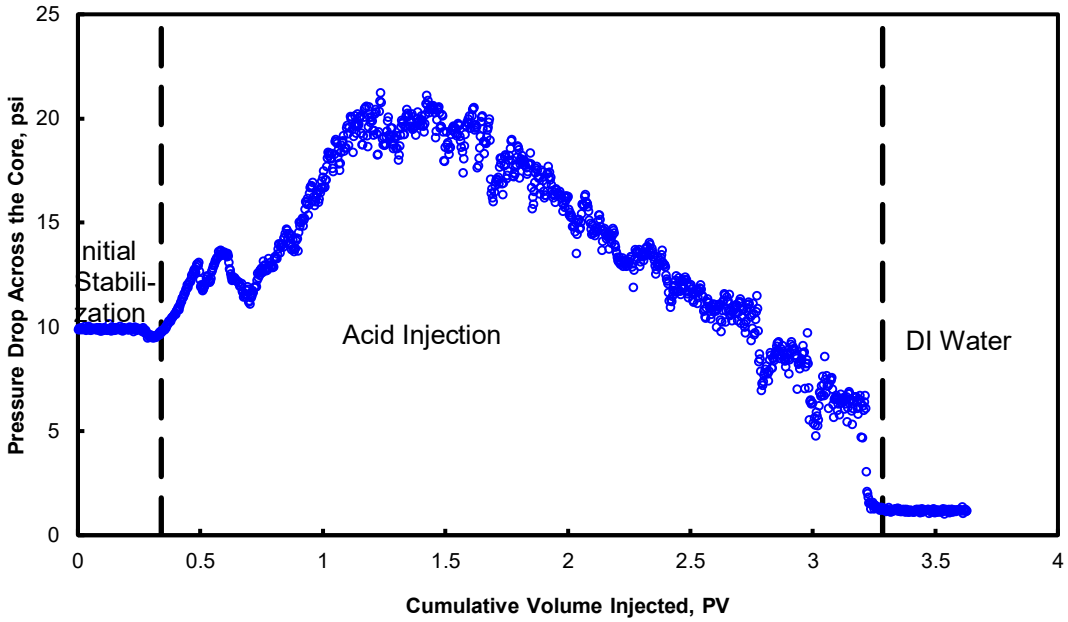

Figure 25 - Pressure drop across the core for 5:5 wt% HCl:MSA at 2 cm^3/min as a function of the cumulative volume injected at 250°F.

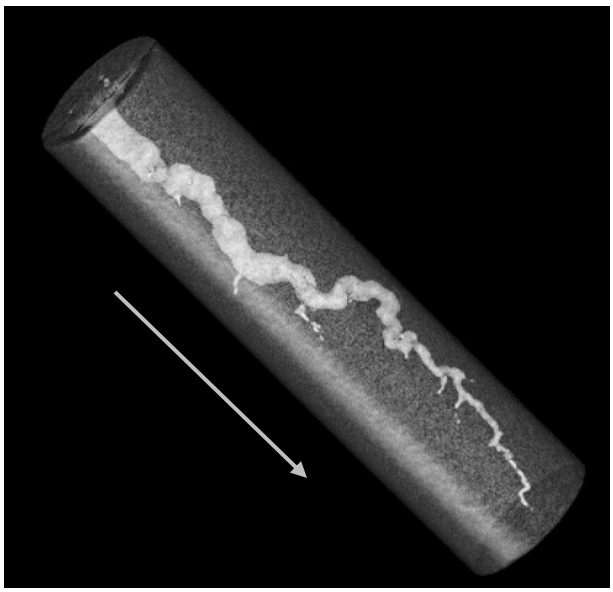

Figure 26 - CT scan image of Indiana limestone core after acidizing by 5:5 wt% HCl:MSA blend at 2 cm^3/min.

CT scan image reveals face dissolution and thick wormhole at the inlet of the core (**Fig. 26**), which tapers close to the outlet. Since the acid mixture had long residence time at 2 cm^3/min, it caused a large volume of acid consumption at the entrance of the core. This resulted in a negligible increase in the conductivity of the core as wormhole propagation was limited due to the enlargement of its diameter at the entrance. Maximum calcium ions dissolved was about 36,500 mg/L (**Fig. 27**). The unconsumed acid concentration in the core effluent samples at breakthrough was about 0.5 wt% equivalent HCl (**Fig. 28**). Thus, most of the acid was consumed on the walls of the wormhole when the residence time of the acid in the core was long. Negligible acid was left for further penetration of the wormhole at the same PV of acid corresponding to the breakthrough.

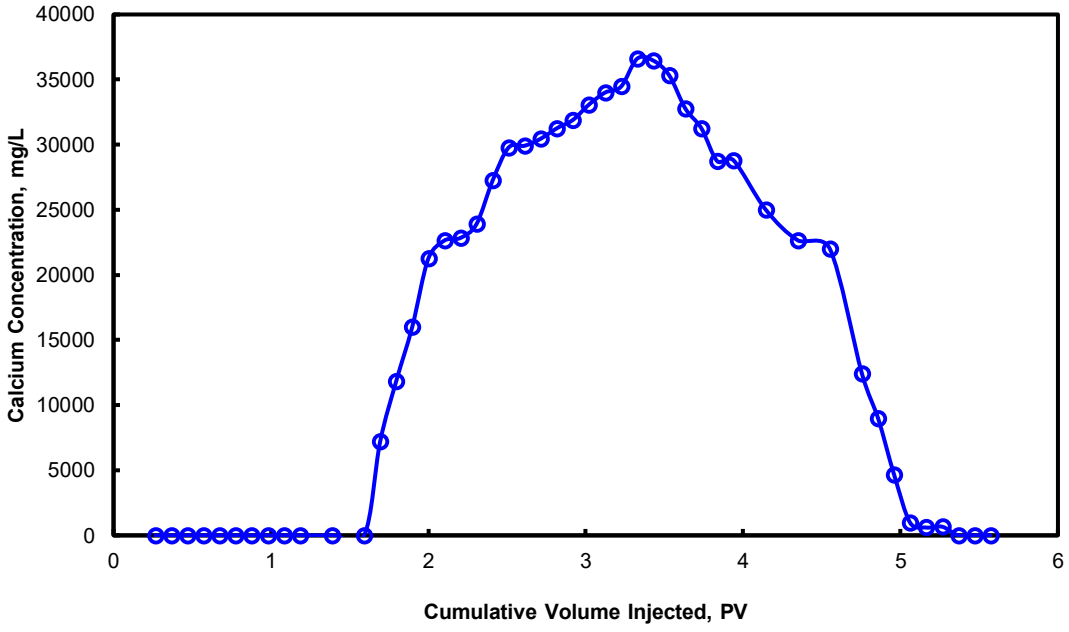

Figure 27 - Calcium ion concentration for 5:5 wt% HCl:MSA at 2 cm^3/min as a function of the cumulative volume injected at 250°F.

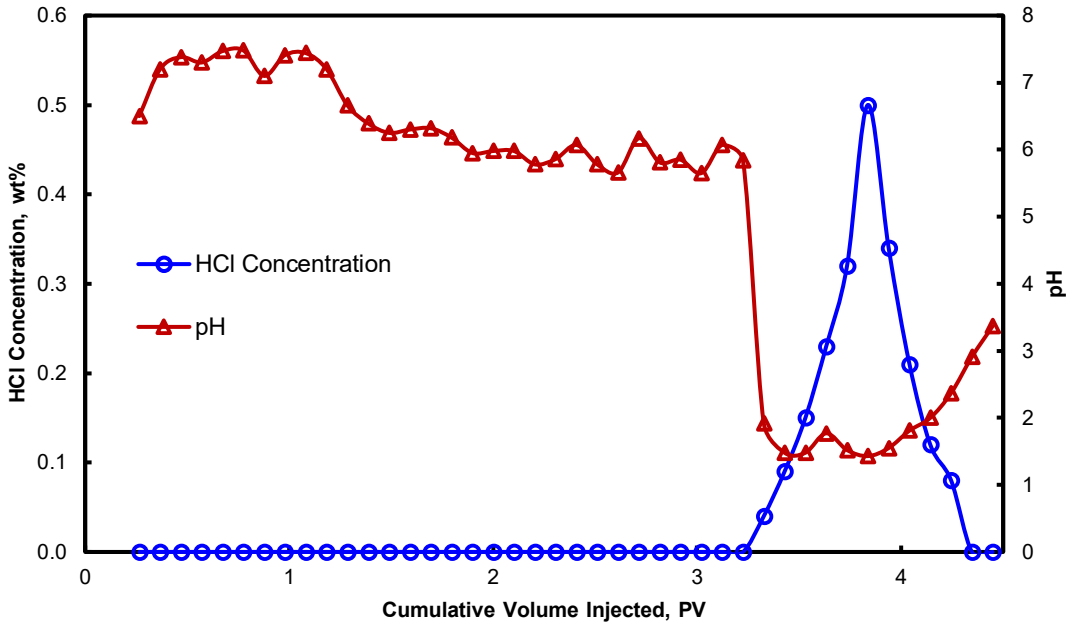

Figure 28 - Acid concentration in terms of equivalent HCl and pH of core effluent samples for 5:5 wt% HCl:MSA at 2 cm^3/min as a function of the cumulative volume injected at 250°F.

<u>At injection rate 5 cm^3/min:</u>

About 1.59 PV of 5:5 wt% HCl:MSA acid blend was required to reach breakthrough, which was the same as the one obtained with the previous blend (2.5:7.5 wt% HCl:MSA) at 5 cm^3/min. The pressure drop profile showed a slight elevation when the acid reached the core inlet (**Fig. 29**) due to some CO_2 in gaseous phase that was not completely left behind by the propagating wormhole at an intermediate residence time of the acid in the core.

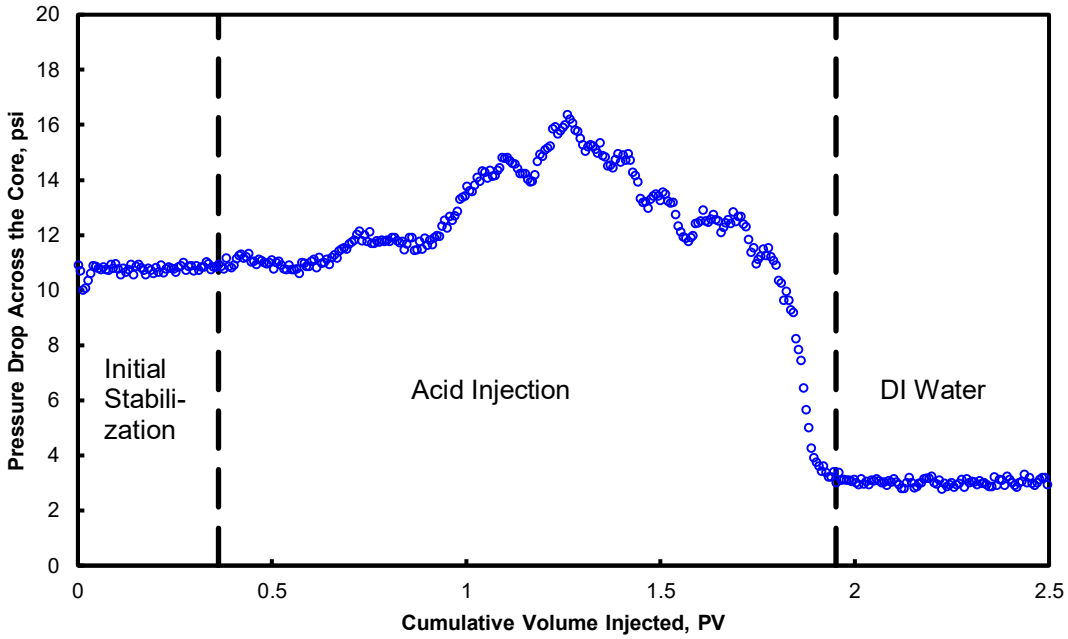

Figure 29 - Pressure drop across the core for 5:5 wt% HCl:MSA at 5 cm^3/min as a function of the cumulative volume injected at 250°F.

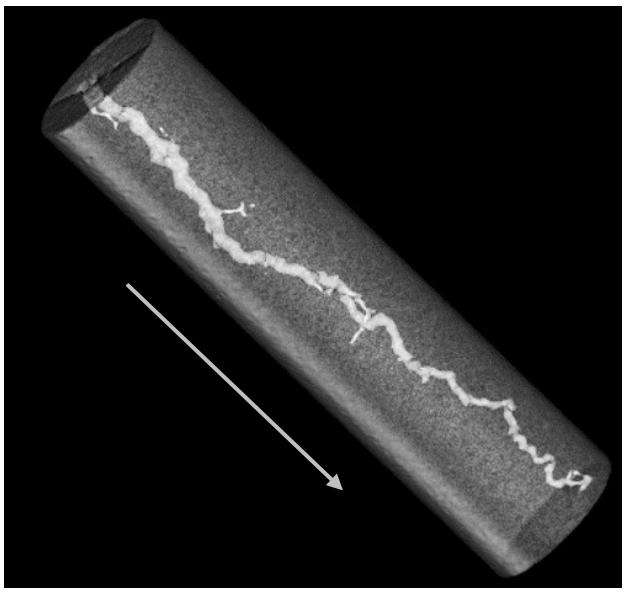

Figure 30 - CT scan image of Indiana limestone core after acidizing by 5:5 wt% HCl:MSA blend at 5 cm^3/min.

Conical wormhole was observed at the injection face of the core (**Fig. 30**). The CT image shows a single wormhole propagating throughout the core. The diameter of the wormhole at the inlet is greater than that in the outlet, which is due to the retardation effect of the gaseous CO_2 partly accumulating at the wormhole tip. Maximum calcium ions dissolved as shown by the peak in **Fig. 31** was 36,600 mg/L. It was higher than the respective 2.5:7.5 wt% HCl:MSA blend dissolution. This is because the overall strength of the acid in terms of total H^+ ions is higher in 5:5 wt% HCl:MSA than 2.5:7.5 wt% HCl:MSA blend. The acid concentration at breakthrough as measured in the effluent samples was close to 1 wt% (**Fig. 32**). Thus, little live acid was left to extend the wormhole deeper into the formation at the PV of acid corresponding to breakthrough.

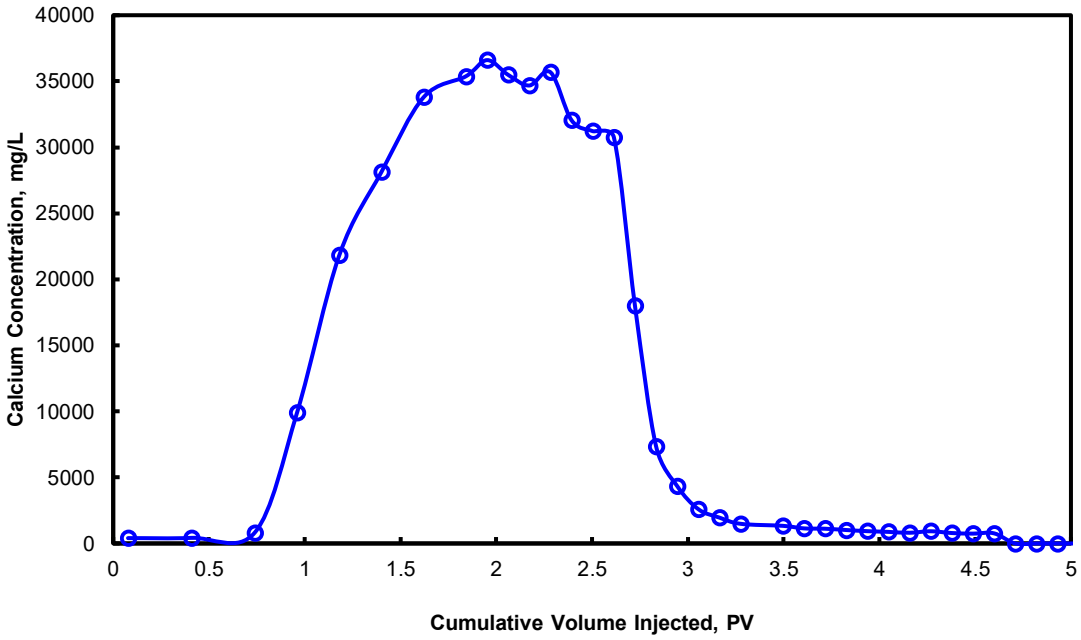

Figure 31 - Calcium ion concentration for 5:5 wt% HCl:MSA at 5 cm^3/min as a function of the cumulative volume injected at 250°F.

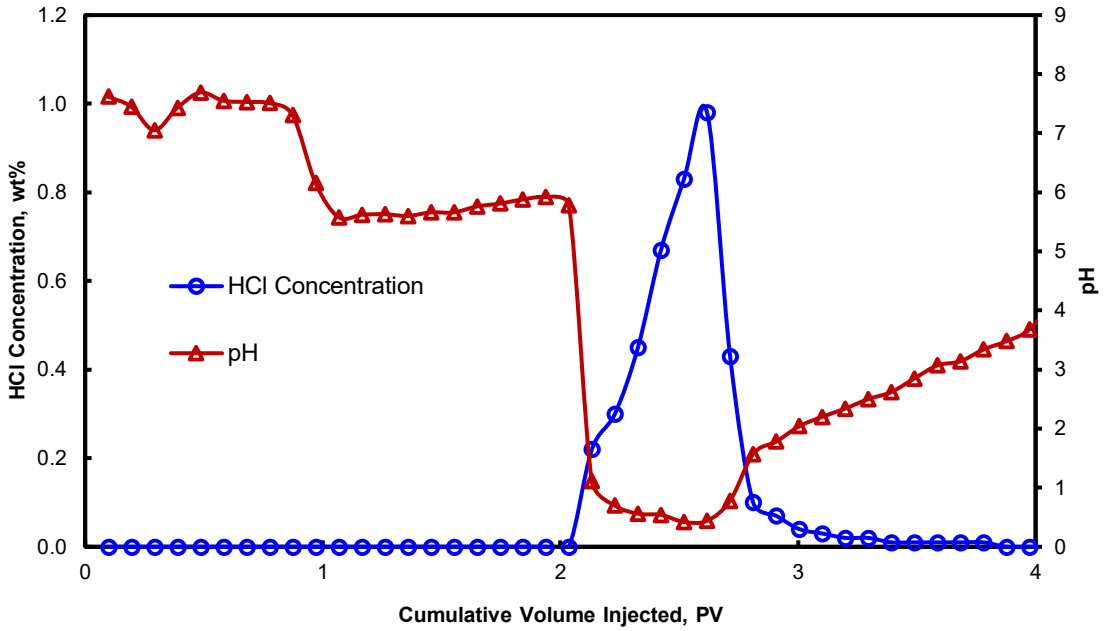

Figure 32 - Acid concentration in terms of equivalent HCl and pH of core effluent samples for 5:5 wt% HCl:MSA at 5 cm^3/min as a function of the cumulative volume injected at 250°F.

<u>At injection rate 7.5 cm^3/min:</u>

The PV required to reach breakthrough was 1.33, which is lower than that for the above-mentioned injection rates. Pressure drop profile showed a linear decline when the acid reached the core inlet (**Fig. 33**). At 7.5 cm^3/min, the residence time of the acid in the core was lower than the previous cases, so the time of exposure of acid to the rock was less, and the reaction was not very vigorous; hence, CO_2 generated was effectively left behind by the linear flow of acid through the wormhole. In other words, the concentration of the live acid was higher at the tip than the one contacting the surface of the wormhole.

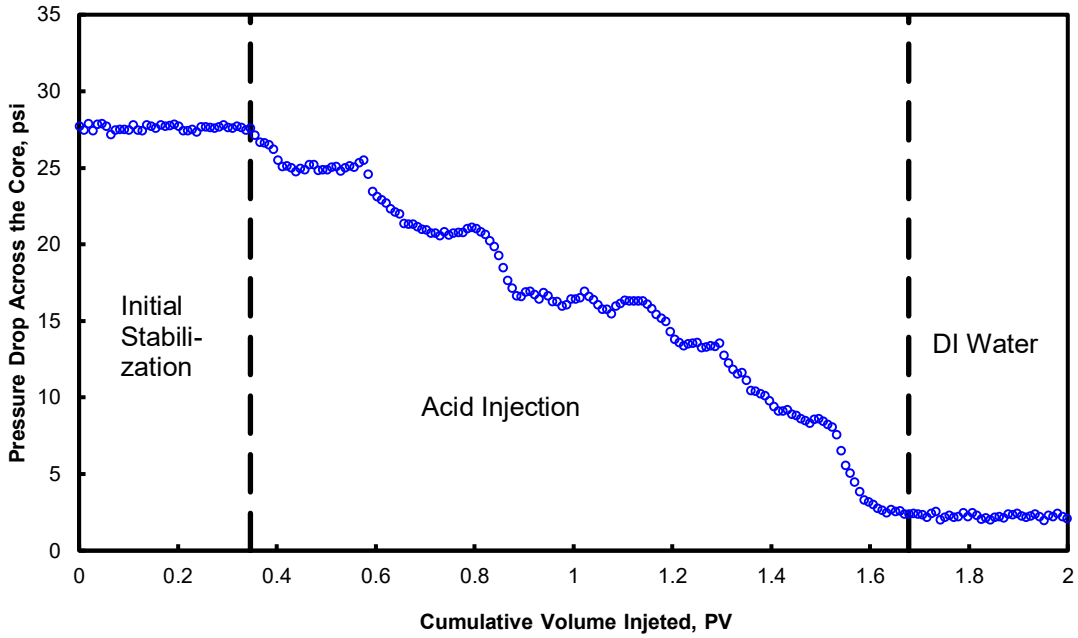

Figure 33 - Pressure drop across the core for 5:5 wt% HCl:MSA at 7.5 cm^3/min as a function of the cumulative volume injected at 250°F.

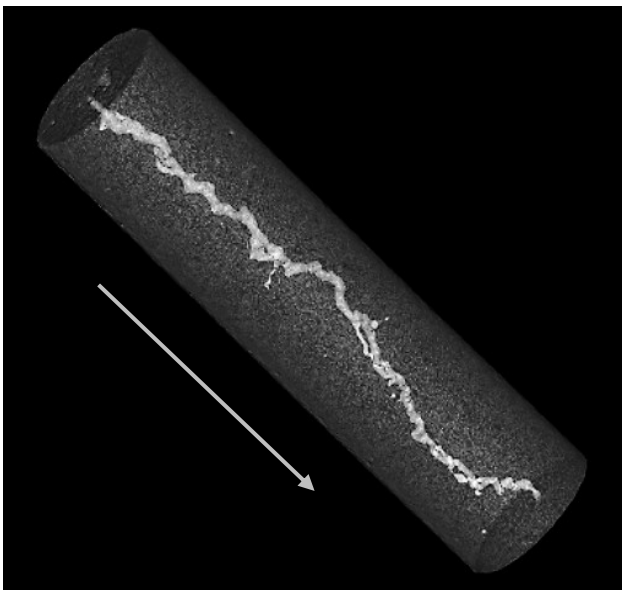

Figure 34 - CT scan image of Indiana limestone core after acidizing by 5:5 wt% HCl:MSA blend at 7.5 cm^3/min.

A significantly straight, single, least tortuous and dominant wormhole was observed from the CT scan image (**Fig. 34**). A relatively thinner wormhole was noted than that for 2 and 5 cm^3/min, and the diameter of the wormhole was more or less uniform throughout its propagation in the core. A less tortuous wormhole consumes less volume of acid to breakthrough and ensures deeper penetration in the formation. Maximum calcium ions dissolved at the peak was about 35,200 mg/L (**Fig. 35**). Acid concentration in the effluent samples at breakthrough was 1.72 wt% equivalent HCl (**Fig. 36**). Higher unspent acid concentration displays deeper wormhole propagation ability of the blend at 7.5 cm^3/min.

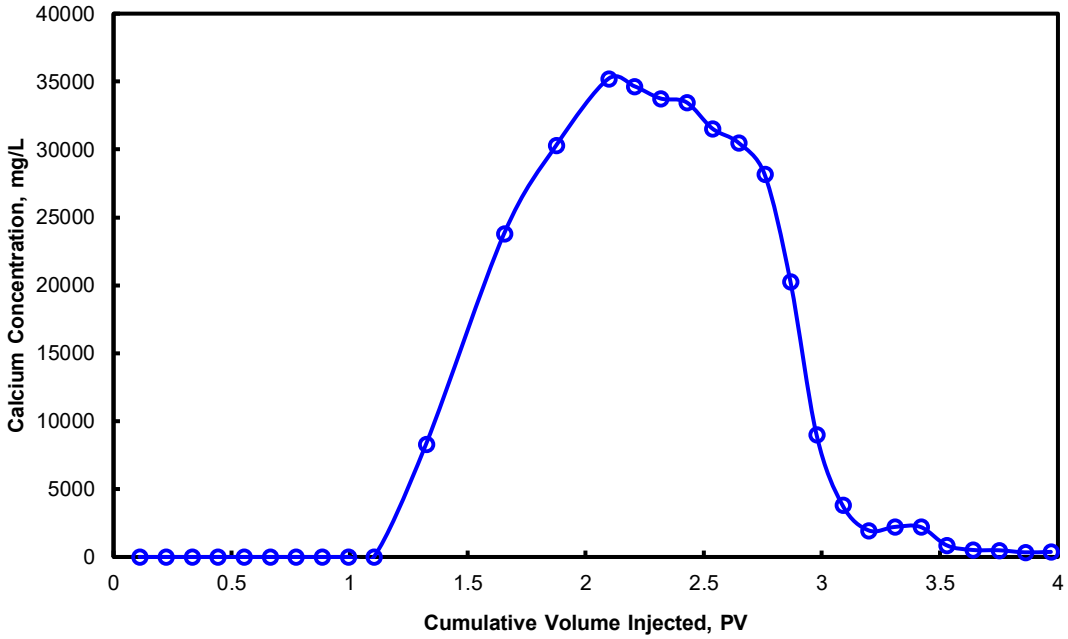

Figure 35 - Calcium ion concentration for 5:5 wt% HCl:MSA at 7.5 cm^3/min as a function of the cumulative volume injected at 250°F.

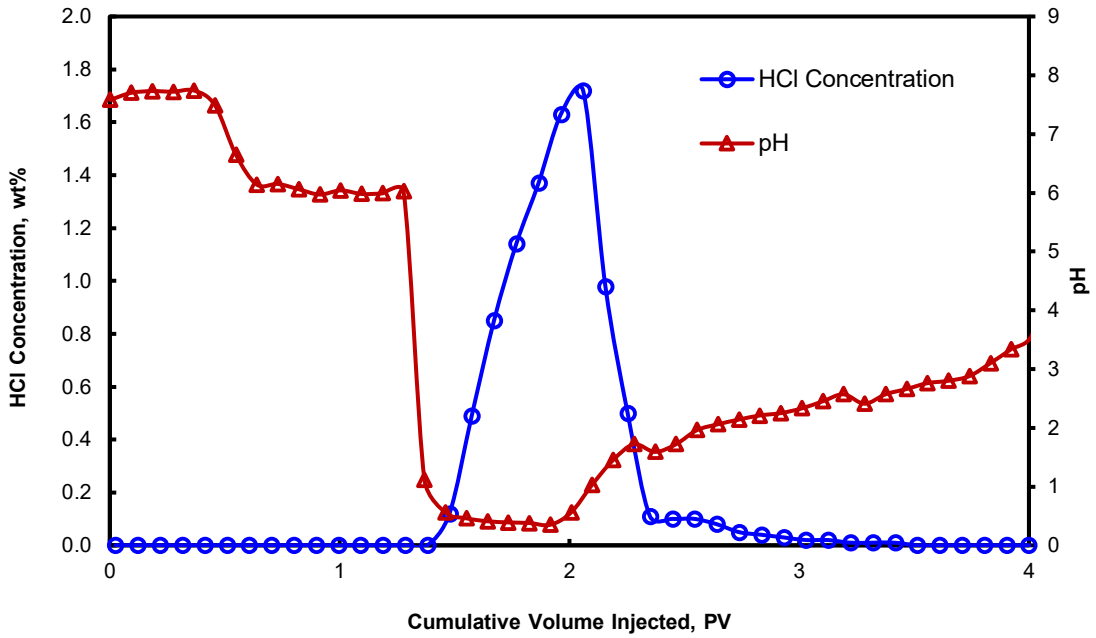

Figure 36 - Acid concentration in terms of equivalent HCl and pH of core effluent samples for 5:5 wt% HCl:MSA at 7.5 cm^3/min as a function of the cumulative volume injected at 250°F.

At injection rate 10 cm^3/min:

About 1.54 PV of the acid blend was required to breakthrough the core. Thus, the optimum injection rate, which requires the least PV of acid to breakthrough, is 7.5 cm^3/min. No increase in pressure drop was observed when the acid injection was carried out (**Fig. 37**). The residence time of the acid in the core was lower than all the previous injection rates.

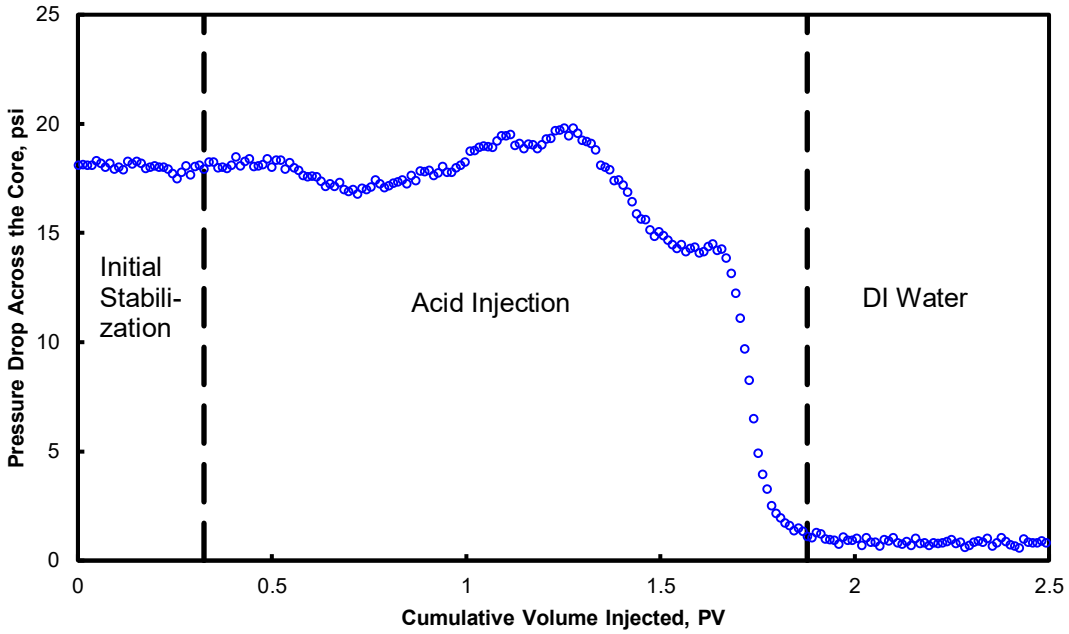

Figure 37 - Pressure drop across the core for 5:5 wt% HCl:MSA at 10 cm^3/min as a function of the cumulative volume injected at 250°F.

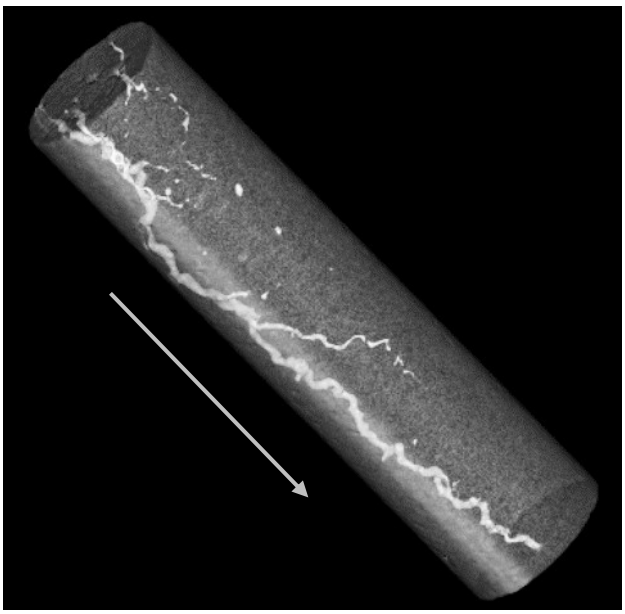

Figure 38 - CT scan image of Indiana limestone core after acidizing by 5:5 wt% HCl:MSA blend at 10 cm^3/min.

From the CT scan image, the core has severely branched wormholes with four inlets (**Fig. 38**). At such high injection rates, where transport of the acid is faster than the dissolution reaction, more uniform acid attack occurs (Hoefner and Fogler 1988). Thus, the diameter of the wormhole remained consistent throughout the core; however, high acid flux increased filtration losses (Bazin 2001). Both CT scan profile and acid volume requirement confirm that 7.5 cm^3/min is the optimum injection rate. Maximum calcium ion dissolved was 29,500 mg/L (**Fig. 39**). The dissolved calcium concentration is the same as that at 7.5 cm^3/min. Maximum unconsumed acid concentration in the effluent samples reached 1.5 wt% equivalent HCl (**Fig. 40**). Thus, the highest acid concentration in the samples corresponding to breakthrough was noticed at 7.5 cm^3/min.

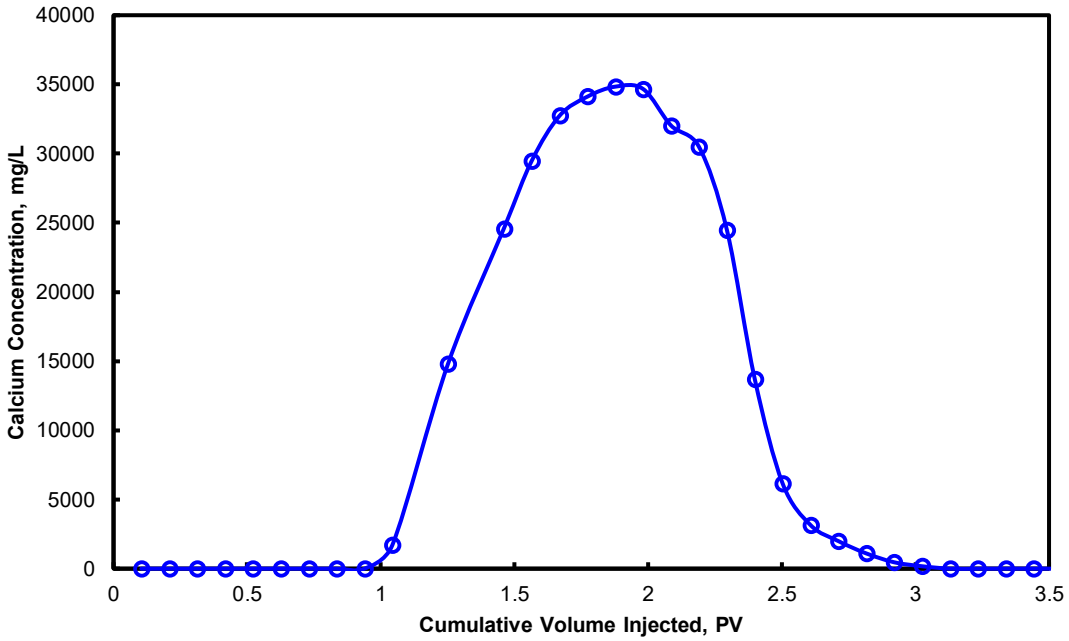

Figure 39 - Calcium ion concentration for 5:5 wt% HCl:MSA at 10 cm^3/min as a function of the cumulative volume injected at 250°F.

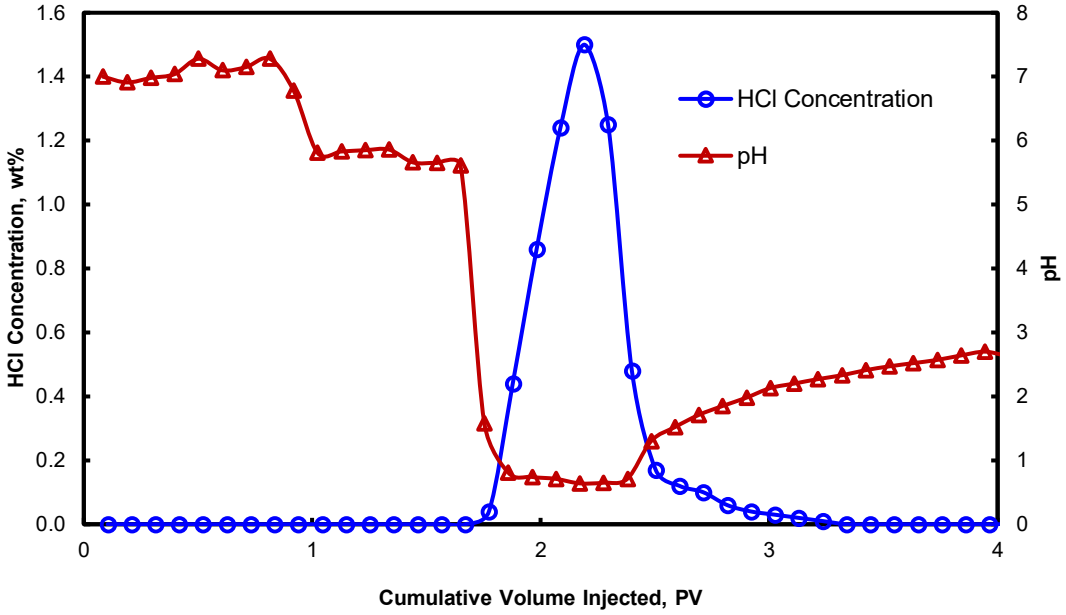

Figure 40 - Acid concentration in terms of equivalent HCl and pH of core effluent samples for 5:5 wt% HCl:MSA at 10 cm^3/min as a function of the cumulative volume injected at 250°F.

<u>At optimum injection rate 7.5 cm^3/min:</u>

The acid efficiency curve is shown in **Fig. 41**. The optimum injection rate is 7.5 cm^3/min for this blend, as minimum volume of acid is required to reach breakthrough. At low injection rates (2 cm^3/min), face dissolution was observed, whereas a high flow rate (10 cm^3/min) was associated with ramified branched wormholes. Two control experiments with equivalent concentrations of individual HCl and MSA were also performed at 7.5 cm^3/min. Lower PV of acid is needed for the acid blend, at its optimum injection rate, to breakthrough (1.33 PV) when compared to the equivalent concentration of 7.2 wt% HCl control (1.84 PV), whereas almost the same PV of acid was required for 17.7 wt% MSA control (1.39 PV).

Fig. 42 shows the pressure drop profile for 5:5 wt% acid blend at optimum injection rate. The pressure drop started to decline as soon as the acid reached the inlet of the core. A similar observation was noted with an equivalent concentration of MSA (control). However, the pressure drop increased for HCl (control) before reaching breakthrough. It can be inferred that HCl reacted vigorously with the calcite core, generating more gaseous CO_2, which increased the pressure drop across the core. In general, the solubility of CO_2 in solution decreases significantly as the concentration of $CaCl_2$ increases (Prutton and Savage 1945). For example, at 250°F and 1,100 psi, 0.5 and 0.15 moles of CO_2 is dissolved in solution per mole of $CaCl_2$ in the original solution of 10 and 20 wt% $CaCl_2$, respectively. Since the concentration of $CaCl_2$ produced from the dissolution reaction is higher for HCl (control) than the blend, more CO_2 is expected to be in the gaseous phase in the case of HCl (control).

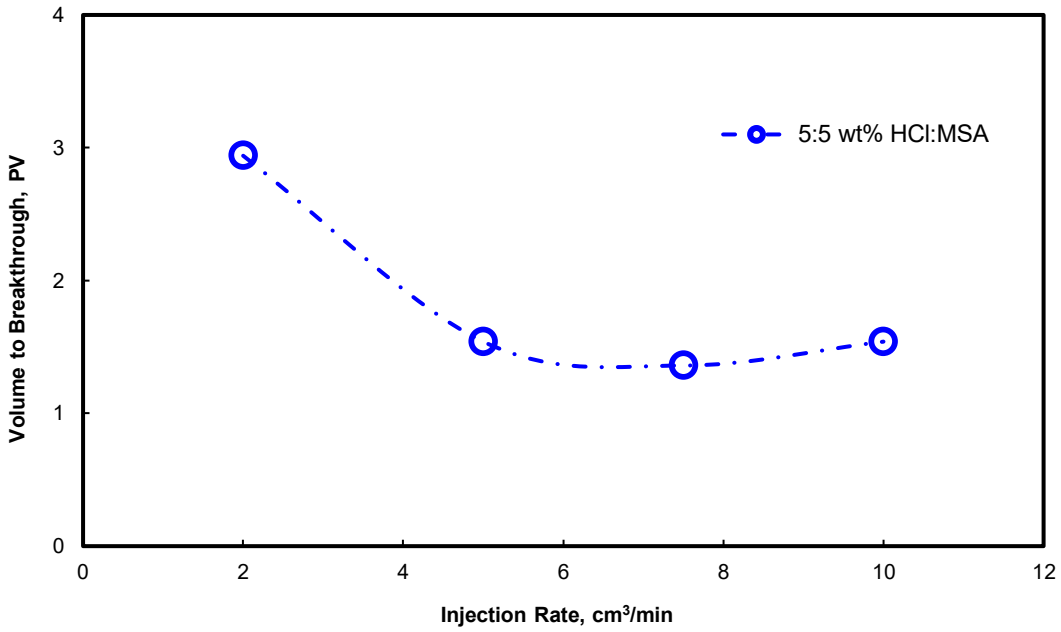

Figure 41 - Acid efficiency curve for 5:5 wt% HCl:MSA at 250°F (Reprinted with permission from Kankaria et al., 2017).

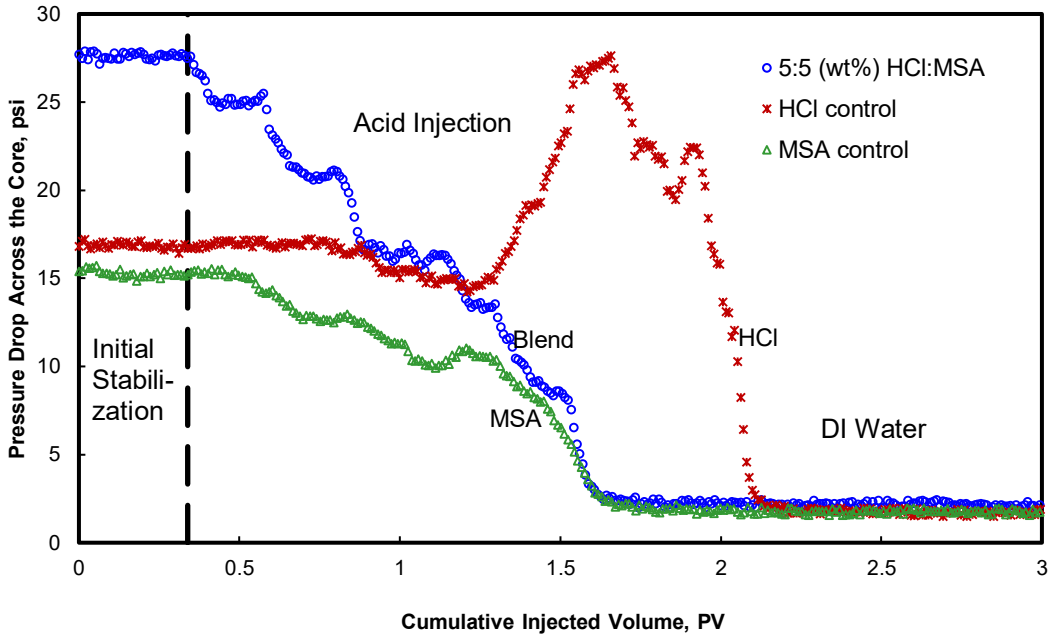

Figure 42 - Pressure drop across the core for 5:5 wt% HCl:MSA and its respective HCl and MSA controls at 7.5 cm^3/min as a function of the cumulative volume injected at 250°F (Reprinted with permission from Kankaria et al., 2017).

The calcium concentration in the core effluent samples as a function of cumulative volume injected is shown in **Fig. 43**. The amount of calcium ions dissolved by 5:5 wt% acid blend is almost equal to that of HCl control, while the MSA control dissolved the least amount of calcium ions as evident from the generated curve of calcium concentration profile. Acid concentrations in the core effluent samples left after the dissolution of the calcite core were measured as shown in **Fig. 44**. Higher acid concentration was observed for the blend compared to the controls, which ensures deeper acid penetration at the same PV of acid injection corresponding to breakthrough. This indicates lower reactivity of the acid blend, where HCl is consumed first, followed by MSA continuing the wormhole propagation.

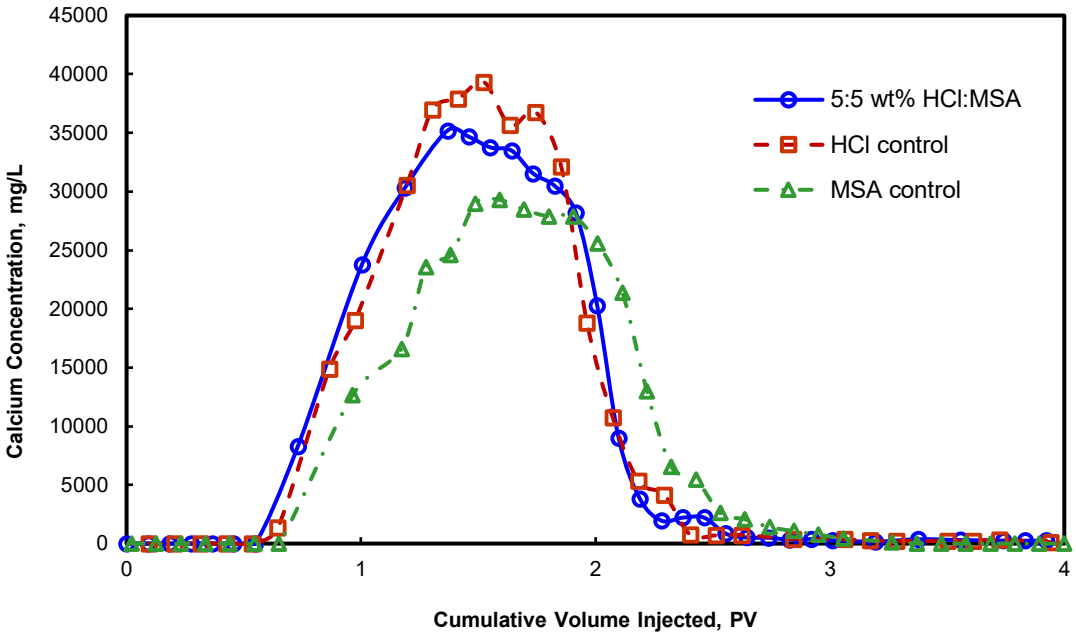

Figure 43 - Calcium ion concentration for 5:5 wt% HCl:MSA and its respective HCl and MSA controls at 7.5 cm^3/min as a function of the cumulative volume injected at 250°F (Reprinted with permission from Kankaria et al., 2017).

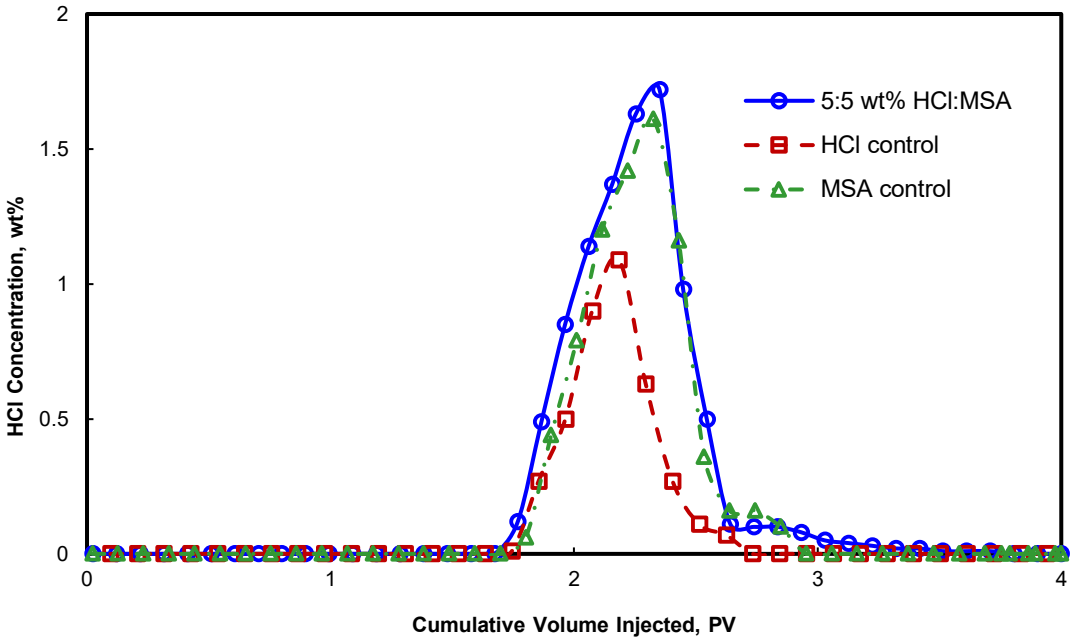

Figure 44 - Acid concentration in terms of equivalent HCl concentration for 5:5 wt% HCl:MSA and its respective HCl and MSA controls at 7.5 cm^3/min as a function of the cumulative volume injected at 250°F (Reprinted with permission from Kankaria et al., 2017).

A comparison between wormholes for 5:5 wt% HCl:MSA acid blend and its corresponding controls is shown in **Fig. 45**. A straight, dominant wormhole for the acid blend with lower tortuosity was observed. A more tortuous, slightly branched and enlarged wormhole was noted for HCl (control), whereas thinner, but branched wormhole was seen in the case of MSA (control). This indicates that the consumption of the acid blend contributed entirely to the dominant wormhole propagation, which was the most efficient way to transport acid to the wormhole tip. On the contrary, HCl (control) transport to the tip was least effective because more acid was consumed on the walls of the wormhole, thereby increasing its diameter, its side branches, and the rate of its propagation.

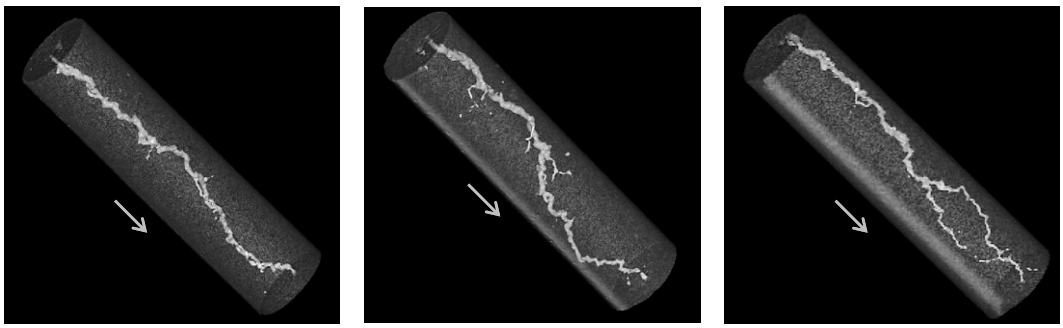

5:5 wt% HCl:MSA	7.2 wt% HCl control	17.7 wt% MSA control

Figure 45 - CT scan images of Indiana limestone cores after acidizing by 5:5 wt% HCl:MSA, 7.2 wt% HCl control, and 17.7 wt% MSA control equivalent at 7.5 cm^3/min (Reprinted with permission from Kankaria et al., 2017).

VI.3.3 Acid blend 7.5:2.5 wt% HCl:MSA

Coreflood experiments were carried out with 7.5:2.5 wt% acid blend at 2, 5, 7.5 and 10 cm^3/min injection rates.

At injection rate 2 cm^3/min:

The PV of acid required to breakthrough was found to be 2.96. The pressure drop increased when the acid reached the core face (**Fig. 46**), due to CO_2 in the gaseous phase. The presence of two-phase causes a spike in the pressure drop. As the concentration of HCl is increased in this blend compared to the previous two blends, more CO_2 is expected to be in the gaseous state due to its lowered solubility in high concentration of $CaCl_2$ produced during the reaction. A thick, large diameter wormhole is observed towards the core inlet side, which progressively decreases in the diameter towards the outlet (**Fig. 47**). The long residence time of the acid in the core and the generation of a lot of gaseous CO_2 resulted in a large volume of acid consumption at the entrance of the core.

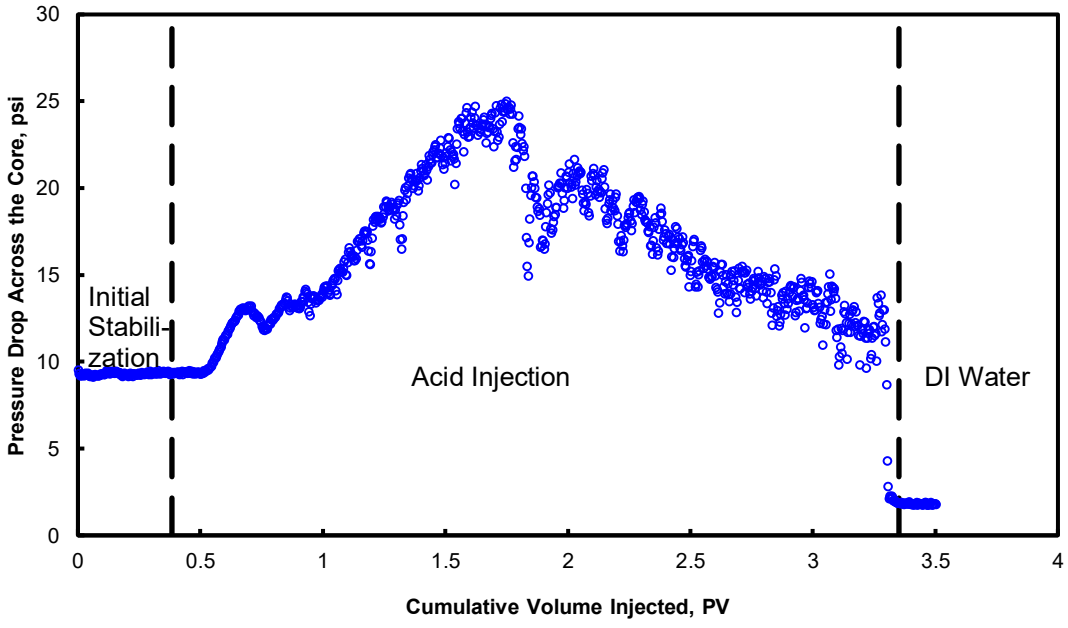

Figure 46 - Pressure drop across the core for 7.5:2.5 wt% HCl:MSA at 2 cm^3/min as a function of the cumulative volume injected at 250°F.

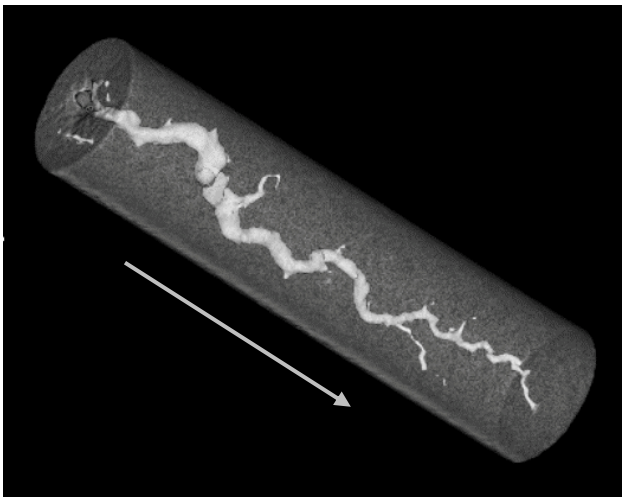

Figure 47 - CT scan image of Indiana limestone core after acidizing by 7.5:2.5 wt% HCl:MSA blend at 2 cm^3/min.

The calcium concentration at the peak was 56,700 mg/L (**Fig. 48**), much higher than the previous two blends due to higher acid strength. The unspent acid concentration in the core effluent samples at breakthrough was about 1 wt% equivalent HCl (**Fig. 49**), which means most of the acid was consumed on the enlargement of the diameter of the wormhole. Negligible acid was left for further penetration of the wormhole at the same PV of acid corresponding to breakthrough.

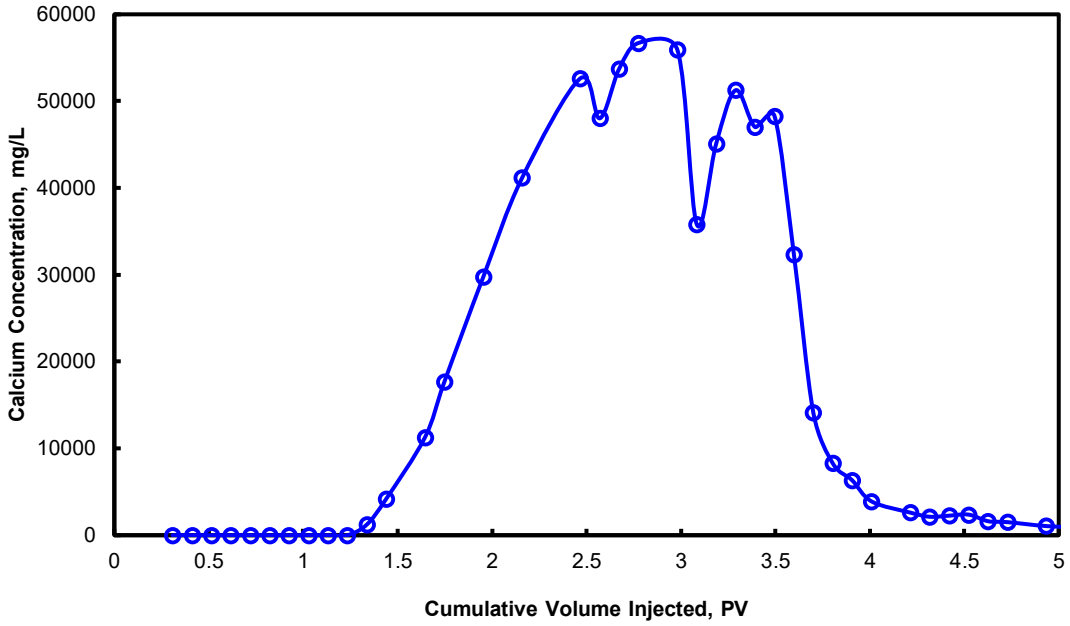

Figure 48 - Calcium ion concentration for 7.5:2.5 wt% HCl:MSA at 2 cm^3/min as a function of the cumulative volume injected at 250°F.

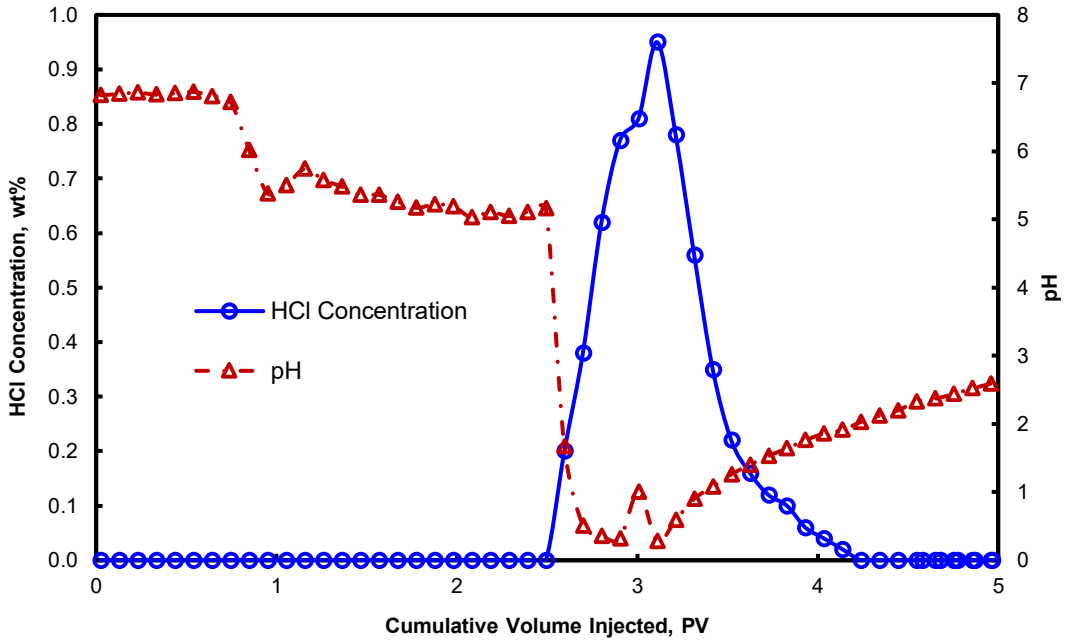

Figure 49 - Acid concentration in terms of equivalent HCl and pH of core effluent samples for 7.5:2.5 wt% HCl:MSA at 2 cm^3/min as a function of the cumulative volume injected at 250°F.

At injection rate 5 cm^3/min:

About 0.99 PV of 7.5:2.5 wt% HCl:MSA acid blend was required to reach breakthrough. It is lower than the previous two blends due to its higher acid strength. Pressure drop increased (**Fig. 50**) when the acid reached the core inlet due to some CO_2 in the gas phase that is not dissolved in the solution at the applied back pressure. The CT image shows a single, dominant, and highly tortuous wormhole propagating throughout the core (**Fig. 51**). The wormhole at the inlet has a larger diameter that tapers as it gets close to the outlet. The injection rate is not high enough to diminish the negative effect of CO_2 retardation on wormhole propagation.

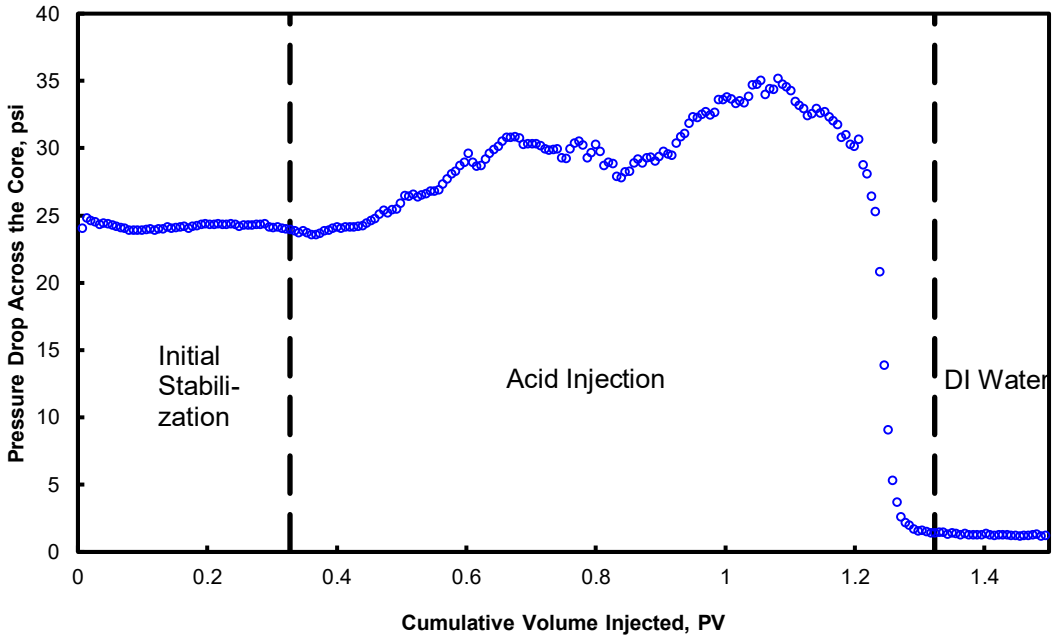

Figure 50 - Pressure drop across the core for 7.5:2.5 wt% HCl:MSA at 5 cm^3/min as a function of the cumulative volume injected at 250°F.

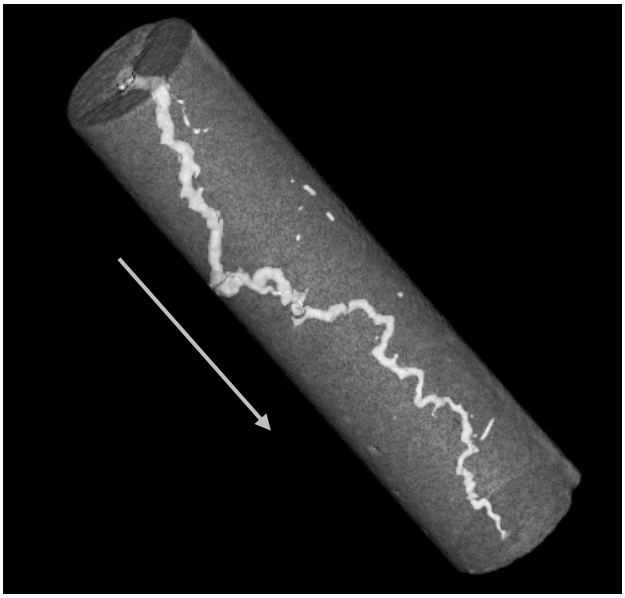

Figure 51 - CT scan image of Indiana limestone core after acidizing by 7.5:2.5 wt% HCl:MSA blend at 5 cm^3/min.

Maximum calcium ions dissolved as shown by the peak in **Fig. 52** was about 42,000 mg/L. The maximum acid concentration at breakthrough as shown by the peak was 0.93 wt% (**Fig. 53**). Thus, there was not much live acid left to extend the wormhole deeper in formation corresponding to the PV of acid corresponding to breakthrough.

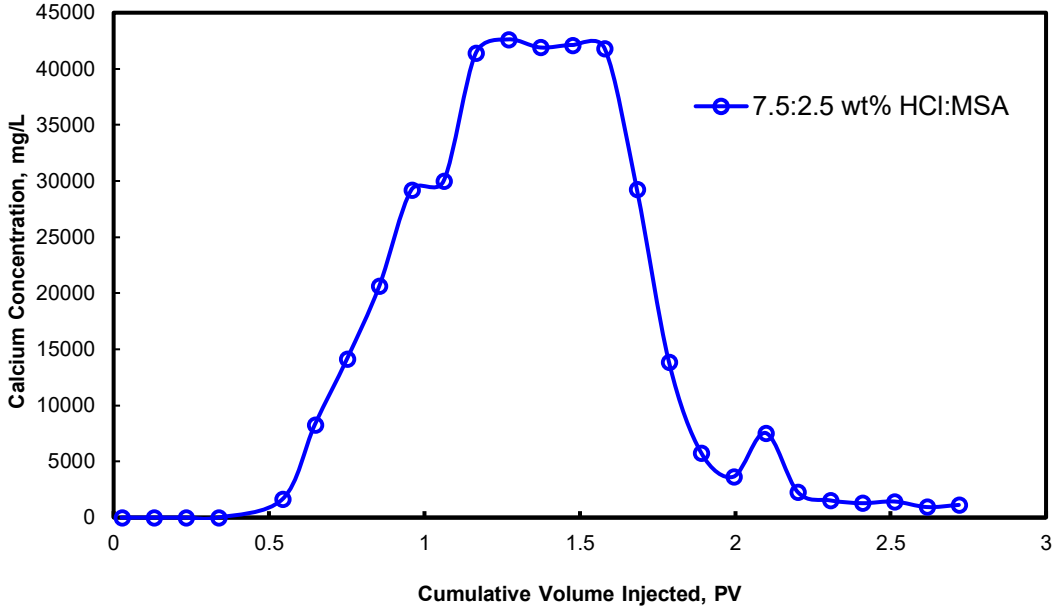

Figure 52 - Calcium ion concentration for 7.5:2.5 wt% HCl:MSA at 5 cm^3/min as a function of the cumulative volume injected at 250°F.

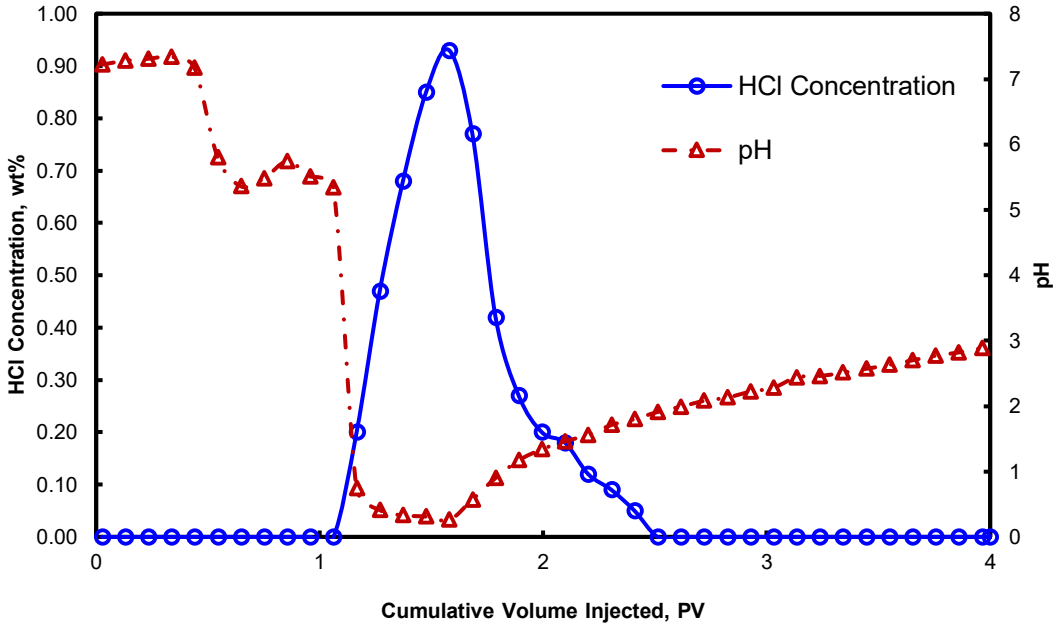

Figure 53 - Acid concentration in terms of equivalent HCl and pH of core effluent samples for 7.5:2.5 wt% HCl:MSA at 5 cm^3/min as a function of the cumulative volume injected at 250°F.

At injection rate 7.5 cm^3/min:

About 1.2 PV of acid was required to reach breakthrough at 7.5 cm^3/min. This was higher than that at 5 cm^3/min, which indicates that the latter is the optimum injection rate for 7.5:2.5 wt% HCl:MSA blend. The pressure drop profile showed a spike when the acid reached the core inlet (**Fig. 54**). This observation is consistent for all the flow rates of this blend. The acid strength is high for 7.5:2.5 wt% HCl:MSA mixture and the concentration of MSA is low, such that the effect of an organic acid in retardation of HCl is almost negligible. Hence, the vigorous reaction of HCl with calcite results in a significant amount of CO_2 generation in gaseous phase whose solubility decreases with increase in $CaCl_2$ in the solution. This causes an increase in the pressure drop. A slightly tortuous and branched wormhole was observed from the CT scan image (**Fig. 55**).

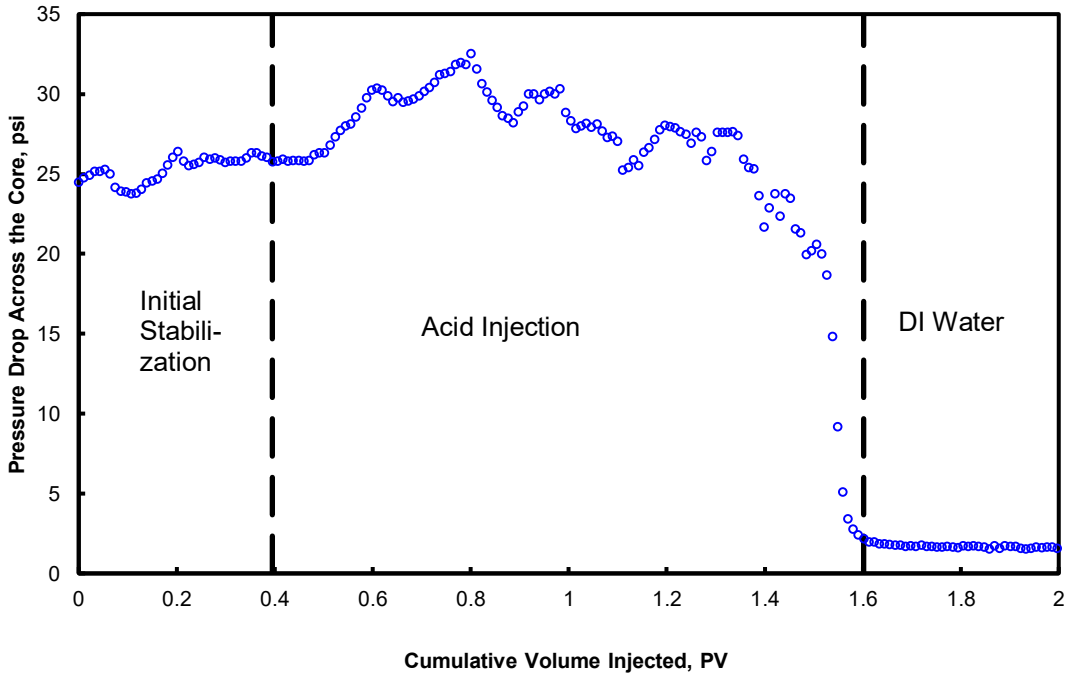

Figure 54 - Pressure drop across the core for 7.5:2.5 wt% HCl:MSA at 7.5 cm^3/min as a function of the cumulative volume injected at 250°F.

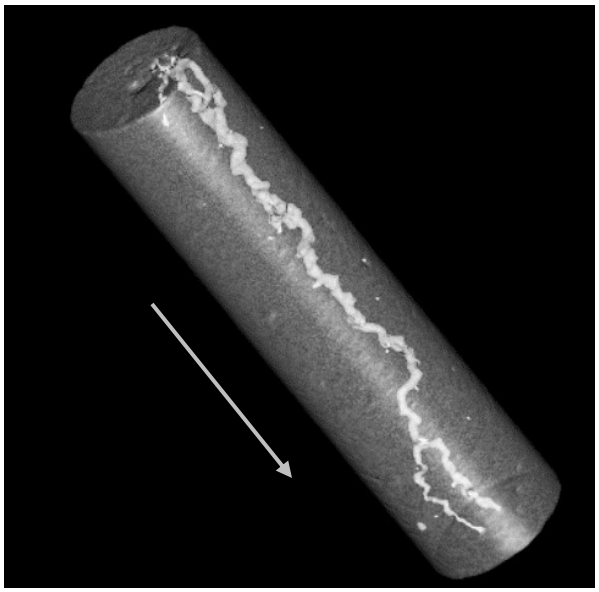

Figure 55 - CT scan image of Indiana limestone core after acidizing by 7.5:2.5 wt% HCl:MSA blend at 7.5 cm^3/min.

Maximum calcium ions dissolved at the peak was about 42,800 mg/L as shown in **Fig. 56**. At breakthrough, the maximum acid concentration is 2.5 wt% equivalent HCl (**Fig. 57**), which indicates its deeper penetration ability.

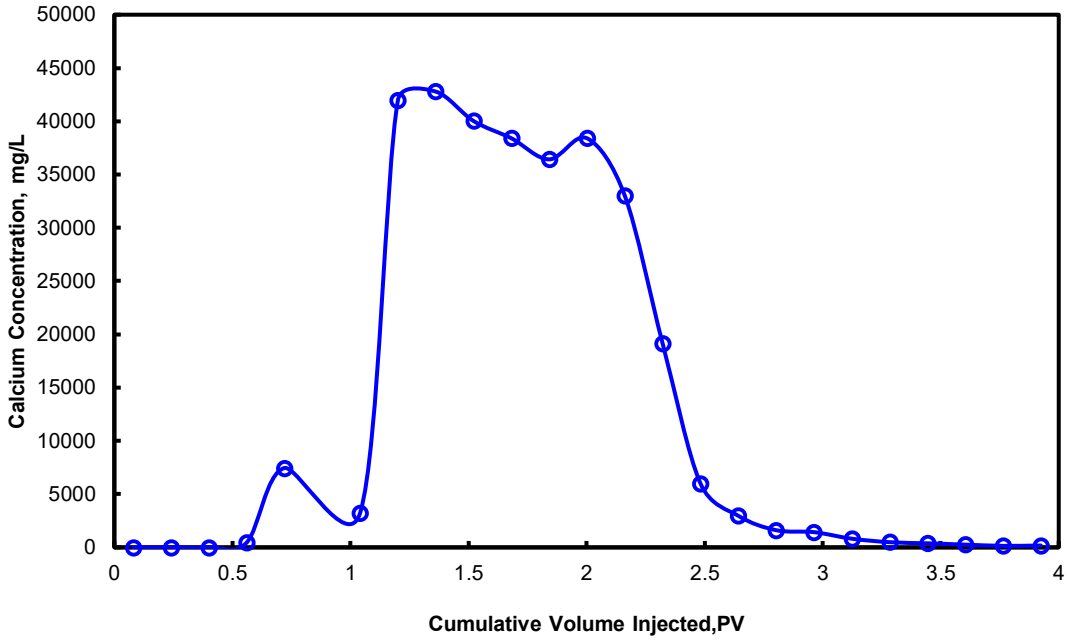

Figure 56 - Calcium ion concentration for 7.5:2.5 wt% HCl:MSA at 7.5 cm^3/min as a function of the cumulative volume injected at 250°F.

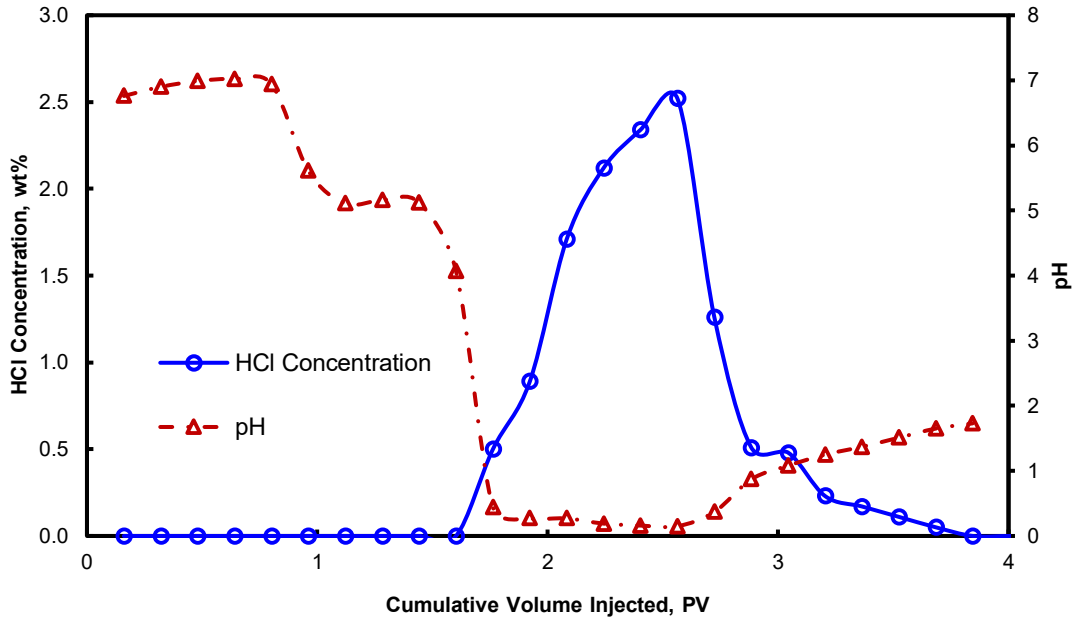

Figure 57 - Acid concentration in terms of equivalent HCl and pH of core effluent samples for 7.5:2.5 wt% HCl:MSA at 7.5 cm^3/min as a function of the cumulative volume injected at 250°F.

At injection rate 10 cm^3/min:

The PV of blend required to breakthrough at 10 cm^3/min was 1.2 PV. The pressure drop showed an increase as expected when the acid injection was carried out (**Fig. 58**). The residence time of the acid in the core was lower than all the previous injection rates. From the CT scan image, the core has severely branched wormholes (**Fig. 59**), which is expected when the dissolution is shifted towards the surface-reaction-limited regime.

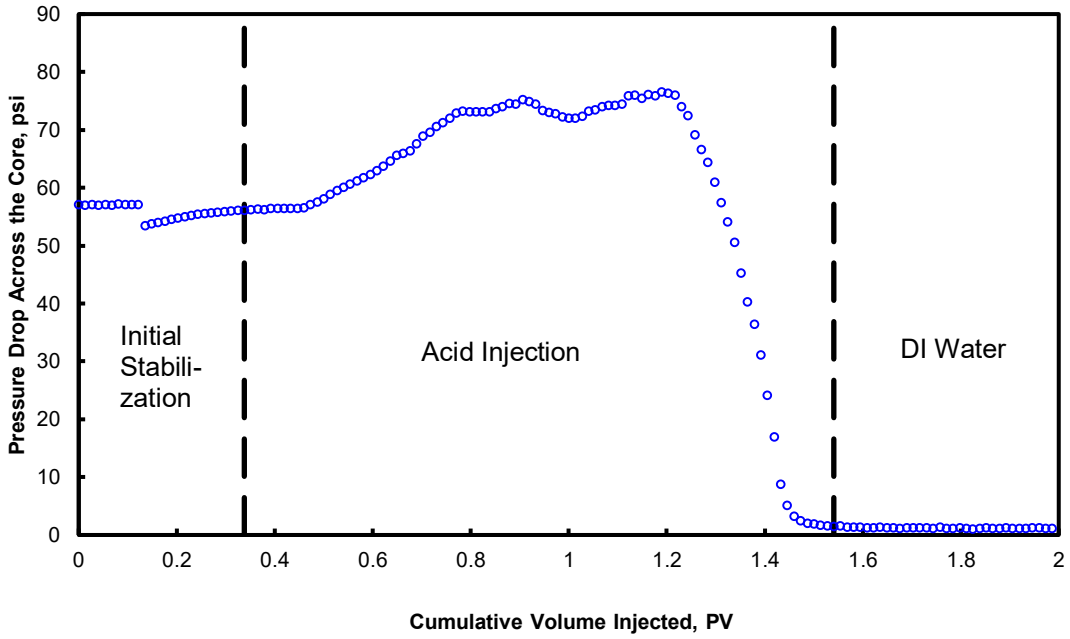

Figure 58 - Pressure drop across the core for 7.5:2.5 wt% HCl:MSA at 10 cm^3/min as a function of the cumulative volume injected at 250°F.

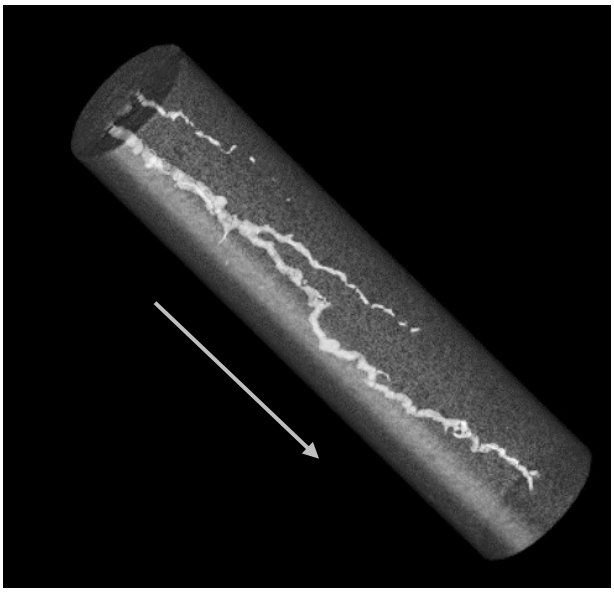

Figure 59 - CT scan image of Indiana limestone core after acidizing by 7.5:2.5 wt% HCl:MSA blend at 10 cm^3/min.

Maximum calcium ion dissolved was 42,600 mg/L (**Fig. 60**), which is almost equal to that at 7.5 cm^3/min. Maximum unconsumed acid concentration in the effluent samples reached 2.8 wt% equivalent HCl (**Fig. 61**).

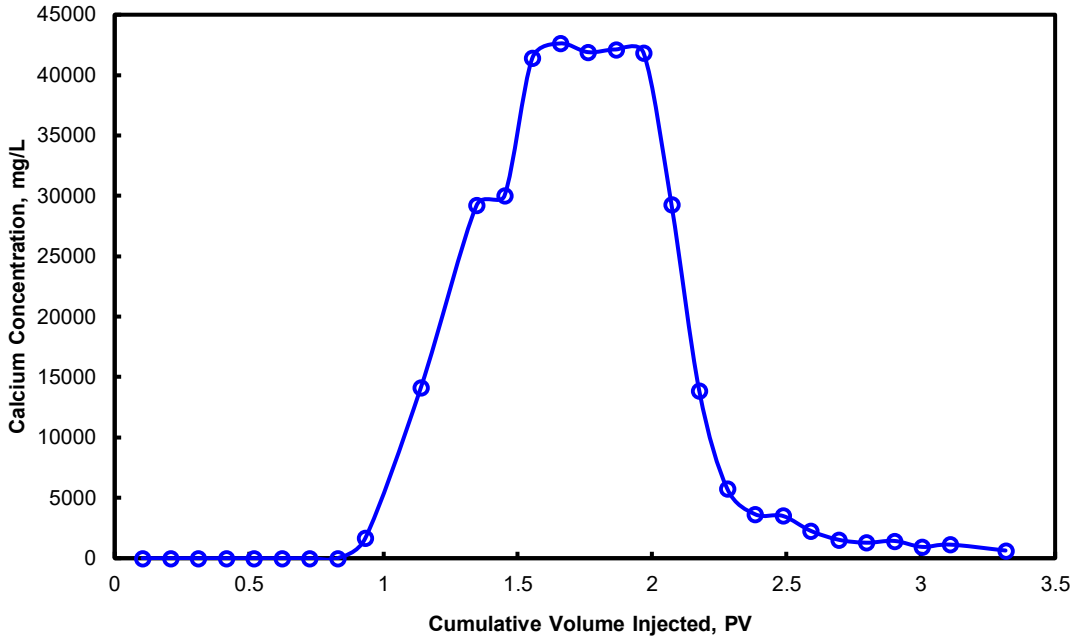

Figure 60 - Calcium ion concentration for 7.5:2.5 wt% HCl:MSA at 10 cm^3/min as a function of the cumulative volume injected at 250°F.

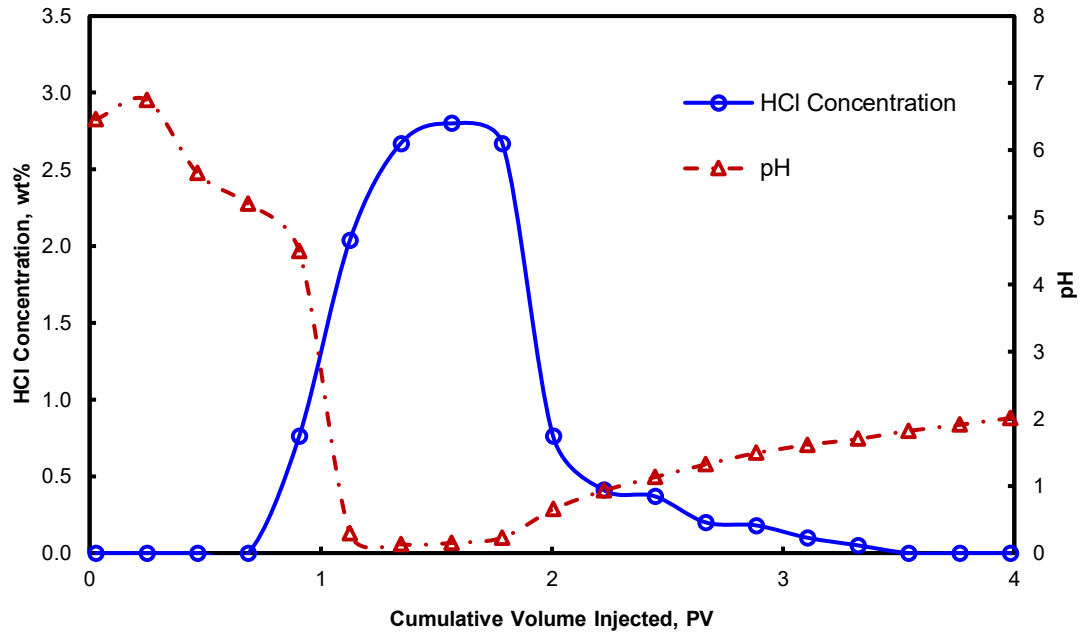

Figure 61 - Acid concentration in terms of equivalent HCl and pH of core effluent samples for 7.5:2.5 wt% HCl:MSA at 10 cm^3/min as a function of the cumulative volume injected at 250°F.

At optimum injection rate 5 cm^3/min:

The acid efficiency curve became progressively flatter as injection rate increased beyond 5 cm^3/min (**Fig. 62**), which is essentially an indication of the approach to a surface-reaction-limited regime. However, optimum injection rate was noted at 5 cm^3/min where least number of PVs of acid (0.99 PV) was required to reach breakthrough. The control experiments were carried out at this injection rate with an equivalent concentration of individual HCl and MSA. The 8.8 wt% HCl control required 0.97 PV of acid while 21.31 wt% MSA control required lesser PV of acid to reach breakthrough (0.79 PV); however, the difference in the volume of the acid requirement for breakthrough is not considerable. Thus, the effect of mixing an organic acid is no longer significant when HCl concentration is raised and MSA concentration is reduced from 5:5 to 7.5:2.5 wt% HCl:MSA.

The blend showed an increase in the pressure drop for the four tested injection rates. HCl control also showed a spike in the pressure drop at an optimum acid injection rate of 5 cm^3/min (**Fig. 63**). When the concentration of MSA is reduced to as low as 2.5 wt% in the blend, the vigorous reaction of the acid with calcite produces a concentration of $CaCl_2$ large enough to reduce CO_2 solubility in the solution. However, the MSA control does not show an elevation in the pressure drop, which is a clear indication of no CO_2 in the gas phase.

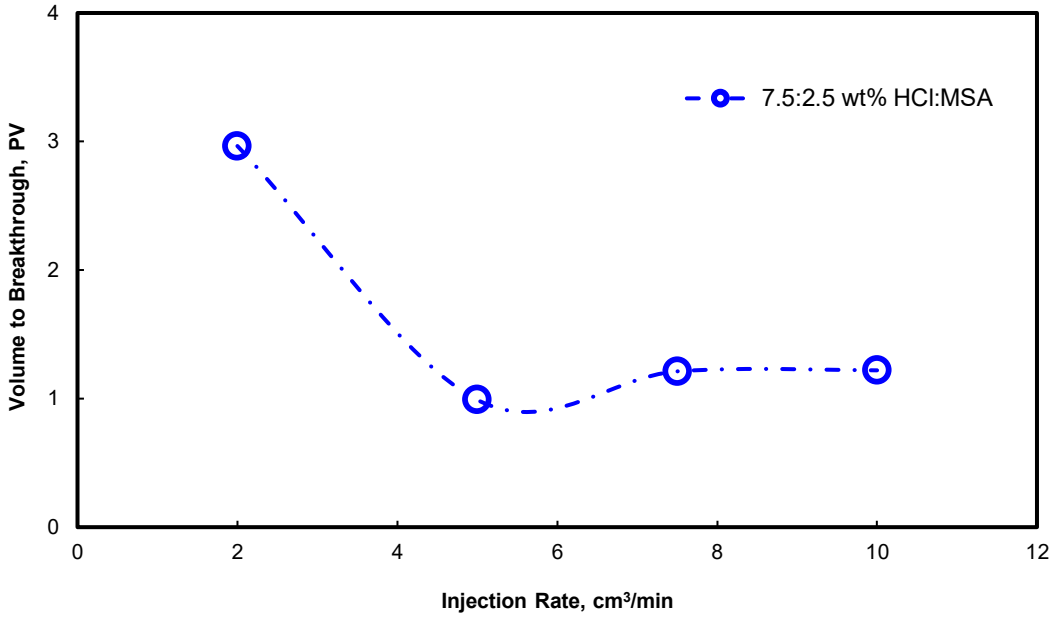

Figure 62 - Acid efficiency curve for 7.5:2.5 wt% HCl:MSA at 250°F (Reprinted with permission from Kankaria et al., 2017).

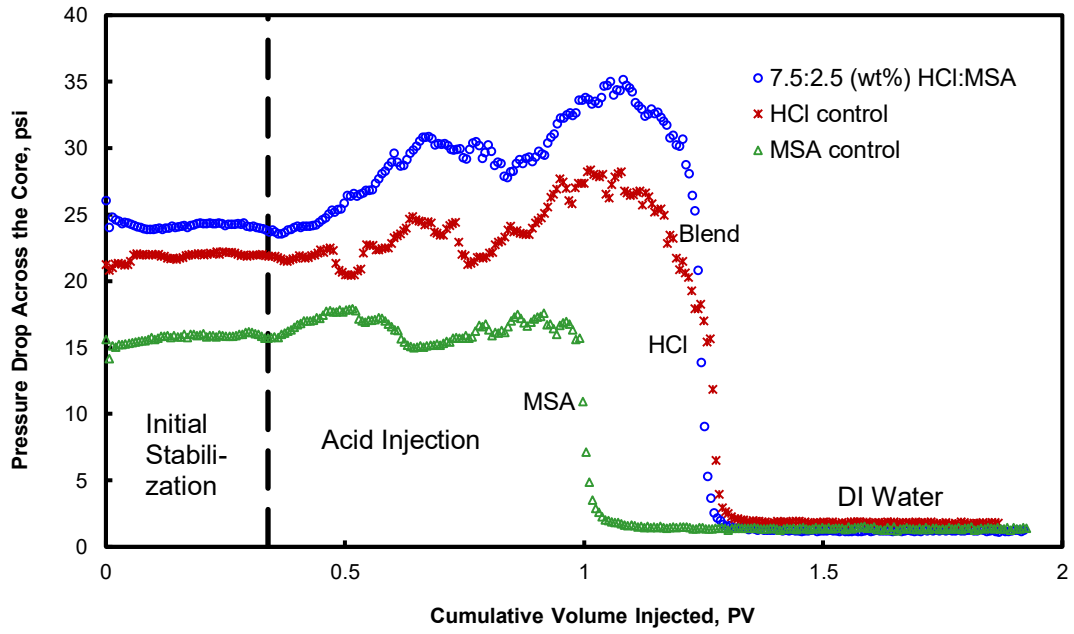

Figure 63 - Pressure drop across the core for 7.5:2.5 wt% HCl:MSA and its respective HCl and MSA controls at 5 cm^3/min as a function of the cumulative volume injected at 250°F (Reprinted with permission from Kankaria et al., 2017).

Fig. 64 shows the calcium concentration for the acid blend and controls as a function of the cumulative volume injected. An intermediate amount of calcium is dissolved by acid mixture when compared to the two controls, as evident from the area under the generated curve. Acid concentrations in core effluent samples were measured and plotted as a function of cumulative PV injected (**Fig. 65**). Much higher acid concentration was found for the controls compared to the blends, which can be utilized for further acid penetration. The wormhole formed for the acid blend is of slightly lower thickness and higher tortuosity than that of the HCl control (**Fig. 66**). On the other hand, the MSA control created a much thinner and less tortuous wormhole.

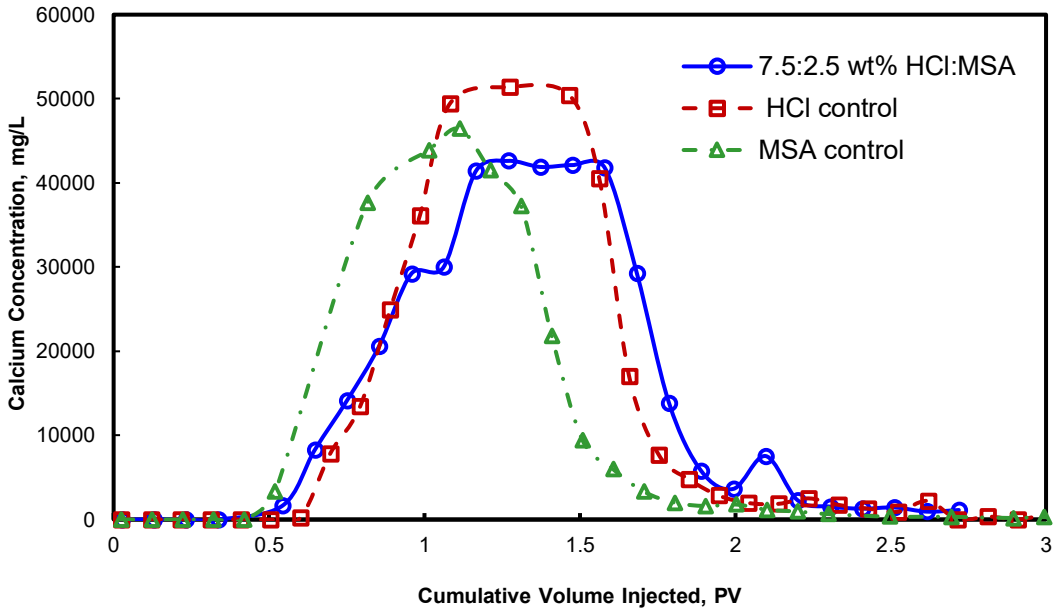

Figure 64 - Calcium ion concentration for 7.5:2.5 wt% HCl:MSA and its respective HCl and MSA controls at 5 cm^3/min as a function of the cumulative volume injected at 250°F (Reprinted with permission from Kankaria et al., 2017).

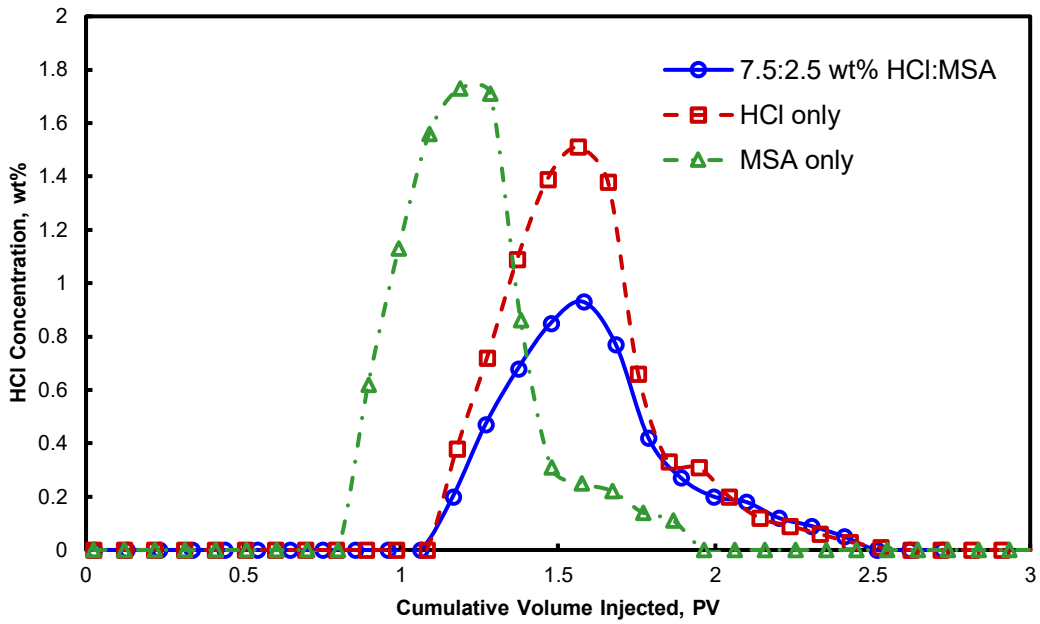

Figure 65 - Acid concentration in core effluent samples in terms of equivalent HCl concentration for 7.5:2.5 wt% HCl:MSA and its respective HCl and MSA controls at 5 cm^3/min as a function of the cumulative volume injected at 250°F (Reprinted with permission from Kankaria et al., 2017).

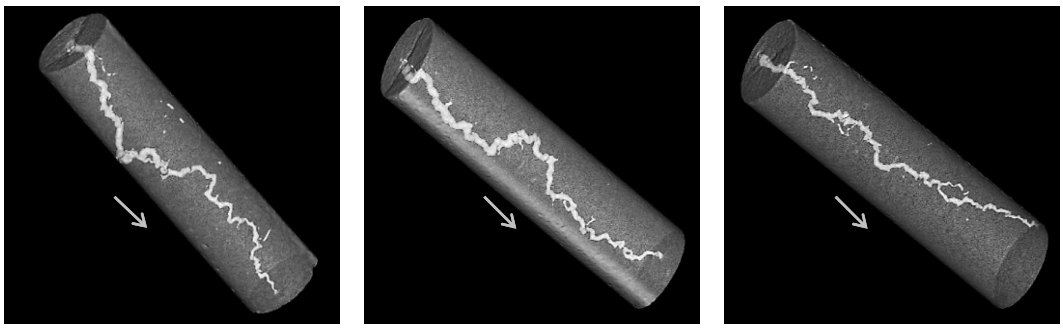

7.5:2.5 wt% HCl:MSA	8.8 wt% HCl control	21.31 wt% MSA control

Figure 66 - CT scan images of Indiana limestone cores after acidizing by 7.5:2.5 wt% HCl:MSA, 8.8 wt% HCl control, and 21.31 wt% MSA control equivalent at 5 cm^3/min (Reprinted with permission from Kankaria et al., 2017).

VI.3.4 Comparative study

All the cores after the coreflood experiments were scanned in a CT scanner, and the 3D wormhole images were generated using Osirix software. Tortuosity is defined as the ratio of the effective wormhole length to the length of the core (L/L_0). The CT scan images were processed using ImageJ software to get slices of the core along its diameter. Based on the CT numbers (which is negative for the wormhole and positive for the solid), the position of the center of the wormhole for each slice was detected. The length of the wormhole was determined by simple VBA code on excel, written by Mahmoud Taha Ali (shown in Appendix A), and tortuosity was calculated. Lower tortuosity implies a more effective way of acid transport across the core as it corresponds to lower acid consumption.

Fig. 67 shows the comparison of wormhole structures for different acid blend ratios at their optimum injection rates ($I.R._{opt}$) along with their controls. **Figs. 67a** through **67c** show the conductive channels formed for the experiment set of 2.5:7.5 wt% HCl:MSA, along with its equivalent controls. The tortuosity of the wormhole was slightly greater for the 2.5:7.5 wt% HCl:MSA blend than that of the controls. The HCl control created branching in the channel while the blend formed a single path with no branching. Minor splitting of channel pathways can be noted from all the images which are indicative of branching at pore scale due to varying pore size distribution across the core.

Figs. 67d through **67f** shows a comparison between wormholes for 5:5 wt% HCl:MSA acid blend and its corresponding controls. A straight, dominant wormhole for

the acid blend with lower tortuosity (1.68) was observed. A more tortuous (2.11), slightly branched and enlarged wormhole was noted for HCl (control), whereas thinner, but branched wormhole was observed in case of MSA (control). The tortuosity of blend and MSA control are almost equal, which complies with almost similar acid volume requirement to breakthrough. This indicates that the consumption of the acid blend contributed entirely to the dominant wormhole propagation, which was the most efficient way to transport acid to the wormhole tip. On the contrary, HCl (control) transport to the tip was least effective because more acid was consumed on the walls of the wormhole, thereby increasing its diameter, its side branches, and the rate of its propagation.

In accordance with Le Chatelier principle, reduced ionization of MSA in the presence of HCl generates less CO_2 than that produced by the corresponding HCl control. Additionally, higher mole fraction of CO_2 is liberated in the gaseous phase with HCl control due to a higher concentration of $CaCl_2$. The CO_2-rich vapor phase tends to accumulate at the wormhole tip, thereby reducing its propagation velocity. This causes diversion of the acid away from the tip by enlarging the wormhole diameter, imparting more tortuosity, and creating side branches. The retardation effect of CO_2 also explains higher acid PV requirement and lower unreacted acid concentration in case of HCl control compared to the blend. On the other hand, most of the CO_2 produced by the blend remains in solution that buffers the H^+ ions transport to the rock surface resulting in higher live acid concentration at wormhole tip (Qiu et al. 2014).

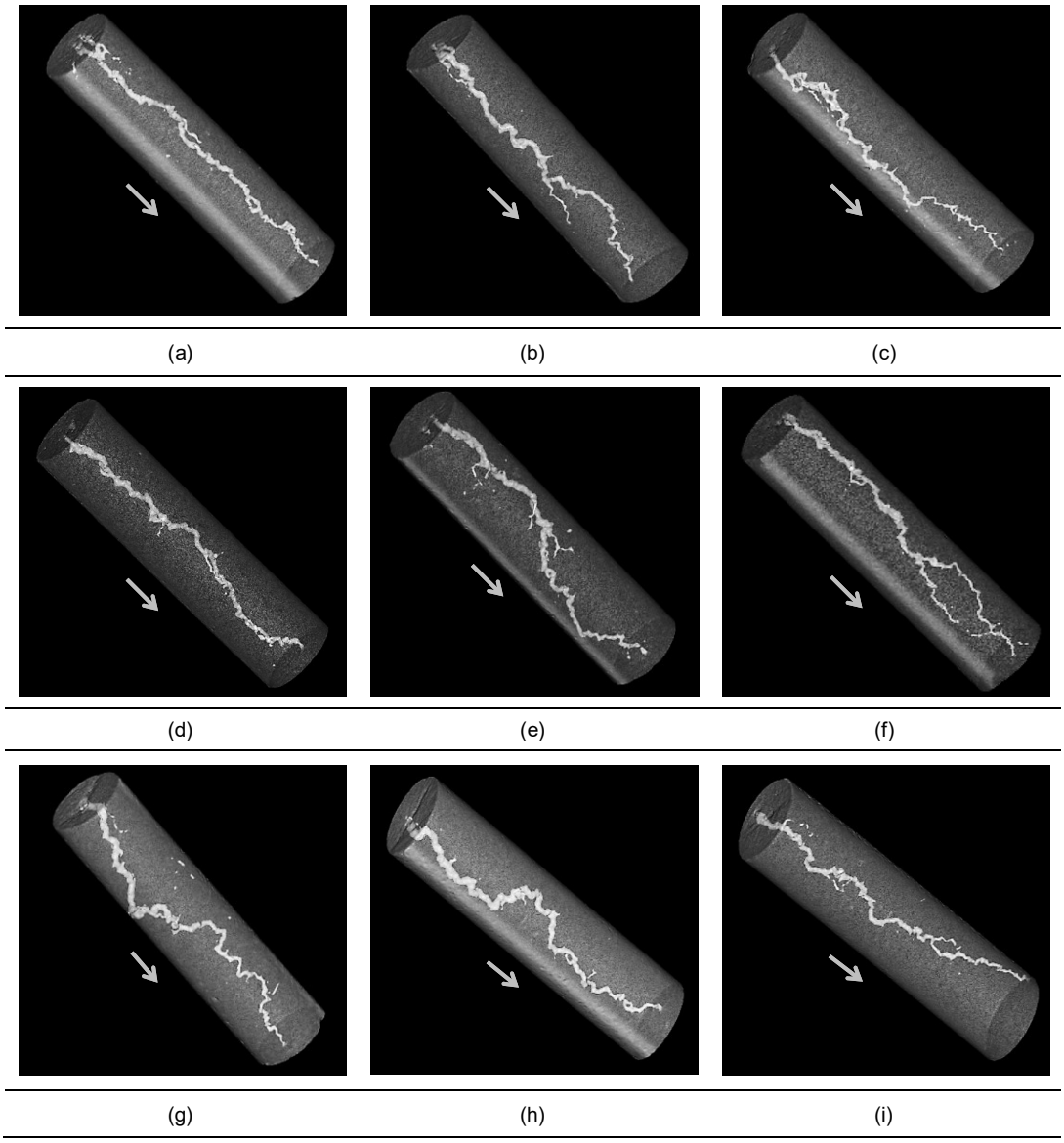

Figure 67 - CT scan images of Indiana limestone cores after acidizing by different acid blends and their controls at the optimum injection rate. (a) 2.5:7.5 wt% HCl:MSA blend at 7.5 cm^3/min (b) HCl control equivalent to 2.5:7.5 wt% HCl:MSA blend at 7.5 cm^3/min (c) MSA control equivalent to 2.5:7.5 wt% HCl:MSA blend at 7.5 cm^3/min (d) 5:5 wt% HCl:MSA blend at 7.5 cm^3/min (e) HCl control equivalent to 5:5 wt% HCl:MSA blend at 7.5 cm^3/min (f) MSA control equivalent to 5:5 wt% HCl:MSA blend at 7.5 cm^3/min (g) 7.5:2.5 wt% HCl:MSA blend at 5 cm^3/min (h) HCl control equivalent to 7.5:2.5 wt% HCl:MSA blend at 5 cm^3/min (i) MSA control equivalent to 7.5:2.5 wt% HCl:MSA blend at 5 cm^3/min (Reprinted with permission from Kankaria et al., 2017).

The conductive channels formed for acid blend 7.5:2.5 wt% HCl:MSA, along with its controls, are shown in **Figs. 67g** through **67i .**The wormhole formed for the acid blend is of slightly lower thickness and higher tortuosity than that of the HCl control. On the other hand, the MSA control created a much thinner and less tortuous wormhole. This result clearly indicates the negligible effectiveness of 7.5:2.5 wt% HCl:MSA acid blend, as the MSA concentration is progressively reduced with a simultaneous increase in HCl concentration.

Fig. 68 shows a comparison of PVs to breakthrough for three acid blends at their optimum injection rates along with their respective controls. As the overall acid concentration of the solution increases from 2.5:7.5 to 7.5:2.5 wt% HCl:MSA, acid PV required to reach breakthrough decreases. It is worthwhile to note that 5:5 wt% acid blend best optimizes the performance of individual acids. Almost equal PVs of acid are required to reach breakthrough for 2.5:7.5 and 5:5 wt% acid blend. Since MSA is much more expensive than HCl, it is a reasonable approach to increase HCl concentration in the mixture, with a simultaneous decrease in MSA concentration, while preserving the overall performance of the blend.

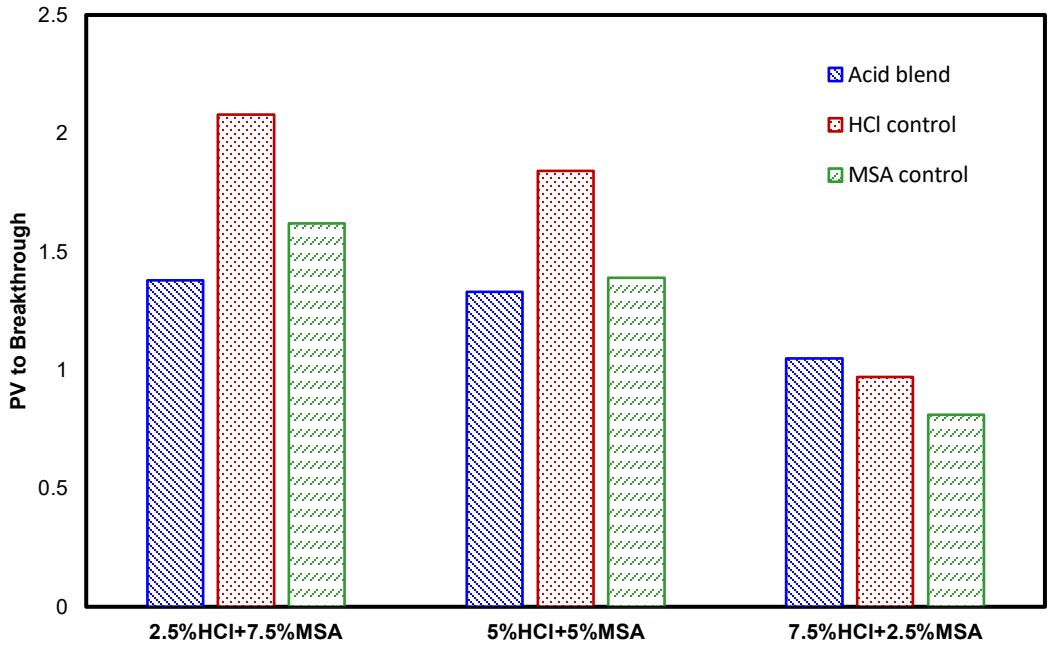

Figure 68 - Comparison of acid volume required to reach breakthrough between different acid blends and their respective HCl and MSA controls at optimum injection rates (Reprinted with permission from Kankaria et al., 2017).

The comparison of all the analyses of different acid blends with their respective controls is tabulated in **Table 5**. Almost equal calcium ion dissolution is noted with all three blends tested. It is desirable to retain the dissolving power of individual acids of the blend while ensuring its ability to penetrate deeper into formation with least volume of acid requirement. The wormhole structure for 5:5 wt% HCl:MSA blend exhibits the least tortuosity compared to other blends as well as its own controls. Unconsumed acid concentration in core effluent sample corresponding to breakthrough increases as the concentration of the blend increases. The more acid left unreacted, the more of it can be used for deeper penetration of acid. The reduced ionization of organic acid in the

presence of HCl imparts extension of reaction time. HCl will react to completion before MSA starts to dissociate and penetrate further. Thus, 5:5 wt% HCl:MSA blend can penetrate deeper into the formation than their respective controls. Although lesser PVs of acid is required to breakthrough for 7.5:2.5 wt% acid blend, the wormhole structures indicate a negligible advantage of blend over the individual controls in terms of wormhole thickness and tortuosity.

Combining all the factors mentioned above, 5:5 wt% HCl:MSA serves as the best and optimum choice compared to other two blends tested in terms of lesser acid PV required to breakthrough, almost equal calcium dissolution, straight, dominant, less tortuous and thinner wormhole compared to HCl control, and its ability to penetrate deeper into the formation.

Set	Core ID	Volume to breakthrough, PV	Total Calcium ions dissolved, g	Maximum unconsumed acid concentration, wt% HCl	Tortuosity, L/L_0	Wormhole structure
2.5:7.5 wt% HCl:MSA I.R.$_{opt}$ = 7.5 cm^3/min	20 (Blend)	1.38	1.04	0.85	1.65	Single and dominant
	26 (HCl control)	2.08	1.29	0.94	1.50	Branched and relatively enlarged
	27 (MSA control)	1.62	0.87	0.85	1.56	Slightly branched and relatively thinner
5:5 wt% HCl:MSA I.R.$_{opt}$ = 7.5 cm^3/min	5 (Blend)	1.33	1.08	1.72	1.68	Single, straight and dominant
	8 (HCl control)	1.84	1.09	1.09	2.11	Branched, tortuous and relatively enlarged
	9 (MSA control)	1.39	0.81	1.61	1.70	Branched and relatively thinner
7.5:2.5 wt% HCl:MSA I.R.$_{opt}$ = 5 cm^3/min	12 (Blend)	0.99	0.97	0.93	1.99	Tortuous
	18 (HCl control)	0.97	1.06	1.51	1.66	Tortuous and relatively enlarged
	19 (MSA control)	0.79	0.86	1.73	1.69	Tortuous but thinner

Table 5 - Comparison of various post-coreflood parameters between different acid blends and their respective HCl and MSA controls at optimum injection rates (Reprinted with permission from Kankaria et al., 2017).

CHAPTER VII

ROTATING DISK APPARATUS (RDA) STUDIES

The optimum blend of HCl:MSA (5:5 wt% HCl:MSA) was chosen for RDA studies with calcite marble disk. RDA approach was used to quantify the observations of coreflood studies. Two sets of tests were carried out: at 77 and 250°F. Four different rotational speeds, ranging from 100 to 800 rpm were selected to conduct the experiments at each of the temperatures. In total, 8 RDA tests were conducted, and some were repeated to check the reproducibility of the data. The results were compared to that with equivalent 7.2 wt% HCl provided in the literature. The comparison was made in terms of diffusivity value in the mass-transfer regime. Lower diffusivity of HCl-MSA blend would indicate reduced ionization of MSA (in accordance with Le Chatelier principle) as opposed to regular HCl.

VII.1 Experimental Procedure

VII.1.1 Components of RDA

Fig. 69 shows a picture of the RDA set-up. It consists of the following components:

1. Two Hastelloy® vessels, reservoir and reactor, to hold the fluids.
2. Spindle on the reactor lid, where the rock is mounted, assembled with a motor that provides rotation.
3. Two temperature controllers to set the test temperature of reservoir and reactor.

4. Rotation speed controller for the motor on the reactor.
5. Seven flow and pressure valves.
6. Two pressure gauges for the reservoir and the reactor to monitor the pressure in the respective vessels over time.
7. A nitrogen cylinder to apply the pressure in the vessels.
8. Gas booster controller to drive air to the booster pump.
9. Pressure release valves to release pressure from the vessels after the test.
10. Sampling line to collect the effluent samples.

Figure 69 – Rotating disk reactor.

VII.1.2 Disk preparation

Marble disks of 1.5 in. diameter and 0.65 in. thickness were drilled from a marble block and cut into the disk shape. The disks were polished using sandpaper to remove any irregularities in them. 0.1M HCl solution was used to soak the polished disks for 35 minutes to make the surface smooth and remove any further kinks. Next, the disks were thoroughly rinsed and soaked in DI water. The porosity of the disks was determined to be negligible.

VII.1.3 RDA experiments

The reacting disk was laminated with the heat-shrinkable Teflon rollcover and then mounted on the spindle in the reactor. Both the reservoir filled with reacting fluid and the reactor were heated to the test temperature. A pressure above 1,100 psi was maintained to ensure most of the CO_2 is dissolved in the solution. The reaction began when the acid solution was injected from the reservoir under pressure to the reactor where the disk was loaded. The disk was rotated at the pre-set rotational speed. 3 ml samples were withdrawn every minute for 10 minutes and were further diluted to measure the dissolved calcium concentration using ICP-OES.

VII.2 Theory of RDA

RDA is a widely used method to calculate the kinetic parameters such as; calcite dissolution rate, reaction constant, reaction order, diffusivity, and activation energy of

acid-carbonate stimulation (Fredd and Fogler 1998b; Taylor et al. 2004; Lund et al. 1975). RDA also guides whether a reaction is mass-transfer or surface-reaction limited.

Heterogeneous reactions, like that between solid-liquid, are associated with overall three steps (Lund et al. 1975): 1) H^+ ions diffusion from the bulk acid solution to the solid-liquid interface, 2) reaction at the interface and 3) products diffusion back into the bulk solution. According to kinetics rule, the slowest step controls the rate of the reaction. If the diffusion is the slowest step, the reaction is mass-transfer limited (Taylor and Nasr-El-Din 2009). If the slowest step is the reaction at the solid-liquid interface, the reaction is surface-reaction limited.

The calcium concentration data from RDA test is converted to calcite dissolution rate for each of the disk rotational speed. Then, the rate of dissolution is plotted against the square root of angular velocity. If the slope is positive (linear relationship), the reaction is mass-transfer limited. On the other hand, if the rate of dissolution is independent of rotational speed, it is in surface-reaction limited regime (Taylor et al. 2004). It is possible to have both regimes in a RDA study (**Fig. 70**). At low rotational speed, the rate of calcite dissolution increases with rotational speed due to shrinkage in the diffusion boundary layer near the disk. This is mass-transfer limited regime. At higher rotational speed, the reaction is surface-reaction limited where the dissolution rate is constant.

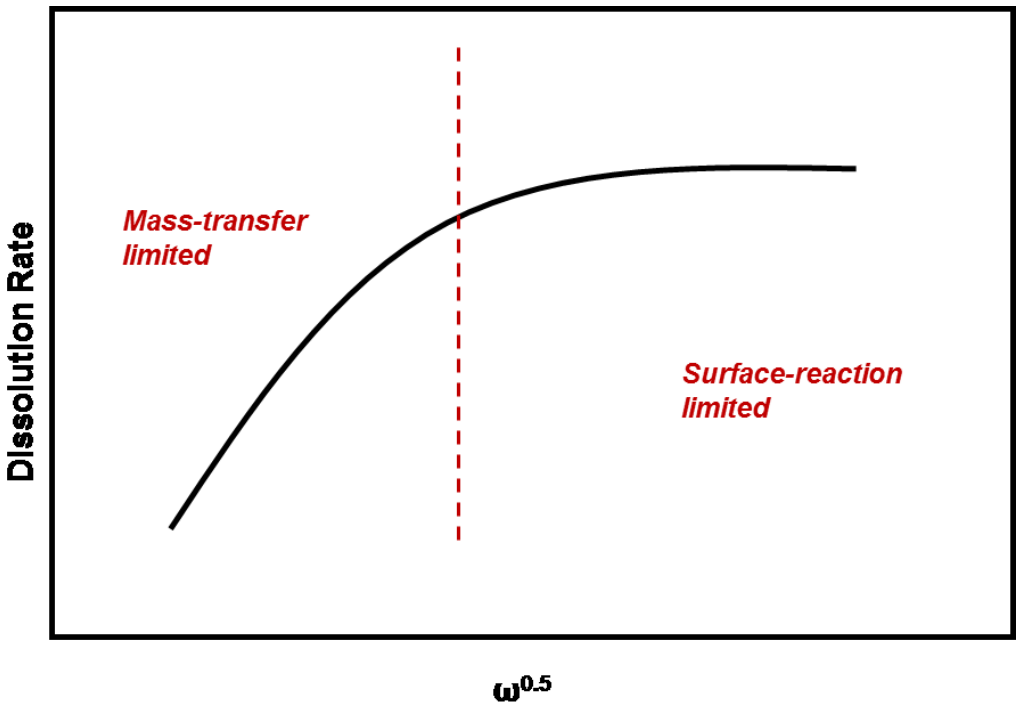

Figure 70 – A typical plot of dissolution rate vs. square root of disk rotational speed.

For the mass-transfer limited regime, the value of diffusion coefficient is calculated using **eq. 4,** where the rate of mass transfer, rotational speed, kinematic viscosity, and bulk acid concentration is known for the Newtonian fluid under laminar flow conditions (Newman 1966). It is worthwhile to note that the surface concentration is negligible for the mass-transfer limited regime.

$$J_{mt} = \frac{0.62048\, Sc^{-2/3} (\nu\omega)^{1/2}\, (C_b - C_s)}{1 + 0.2980\, Sc^{-1/3} + 0.1451\, Sc^{-2/3}} \quad \text{. ……..……..…….. (4)}$$

where J_{mt} is the rate of mass transfer in mol/cm^2.s, ν is kinematic viscosity in cm^2/s, ω is disk rotational speed in rad/s, C_b and C_s are bulk and surface concentration in moles/cm^3, Sc is Schmidt number (=ν/D), D is diffusivity in cm^2/s.

If the reaction is surface-reaction limited, the kinetic parameters are calculated using **eq. 5** (Lund et al. 1975).

$$-r_{HCl} = KC_s^n \quad . \quad \ldots\ldots\ldots\ldots\ldots\ldots\ldots\ldots\ldots\ldots\ldots\ldots\ldots\ldots\ldots\ldots \quad (5)$$

where $-r_{HCl}$ is the rate of consumption of HCl in mol/cm^2.s, K is specific reaction rate in (moles/cm^2.s)(moles/cm^3)$^{-n}$, and n is the reaction order.

VII.3 Results and Discussions

Two sets of experiments, at 77 and 250°F were performed to quantify the diffusivity of the 5:5 wt% HCl:MSA blend. The results were then compared to that of 7.2 wt% HCl. Four rotational speeds, including 100, 300, 500, and 800, were used to conduct the RDA tests with the blend and marble disks. Pressure was always maintained between 1,100 and 1,300 psi. From the ICP analysis of the effluent samples, calcium concentrations were measured. **Fig. 71** and **72** show the plots of calcium concentration against time at different rotational speeds at 77 and 250°F, respectively. The slope indicates the rate of calcite dissolution in gmol/min. In the reaction of carbonate with HCl:MSA blend, 2 moles of H^+ ions react with 1 mole of Ca^{2+}. Thus, the amount of spent acid can be calculated from dissolved calcium data. In turn, the amount of H^+ left in solution unreacted can be calculated by subtracting the spent acid amount from the initial amount of acid taken. For 5:5 wt% HCl:MSA, the concentration of H^+ was 1.97M, which corresponds to 0.97 gmol of H^+ ions in the solution of 500 ml.

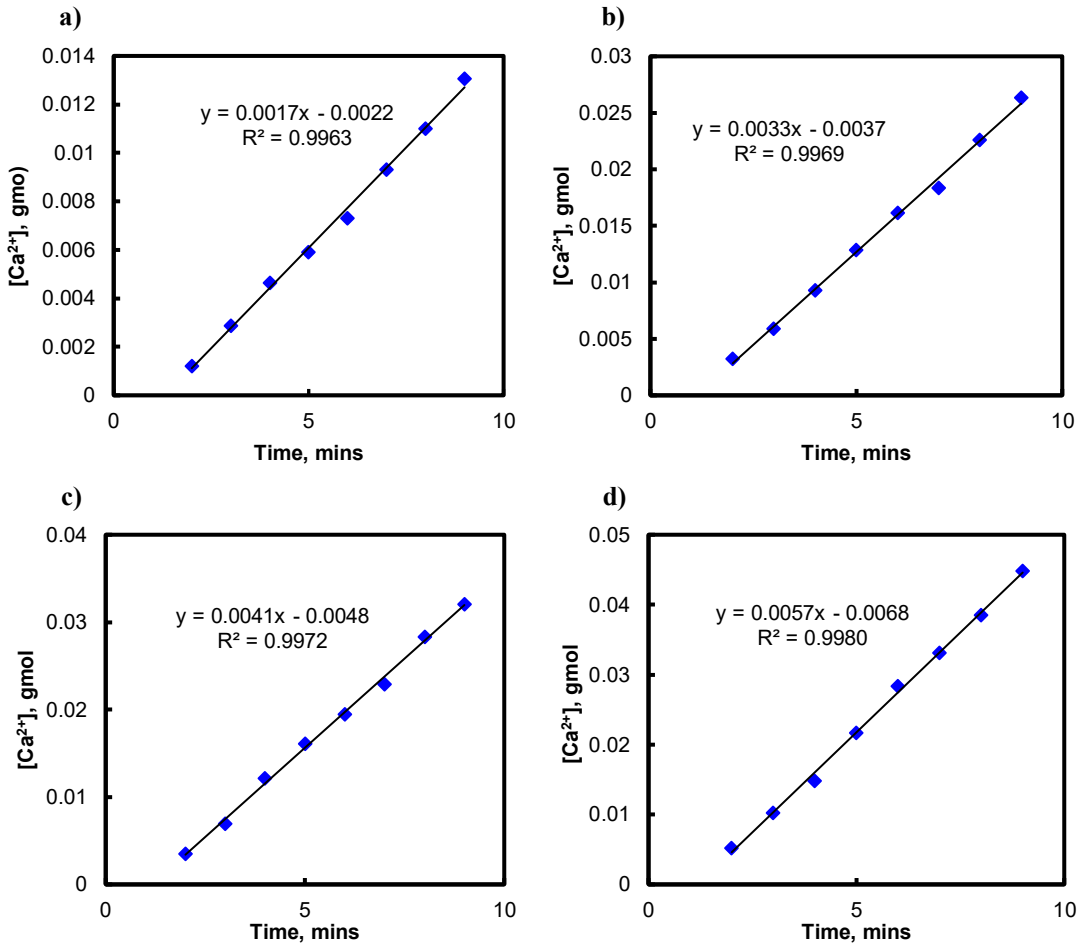

Figure 71 – Dissolved Ca^{2+} vs. time plots for RDA tests at 77°F with 5:5 wt% HCl:MSA blend at a) 100, b) 300, c) 500, and d) 800 rpm.

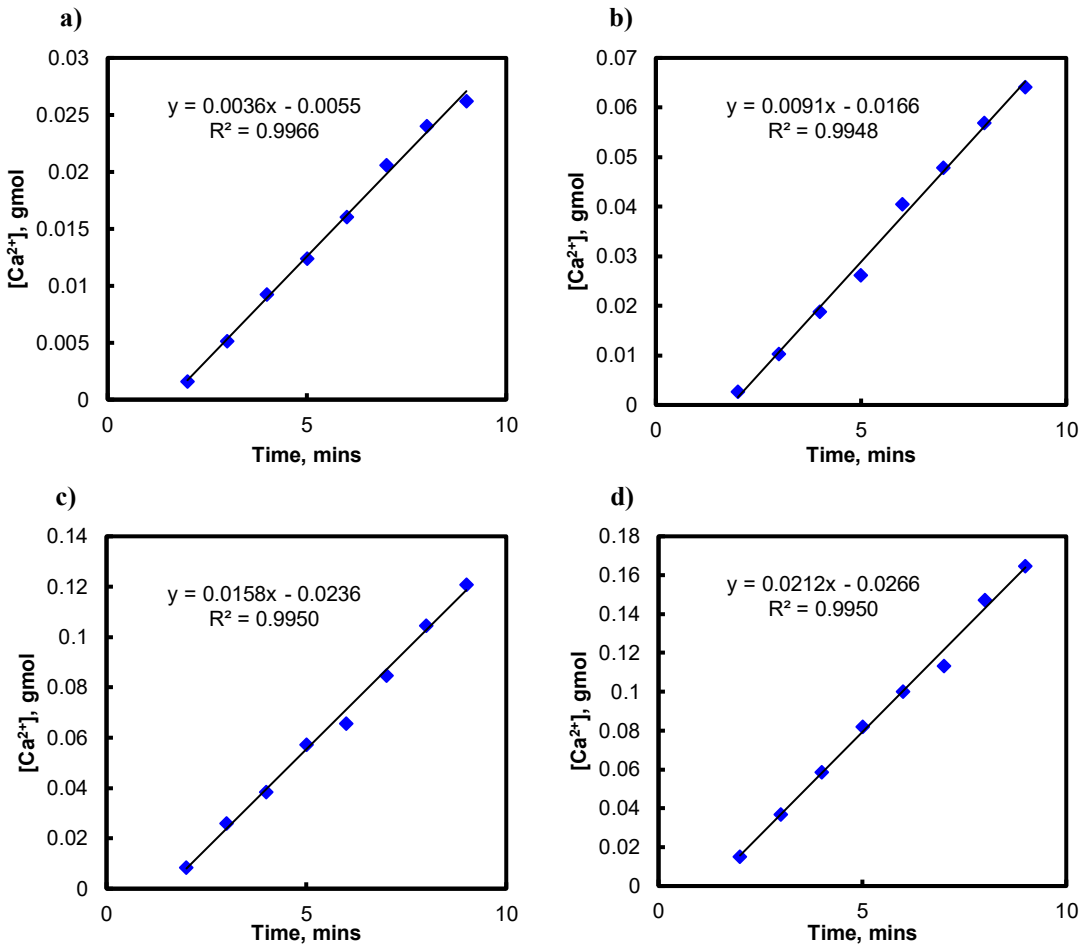

Figure 72 - Dissolved Ca^{2+} vs. time plots for RDA tests at 250°F with 5:5 wt% HCl:MSA blend at a) 100, b) 300, c) 500, and d) 800 rpm.

Fig. 73 and **74** show the plot of unreacted H^+ in gmol against time at 77 and 250°F, respectively. The slope was found to be negative which implies the unreacted H^+ ions decreases with time. The first and last few data points were discarded which didn't fit well into the curve due to the surface of the disk becoming irregular.

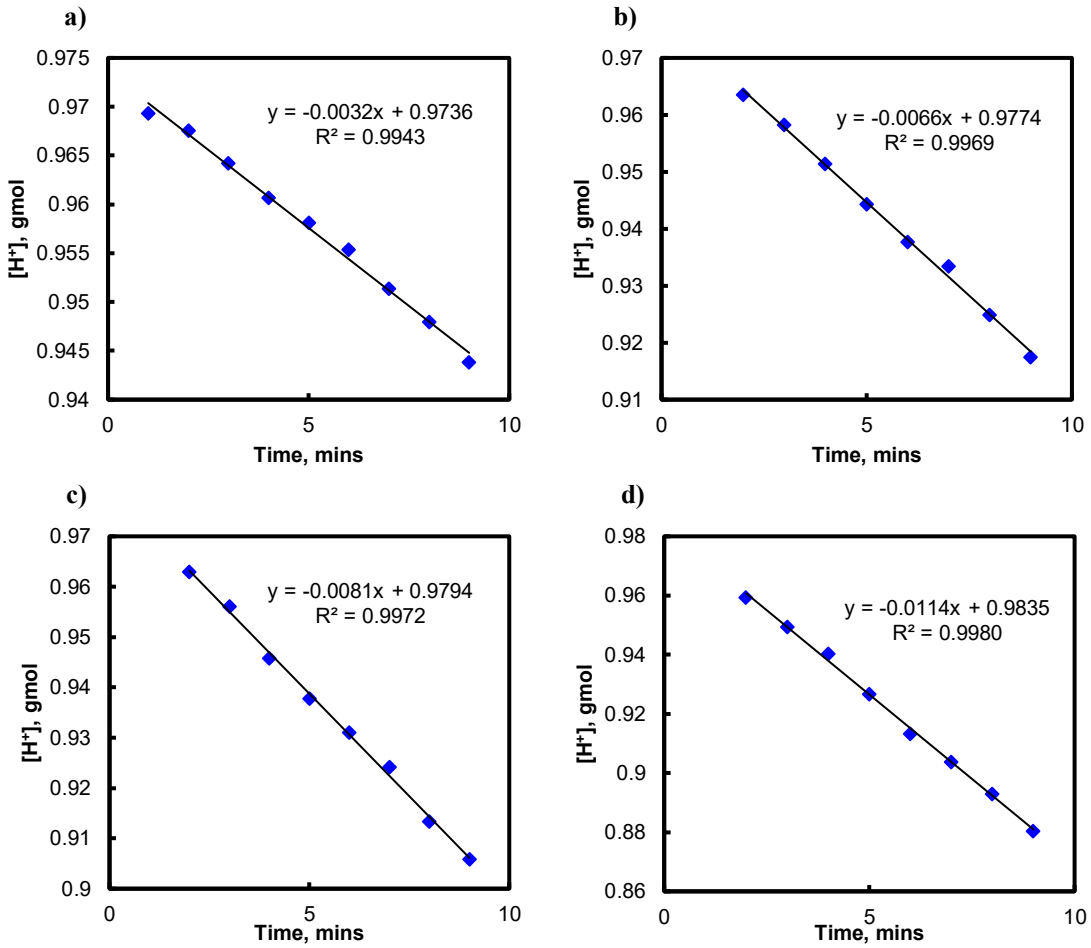

Figure 73 - Dissolved H^+ vs. time plots for RDA tests at 77°F with 5:5 wt% HCl:MSA blend at a) 100, b) 300, c) 500, and d) 800 rpm.

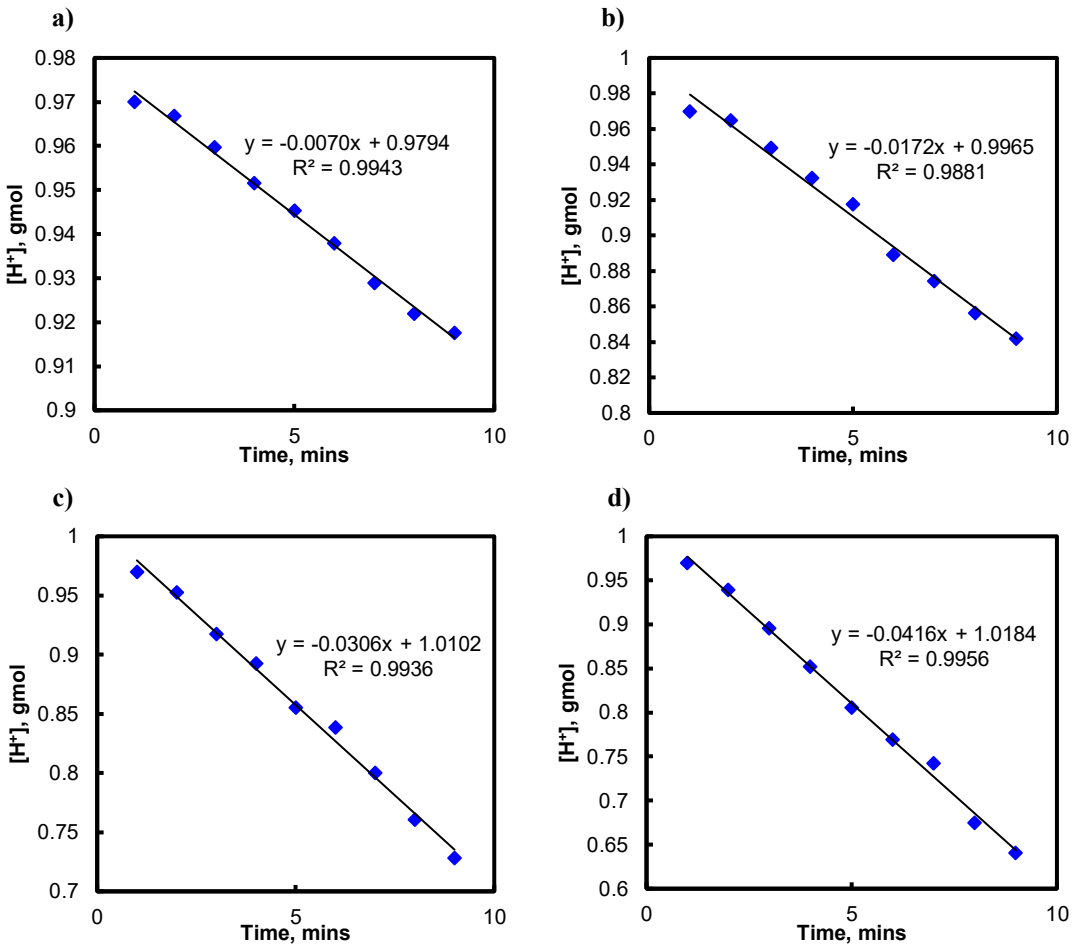

Figure 74 - Dissolved H^+ vs. time plots for RDA tests at 250°F with 5:5 wt% HCl:MSA blend at a) 100, b) 300, c) 500, and d) 800 rpm.

Figs. 75 and **76** show the marble disks after the reaction at 77 and 250°F, respectively. It was observed that as the rotational speed increased, the surface was no longer flat, which is an indirect indication of higher calcite dissolution.

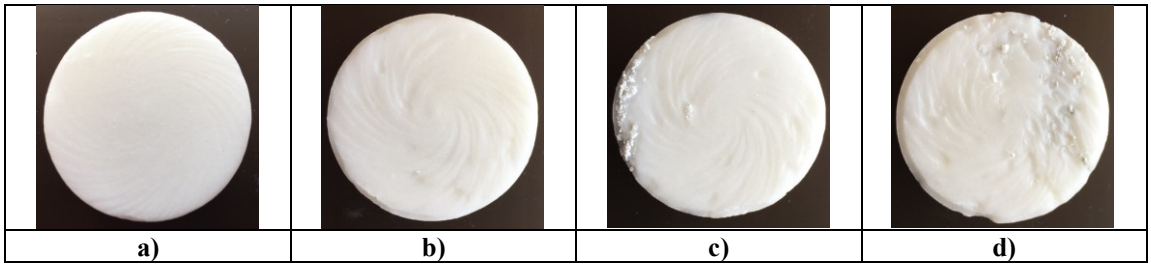

a)	b)	c)	d)

Figure 75 - Marble disks after RDA tests with 5:5 wt% HCl:MSA at 77°F at a) 100, b) 300, c) 500, and d) 800 rpm.

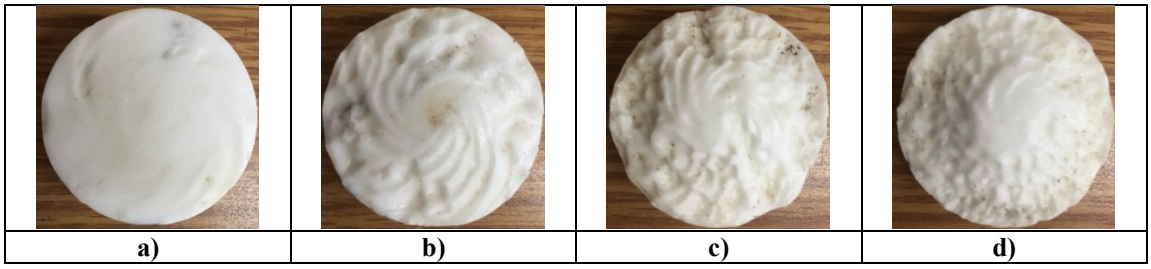

a)	b)	c)	d)

Figure 76 - Marble disks after RDA tests with 5:5 wt% HCl:MSA at 250°F at a) 100, b) 300, c) 500, and d) 800 rpm.

<u>Comparison of results of 5:5 wt% HCl:MSA blend and 7.2 wt% HCl:</u>

The slope of **Figs. 73** and **74** indicate the rate of spending of H^+ in gmol/min. It is then converted into gmol/s, and the rate of reaction is calculated as per **eq. 6**.

$$Reaction\ rate = \frac{slope}{A\ (1-\phi)} \quad . \quad \ldots\ldots\ldots\ldots\ldots\ldots\ldots\ldots\ldots\ldots\ldots\ldots \quad (6)$$

where reaction rate is in $\frac{gmol}{cm^2.s}$, A is surface area in cm^2, slope is in $\frac{gmol}{s}$ and ϕ is porosity.

The linear disk rotational velocity (rpm) was converted to angular velocity, ω (rad/s). The reaction rate was then plotted against the square root of ω (**Fig. 77**) for both 77 and 250°F.

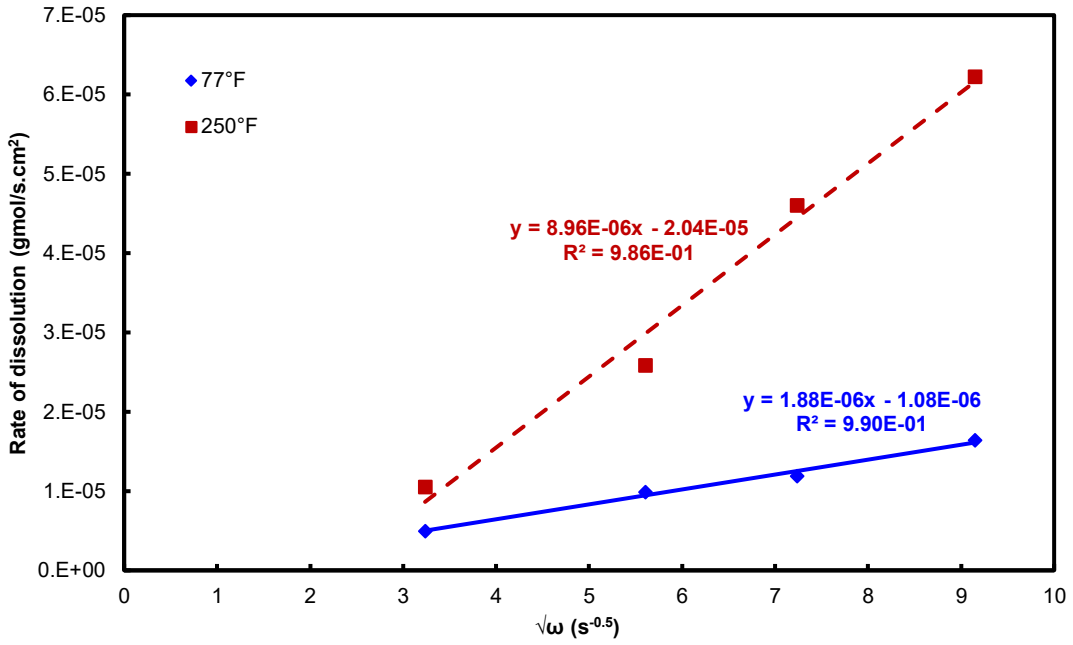

Figure 77 - Rate of dissolution as a function of square root of angular velocity at 77 and 250°F.

The reaction rate increases linearly with $\omega^{0.5}$. The linear positive slope $(\frac{Jmt}{\omega^{0.5}})$ indicates the reaction is in mass-transfer limited regime at both temperatures. The reaction rate is higher at 250°F compared to 77°F in accordance with the Arrhenius law (**eq. 7**).

$$K = K_0 \exp(\frac{-E_a}{RT}) \quad \text{. ……..…….. (7)}$$

where K is specific reaction rate in (moles/cm^2.s)(moles/cm^3)$^{-n}$, K_0 is the pre-exponential factor, E_a is activation energy in kJ/gmol, R = 8.314 kJ/gmol.°K, and T is temperature in °K.

In order to calculate diffusivity of the blend at both the temperatures, eq. 4 was used. In this equation, kinematic viscosity, ν, which is a function of temperature, was unknown. Thus, the kinematic viscosity was measured at 77, 86, 104, 122, 140, 158, and 160°F. The results are tabulated in **Table 6**. To obtain the kinematic viscosity value at 250°F, the results were extrapolated as shown in **Fig. 78**.

Temperature (°F)	Density (g/cm^3)	Kinematic viscosity (cm^2/s)
77	1.0427	0.0106488
86	1.0409	0.0097969
104	1.037	0.00862553
122	1.0326	0.00758727
140	1.0277	0.00596333
158	1.0225	0.00500456
176	1.0169	0.00442376

Table 6 – Kinematic viscosity and density as a function of temperature for 5:5 wt% HCl:MSA blend.

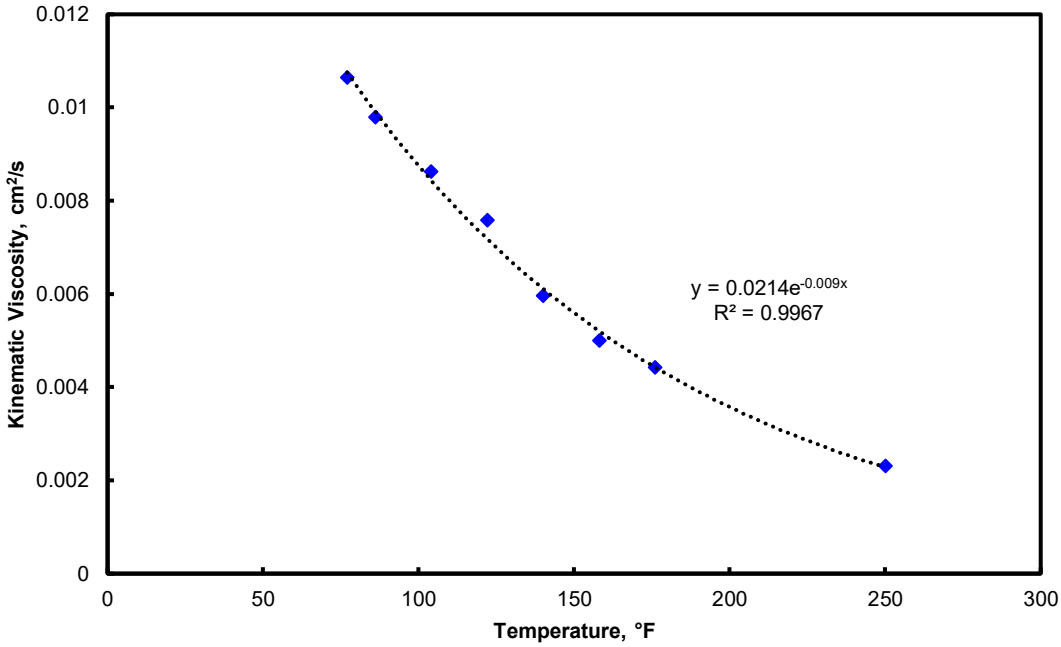

Figure 78 – Kinematic viscosity of 5:5 wt% HCl:MSA blend as a function of temperature.

According to Lund et al. (1973), the surface concentration, C_s, is almost zero in the diffusion-limited regime. Inserting all the variables ($\frac{J_{mt}}{\omega^{0.5}}$, ν, C_b) in eq. 4, diffusivity, D, can be calculated for the blend at both the temperatures. Diffusion coefficient for the blend was found to be 1.45E-05 and 1.6E-04 cm^2/s at 77 and 250°F, respectively. This indicates almost an order of magnitude increase in diffusivity with an increase in temperature. The values of diffusion coefficient of equivalent concentration of HCl (7.2 wt%) and MSA (17.7 wt%) was found from literature (**Table 7** and **8**). By interpolation, the diffusivity of 7.2 wt% HCl is 2.72E-05 and 9.23E-05 cm^2/s at 77 and 250°F, respectively (Taylor et al. 2004). According to interpolation of the data from Reyath et

al. (2015), diffusivity of 17.7 wt% MSA is 9.1E-06 and 1.70E-04 cm^2/s at 77 and 250°F, respectively.

	HCl		
Wt% / T(°F)	**3.59**	**7.07**	**16.9**
73.4	2.95E-05	2.71E-05	2.11E-05
122	4.75E-05	4.49E-05	3.91E-05
185	7.08E-05	6.82E-05	6.24E-05

Table 7 – Diffusion coefficient values of HCl at different concentration and temperature.

	MSA		
Wt% / T(°F)	**5**	**10**	**20**
73	4.40E-05	1.73E-04	7.06E-06
150	3E-04	2.91E-04	9.54E-05
250	9.76E-04	3.82E-04	1.14E-04

Table 8 - Diffusion coefficient values of MSA at different concentration and temperature.

The results indicate lower diffusivity of the blend than both the equivalent controls of HCl and MSA at 77°F. However, at 250°F, the blend shows almost similar diffusivity as equivalent 17.7 wt% MSA and is higher than the HCl control. This shows a necessity of retarding the blend for high temperature applications.

According to Lund et al. (1975), the reaction of HCl with calcite should be mass-transfer controlled at temperatures above 34°F. Though it is valid for concentrations

lower than 1M, it might not be true at higher concentrations, such as 15% HCl. Karale et al. (2016) claimed that the RDA studies are not representative of the downhole conditions due to the lack of exposure to porous media which is a local closed system. In RDA, the reaction occurs only on the flat surface of marble (which has negligible porosity). At 1M concentrations, much less CO_2 is produced that is effectively dissolved in the solution at the applied pressure of 1,100 psi. At higher concentrations of HCl, CO_2 produced from the reaction is not completely dissolved and a local increase in gas phase saturation occurs, as also noted from our coreflood experiments. The solubility of CO_2 decreases in the solution as the concentration of $CaCl_2$ increases as one of the product formed during the reaction (Prutton and Savage 1945). The presence of gaseous CO_2 affects the hydrodynamics of the reaction and the overall dissolution process.

CHAPTER VIII

CONCLUSIONS[4]

Commonly used HCl in the oil industry poses several issues, including face dissolution and corrosion. Several alternatives, such as organic acids, have been tried in the literature. Methanesulfonic acid is one such solution to the problem; however, it is expensive. Thus, blending organic acid with HCl is another viable option. This study examined three different acid blends of HCl:MSA (2.5:7.5, 5:5 and 7.5:2.5 wt%), along with their equivalent HCl and MSA controls at optimum injection rates of the blends to determine the optimum and suitable candidate for carbonate acidizing. The following conclusions were derived based on the results obtained:

1) Lower injection rates for all the blends were associated with an increase in pressure drop and enlarged wormhole diameter close to the core inlet due to gaseous CO_2 retarding the wormhole propagation rate.

2) Injection rate higher than optimum was associated with branched wormholes because of the filtration losses through the wormhole walls.

3) Almost equal PVs of acid are required to reach breakthrough for 2.5:7.5 and 5:5 wt% acid blends. Thus, it is reasonable to increase HCl concentration and decrease MSA concentration, while preserving the overall performance of the blend. Despite

---

[4] Part of this chapter is reprinted with permission from: "Matrix Acidizing of Carbonate Rocks Using New Mixtures of HCl/Methanesulfonic Acid" by Sneha Kankaria, Hisham A. Nasr-El-Din, and Shawn Rimassa, 2017. SPE Proceedings, Copyright [2017] by Society of Petroleum Engineers.

lesser PV of acid required to reach breakthrough by 7.5:2.5 wt% HCl:MSA blend compared to the other two blends, it is not the best choice for acidizing, as the wormhole was thicker and more tortuous than its corresponding controls, as well as the other two blends due to gaseous CO_2 in the system.

4) Both 2.5:7.5 and 5:5 wt% HCl:MSA formed a single, straight, and dominant wormhole, with less tortuosity when compared to their corresponding HCl and MSA controls. This indicates that the consumption of acid blend contributed entirely to the dominant wormhole propagation, which was the most effective way to transport acid to the wormhole tip.

5) Almost equal calcium ions dissolution is noted in 5:5 wt% HCl:MSA blend compared to its corresponding HCl control while forming a dominant wormhole.

6) Both 5:5 and 7.5:2.5 wt% HCl:MSA acid blend exhibited higher unconsumed acid concentrations at breakthrough in the core effluent sample compared to their respective controls. The acid blend of 2.5:7.5 wt% HCl:MSA did not show a considerable unreacted acid concentration at breakthrough. The higher the concentration of acid left at breakthrough, the more potential the acid has for further penetration in the formation.

7) From RDA studies, the diffusivity values suggested a necessity of retardation of the blend at higher temperatures.

8) The RDA studies are not representative of the downhole conditions due to lack of porous media and presence of CO_2 in gaseous phase that affects the overall dissolution process.

In summary, 5:5 wt% HCl:MSA offers the best composition to be considered for carbonates acidizing in terms of wormhole structure, penetration depth, volume of acid required to reach breakthrough, and uniform calcium dissolution. Mixing MSA with HCl renders advantages in terms of deeper wormholes that result in increased well productivity and cost-effectiveness in carbonate stimulation compared to regular HCl treatments.

REFERENCES

Bazin, B. 2001. From Matrix Acidizing to Acid Fracturing: A Laboratory Evaluation of Acid/Rock Interactions. *SPE Prod & Fac* **16** (01): 22-29. SPE-66566-PA. https://doi.org/10.2118/66566-PA.

Bernadiner, M. G., Thompson, K. E., and Fogler, H. S. 1992. Effect of Foams Used During Carbonate Acidizing. *SPE Prod Eng* **7** (04): 350-356. SPE-21035-PA. https://doi.org/10.2118/21035-PA.

Bertkau, W. and Steidl, N. 2012. Alkanesulfonic Acid Microcapsules and Use Thereof in Deep Wells. US Patent No. 2012/0222863 A1.

Bryant, S. L., and Buller, D. C. 1990. Formation damage from acid treatments. *SPE Prod Eng* **5** (04): 455-460. SPE-17597-PA. http://dx.doi.org/10.2118/17597-PA.

Buijse, M., de Boer, P., Breukel, B. et al. 2004. Organic Acids in Carbonate Acidizing. *SPE Prod & Fac* **19** (03): 128-134. SPE-82211-PA. https://doi.org/10.2118/82211-PA.

Chang, F. F., Nasr-El-Din, H. A., Lindvig, T. et al. 2008. Matrix Acidizing of Carbonate Reservoirs Using Organic Acids and Mixture of HCl and Organic Acids. Presented at the SPE Annual Technical Conference and Exhibition, Denver, Colorado, USA, 21-24 September. SPE-116601-MS. https://doi.org/10.2118/116601-MS.

Cheng, H., Zhu, D. and Hill, A. D. 2017. The Effect of Evolved CO_2 on Wormhole Propagation in Carbonate Acidizing. *SPE Prod & Oper* **32** (03): 325-332. SPE-178962-PA. https://doi.org/10.2118/178962-PA.

Clegg, S. L. and Brimblecombe, P. 1985. The Solubility of Methanesulfonic Acid and its Implications for Atmospheric Chemistry. *Environ. Technol. Lett.* **6** (1-11): 269-278. http://dx.doi.org/10.1080/09593338509384344.

Coulter, G. R., and Jennings, A. R. 1999. A Contemporary Approach to Matrix Acidizing. *SPE Prod & Fac* **14** (02): 150-158. SPE-56279-PA. http://dx.doi.org/10.2118/56279-PA.

Crowe, C., Masmonteil, J., and Thomas, R. 1992. Trends in Matrix Acidizing. *Oilfield Review* **4** (4): 24-40.

Daccord, G., Lenormand, R., and Liétard, O. 1993. Chemical Dissolution of a Porous Medium by a Reactive Fluid – I. Model for the "Wormholing" Phenomenon. *Chem. Eng. Sci.* **48** (01): 169-178. https://doi.org/10.1016/0009-2509(93)80293-Y.

Da Motta, E. P., Quiroga, M. H. V., Aragäo, A. F. L. et al. 1998. Acidizing Gas Wells in the Merluza Field Using an Acetic/Formic Acid Mixture and Foam Pigs. Presented at the SPE International Symposium on Formation Damage Control, Lafayette, Louisiana, USA, 18-19 February. SPE-39424-MS. https://doi.org/10.2118/39424-MS.

Dill, W. R. 1961. Reaction Times of Hydrochloric-Acetic Acid Solutions on Limestone. Presented at the 16th Southwest Regional Meeting of the American Chemical Society, Oklahoma City, Oklahoma, USA, 1-3 December. SPE-211-MS. https://doi.org/10.2118/211-MS.

Dill, W. R. and Keeney, B. R. 1978. Optimizing HCl-Formic Acid Mixtures for High Temperature Stimulation. Presented at the SPE Annual Fall Technical Conference and Exhibition, Houston, Texas, USA, 1-3 October. SPE-7567-MS. https://doi.org/10.2118/7567-MS.

Finšgar, M. and Jackson, J. 2015. The Corrosion Resistance of 2205 Duplex Steel in Non-Inhibited Methanesulphonic Acid at Elevated Temperature. *Mater Corros* **66** (11): 1299-1304. https://doi.org/10.1002/maco.201408222.

Fredd, C. N. and Fogler, F. H. 1998a. Alternative Stimulation Fluids and Their Impact on Carbonate Acidizing. *SPE J.* **3** (01): 34-41. SPE-31074-PA. https://doi.org/10.2118/31074-PA.

Fredd, C. N. and Fogler, F. H. 1998b. The Kinetics of Calcite Dissolution in Acetic Acid Solutions. *Chem Eng Sci* **53** (22): 3863-3874. https://doi.org/10.1016/S0009-2509(98)00192-4.

Fredd, C. N. and Fogler, H. S. 1999. Optimum Conditions for Wormhole Formation in Carbonate Porous Media: Influence of Transport and Reaction. *SPE J.* **4** (03): 196-205. SPE-56995-PA. http://dx.doi.org/10.2118/56995-PA.

Frenier, W.W., Rainey, M., Wilson, D. et al. 2003. A Biodegradable Chelating Agent Is Developed for Stimulation of Oil and Gas Formations. Presented at the SPE/EPA/DOE Exploration and Production Environmental Conference, San Antonio, Texas, USA, 10-12 March. SPE-80597-MS. https://doi.org/10.2118/68-006.

Gernon, M. D., Wu, M., Buszta, T. et al. 1999. Environmental Benefits of Methanesulfonic Acid: Comparative Properties and Advantages. *Green Chem.* **01** (03): 127-140. https://doi.org/10.1039/A9001157C.

Ghalambor, A., and Economides, M. J. 2000. Formation damage abatement: a quarter-century perspective. Presented at the SPE International Symposium on Formation

Damage Control, Lafayette, Louisiana, USA, 23-24 February. SPE-58744-MS. http://dx.doi.org/10.2118/58744-MS.

Harp, L. J., Carver Jr., J., and Matson, B. G. 1968. Controlled Stimulation of Deep, Hot Wells with Binary and Trinary HCl-Organic Acid Blends. Presented at the Spring Meeting of the Mid-Continent District Division of Production, Amarillo, Texas, USA, April. API-68-006.

Harris, F. N. 1961. Applications of Acetic Acid to Well Completions, Stimulations and Reconditioning. *J Pet Technol* **13** (07): 637-639. SPE-63-PA. https://doi.org/10.2118/63-PA.

Hashem, M. K., Nasr-El-Din, H. A., and Hopkins, J. A. 1999. An Experience in Acidizing Sandstone Reservoirs: A Scientific Approach. Presented at the SPE Annual Technical Meeting, Houston, Texas, USA, 3-6 October. SPE-56528-MS. http://dx.doi.org/10.2118/56528-MS.

Heidenfelder, T., Guzmann, M., Witteler, H. et al. 2009. Methods of Increasing Permeability in Carbonatic Rock Formations with Alkanesulfonic Acids. US Patent No. 7,638,469 B2.

Hoefner, M. L. and Fogler, H. S. 1988. Pore Evolution and Channel Formation During Flow and Reaction in Porous Media. *AIChE* **34** (01): 45-54. https://doi.org/10.1002/aic.690340107.

Houchin, L. R., Dunlap, D. D., and Hutchinson, J. E. 1988. Formation Damage During Gravel-Pack Completions. Presented at the SPE Formation Damage Control Symposium, Bakersfield, California, USA, 8-9 February. SPE-17166-MS. http://dx.doi.org/10.2118/17166-MS.

Huang, T., Hill, A. D., and Schechter, R. S. 2000. Reaction Rate and Fluid Loss: The Keys to Wormhole Initiation and Propagation in Carbonate Acidizing. *SPE J.* **5** (03): 287-292. SPE-65400-PA. https://doi.org/10.2118/65400-PA.

Karale, C., Beuterbaugh, A., Pinto, M. et al. 2016. HP/HT Carbonate Acidizing-Recent Discoveries and Contradictions in Wormhole Phenomenon. Presented at the Offshore Technology Conference Asia, Kuala Lumpur, Malaysia, 22-25 March. OTC-26714-MS. https://doi.org/10.4043/26714-MS.

Kankaria, S., Nasr-El-Din, H. A., and Rimassa, S. 2017. Matrix Acidizing of Carbonate Rocks Using New Mixtures of HCl/Methanesulfonic Acid. Presented at the SPE International Conference on Oilfield Chemistry, Montgomery, Texas, USA, 3-5 April. SPE-184528-MS. http://dx.doi.org/10.2118/184528-MS.

Klotz, J. A., Krueger, R. F., and Pye, D. S. 1974. Maximum Well Productivity in Damaged Formations Requires Deep, Clean Perforations. Presented at the SPE Symposium on Formation Damage Control, New Orleans, Louisiana, USA, 30 January - 2 February. SPE-4792-MS. http://dx.doi.org/10.2118/4792-MS.

Lund, K. and Fogler, H. S. 1975. Acidization–II: The Dissolution of Calcite in Hydrochloric Acid. Chem Eng Sci 30 (8): 825-835. https://doi.org/10.1016/0009-2509(75)80047-9.

McLeod, H. O. 1984. Matrix Acidizing. *J Pet Technol* **36** (12)**:** 2055-2069. SPE-13752-PA. https://doi.org/10.2118/13752-PA.

Muecke, T. W. 1982. Principles of Acid Stimulation. Presented at the International Petroleum Exhibition and Technical Symposium, Beijing, China, 17-24 March. SPE-10038-MS. https://doi.org/10.2118/10038-MS.

Nasr-El-Din, H. A., Solares, J. R., Al-Mutairi, S. H. et al. 2001. Field Application of Emulsified Acid-Based System to Stimulate Deep, Sour Gas Reservoirs in Saudi Arabia. Presented at the SPE Annual Technical Conference and Exhibition, New Orleans, Louisiana, USA, 30 September - 3 October. SPE-71693-MS. http://dx.doi.org/10.2118/71693-MS.

Nasr-El-Din, H. A., Al-Anazi, H. A., and Hopkins, J. A. 1997. Acid/Rock Interactions During Stimulation of Sour Water Injectors in a Sandstone Reservoir. Presented at the International Symposium on Oilfield Chemistry, Houston, Texas, USA, 18-21 February. SPE-37215-MS. http://dx.doi.org/10.2118/37215-MS.

Nasr-El-Din, H. A., Al-Mutairi, S., Al-Malki, B. et al. 2002. Stimulation of Deep Gas Wells Using HCl/Formic Acid System: Lab Studies and Field Application. Presented at the Canadian International Petroleum Conference, Calgary, Alberta, Canada, 11-13 June. PETSOC-2002-289. http://dx.doi.org/10.2118/2002-289.

Nasr-El-Din, H. A., Driweesh, S. M., and Muntasheri, G. A. 2003. Field Application of HCl-Formic Acid System to Acid Fracture Deep Gas Wells Completed with Super Cr-13 Tubing in Saudi Arabia. Presented at the SPE International Improved Oil Recovery Conference in Asia Pacific, Kuala Lumpur, Malaysia, 20-21 October. SPE-84925-MS. https://doi.org/10.2118/84925-MS.

Newman, J. 1966. Schmidt Number Correction for the Rotating Disk. Journal Phys Chem 70 (4): 1327-1328. https://dx.doi.org/1310.1021/j100876a100509.

Ortega, A., Nasr-El-Din, H. A., and Rimassa, S. 2014. Acidizing High Temperature Carbonate Reservoirs Using Methanesulfonic Acid: A Coreflood Study. Presented at the AADE Symposium on Fluids Technical Conference and Exhibition, Houston, Texas, USA, 15-16 April. AADE-14-FTCE-3.

Prutton, C. F. and Savage, R. L. 1945. The Solubility of Carbon Dioxide in Calcium Chloride-Water Solutions at 75, 100, 120° and High Pressures. *J. Am. Chem. Soc.* **67** (9): 1550-1554. http://dx.doi.org/10.1021/ja01225a047.

Qiu, X. W., Zhao, W., Dyer, S. J. et al. 2014. Revisiting Reaction Kinetics and Wormholing Phenomena During Carbonate Acidizing. Presented at the International Petroleum Technology Conference, Doha, Qatar, 19-22 January. https://doi.org/10.2523/IPTC-17285-MS.

Reyath, S. M., Nasr-El-Din, H. A., and Rimassa, S. 2015. Determination of Diffusion Coefficient of Methanesulfonic Acid Solutions with Calcite Using Rotating Disk Apparatus. Presented at the SPE International Symposium on Oilfield Chemistry, The Woodlands, Texas, USA, 13-15 April. SPE-173794-MS. https://doi.org/10.2118/173794-MS.

Shank, R. A. and McCartney, T. R. 2013. Synergistic and Divergent Effects of Surfactants on the Kinectics of Acid Dissolution of Calcium Carbonate Scale. Presented at the Corrosion 2013 NACE International Conference and Exposition, Orlando, Florida, USA, 17-21 March. NACE-2762.

Shukla, S., Zhu, D., and Hill, A. D. 2006. The Effect of Phase Saturation Conditions on Wormhole Propagation in Carbonate Acidizing. *SPE J.* **11** (03): 273-281. SPE-82273-PA. https://doi.org/10.2118/82273-PA.

Sokhanvarian, K., Nasr-El-Din, H. A., and de Wolf, C. A. 2016. Thermal Stability of Oilfield Aminopolycarboxylic Acids/Salts. *SPE Prod & Oper* **31** (1): 12-21. SPE-157426-PA. http://dx.doi.org/157410.152118/157426-PA.

Taylor, K. C., Al-Ghamdi, A. H., and Nasr-El-Din, H. A. 2004. Effect of Additives on the Acid Dissolution Rates of Calcium and Magnesium Carbonates. *SPE Prod & Fac* **19** (03): 122-127. SPE-80256-PA. http://dx.doi.org/10.2118/80256-PA.

Taylor, K. C. and Nasr-El-Din, H. A. 2009. Measurement of Acid Reaction Rates with the Rotating Disk Apparatus. *J Can Pet Technol* **48** (06): 66-70. PETSOC-09-06-66. http:// doi.org/10.2118/09-06-66.

Van Domelen, M. S. and Jennings, A. R., Jr. 1995. Alternate Acid Blends for HPHT Applications. Presented at the SPE Offshore Europe Conference, Aberdeen, United Kingdom, 5-8 September. SPE-30419-MS. https://doi.org/10.2118/30419-MS.

Wang, Y., Hill, A. D., and Schechter, R. S. 1993. The Optimum Injection Rate for Matrix Acidizing of Carbonate Formations. Presented at the SPE Annual Technical Conference and Exhibition, Houston, Texas, USA, 3-6 October. SPE-26578-MS. https://doi.org/10.2118/26578-MS.

APPENDIX

Appendix A – VBA code for wormhole location

```
Sub OpenAllFiles()

Dim macrowb As Workbook
Set macrowb = ActiveWorkbook

Application.ScreenUpdating = False
''''''''''''''''''''''''''''''''''''''''''''''''''''''''''''''''''
'Folder Workbooks Loop
Dim Methodname As String
Dim i As Integer 'rows loop
Dim x As Integer ' columns loop

Dim n As Integer, m As Integer, inumber As Integer, islice As Integer, por As Double
Dim l1, l2, b1, b2, t1, t2, r1, r2, com, con, x1, x2, y1, y2 As Double
Dim counter As Integer

Dim CT_Dry(600, 300, 300) As Double
Dim CT_sat(600, 300, 300) As Double

    Dim objFSO As Object 'dont edit
    Dim objFolder As Object 'dont edit
    Dim objFile As Object 'dont edit

    Set objFSO = CreateObject("Scripting.FileSystemObject") 'dont edit

    Set objFolder = objFSO.GetFolder(ThisWorkbook.Path & "/Final") 'Change
"Collection if needed"
i = 0
x = 0
    For Each objFile In objFolder.Files 'dont edit

        If InStr(objFile, ".txt") Then 'dont edit
            Workbooks.Open (objFile)

For n = 1 To 300
For m = 1 To 300

If Cells(n, m).Value = "" And n = m Then GoTo 100
```

```
CT_Dry(i, n, m) = Cells(n, m).Value

Next
Next

100 ActiveWorkbook.Close False

' Loop on 1000 files only modifiy if more needed
          i = i + 1
          x = x + 1
          If i = 1000 Then
          MsgBox "10 Files Exceeded"
          Exit Sub
          End If
''' """""""""""""
       End If
0
   Next

inumber = n - 1
islice = i - 1

'islice = 3

For i = 0 To islice

l1 = inumber
l2 = inumber
r1 = 0
r2 = 0
t1 = inumber
t2 = inumber
b1 = 0
b2 = 0

com = 0
con = 0

For n = 1 To inumber

con = 0
counter = 0
```

```
For m = 1 To inumber

If CT_Dry(i, n, m) = 0 Then
counter = counter + 1
End If

If CT_Dry(i, n, m) <> 0 And con = 0 And com = 0 Then

   If n < l1 Then
   l1 = n
   End If

   If n > r1 Then
   r1 = n
   End If

   If m < t1 Then
   t1 = m
   End If

   If m > b1 Then
   b1 = m
   End If

If CT_Dry(i, n, m + 1) = 0 Then
con = 1
End If

ElseIf CT_Dry(i, n, m) <> 0 Then

 If n < l2 Then
   l2 = n
   End If

   If n > r2 Then
   r2 = n
   End If

   If m < t2 Then
   t2 = m
   End If

   If m > b2 Then
```

```
   b2 = m
   End If

End If

If counter = inumber And b1 > 0 Then
com = 1
End If

Next
Next

x1 = (l1 + r1) / 2
y1 = (t1 + b1) / 2

If x1 = 25 And y1 = 25 Then GoTo 2323

Sheets("Porosity").Cells(i + 1, 1) = x1
Sheets("Porosity").Cells(i + 1, 2) = y1

x2 = (l2 + r2) / 2
y2 = (t2 + b2) / 2

If x2 = 25 And y2 = 25 Then GoTo 2323

Sheets("Porosity").Cells(i + 1, 5) = x2
Sheets("Porosity").Cells(i + 1, 6) = y2

2323 Next

Application.ScreenUpdating = True

End Sub
''''''''''''''''''''''''''''''''
```